DEPARTMENT OF STATISTICAL PHYSICS

FACULTY OF PHYSICS
LUDWIG-MAXIMILIANS-UNIVERSITÄT MÜNCHEN


MASTER THESIS

---

# Two Species of Self-Propelled Particles Interacting in a Snowdrift Game Scenario

**- Agent Based Approach -**

# Zwei Spezies selbstgetriebener Teilchen wechselwirkend in einem Feiglingsspiel-Szenario

**- Teilchenbasierter Ansatz -**

---

*Author:*
Michael OBERMÜLLER

*Supervisor:*
Prof. Dr. Erwin FREY

12. August 2019

# Contents

**1 On the Combination of Game Theory and Active Matter** **1**

**2 Introduction to Active Matter** **3**
2.1 The State of Active Matter . . . 3
2.2 Self-Propelled Models . . . 4

**3 The Game Theoretical Model** **7**
3.1 The Cooperator-Defector Game . . . 7
3.2 Evolutionary Game Theory . . . 8
3.2.1 Mean Field Limit and Replicator Equations . . . 8
3.2.2 Fixed Point Structure and the Four Games . . . 9
Prisoner's Dilemma . . . 9
Harmony . . . 10
Coordination . . . 10
Snowdrift Game . . . 10

**4 The Agent Based Approach** **13**
4.1 The Microscopic Agent Based Model . . . 13
4.2 Implementation . . . 16
4.2.1 Parallel Programming . . . 16
4.2.2 The Box Algorithm . . . 18
4.3 Results of the Simulation . . . 20
4.3.1 Isotropy, Active Matter Waves and Coherent Motion . . . 20
The Five Phases . . . 22
Merged Wave Phase . . . 26
4.3.2 Game Theoretical Pattern Formation . . . 27
One Dimensional Case and Model . . . 27
Two Dimensional Case . . . 31
Spot Order vs. Diffusion . . . 33
4.3.3 Polar Order Stabilized Species Separation . . . 35
4.4 Central Results of the Agent Based Approach . . . 35

**5 The Kinetic Boltzmann Approach** **39**
5.1 The Microscopic Model . . . 39
5.2 The Boltzmann Equation . . . 41
5.3 The Combined Model . . . 43
5.4 Fourier Transformed Boltzmann equation . . . 43
5.4.1 The Continuity Equation . . . 44
5.4.2 The Isotropic Solution . . . 45

**6 Hydrodynamic Equations and Linear Stability Analysis** **47**
6.1 The Hydrodynamic Equations . . . 47
6.2 Homogeneous Solutions . . . 48

6.3 Inhomogeneous Perturbations . . . . . 50
6.3.1 Stability: Eigenvalues of Jacobian Matrix without game . . . . . 51
6.3.2 Stability: Eigenvalues of Jacobian Matrix with game . . . . . 53
Eigenvectors . . . . . 55

**7 Simulation and Analysis of the Hydrodynamic Equations 57**
7.1 The Algorithm . . . . . 57
7.2 Results and Comparison to the Agent Based Simulation . . . . . 57
7.2.1 The Five Phases and the Density Shift . . . . . 57
7.2.2 The Bifurcation Structure . . . . . 59

**8 Summary and Outlook 61**

**A Detailed Calculations 63**
A.1 Derivation of Fourier transformed Boltzmann terms . . . . . 63
A.2 Linear Stability of Isotropic Solution . . . . . 66
A.3 Derivation of Hydrodynamic Equations . . . . . 67
A.4 Linear Stability of Hydrodynamic Equations . . . . . 69
A.5 Collision Factors . . . . . 71

**Acknowledgements 73**

**Bibliography 75**

**Declaration of Authorship 81**

# Chapter 1

# On the Combination of Game Theory and Active Matter

Competition and Cooperation are phenomena observable almost everywhere in nature. There have been many studies of such behavior for a lot of different systems, ranging from bacteria to humans [2]. The mathematical description of this field, known as Game Theory, tries to find ways to model real life systems, develop theories for optimal behavior and strategies and predict behavior under predefined circumstances.

In nature, when observing living organisms, an optimal strategy most of the time means getting an evolutionary advantage over competitors.

While it is of great interest to understand interactions between different agents locally, it is often insightful to introduce a spatial component and interaction ranges for these systems to closer model nature, where spatial extension often plays a significant role. Especially in the case of many-particle systems this can lead to astounding results differing significantly from not extended or mean-field systems [38] [17] [28] [22].

A famous example for this is the case of the prisoners dilemma, a very basic game theoretical model, where it is beneficial to betray interaction partners in order to maximize the own gain. In the case of a local game this always leads to the extinction of a cooperative strategy [14]. If spatial extension is introduced, cooperation can survive by forming clusters [38].

Particles in nature also move through space, either by diffusion, through some external force or through self-propelled motion [16] [51]. The case of diffusion has been studied and shown to yield interesting results for game theoretical models like spiral patterns in rock-paper-scissors games [17] or the coexistence of species in a prisoners dilemma model [38]. Because self-propelled system can exhibit spatial patterns as well, we want to combine a game theoretical model and self-propelled movement to observe the interplay between alignment and game interaction and how these different mechanisms of possible pattern formation influence each other.

Self-propelled particles is the scientific term for agents which move through space on their own without being guided by an external force, while usually interacting with other active particles around them. This can lead to collective behavior such as swarming, flocking and collective movement and can be observed in the most different of species in nature. From the smallest bacteria colonies [59] to large mammal herds such as wildebeest [46], from fish swarms in the sea [30] to bird flocks in the air [31], coherent motion is a phenomenon present over many scales and environments.

Self propelled particles are part of the broader field called *active matter*. Active matter, the study of active agents, i.e. constituents that consume energy to exercise force or motion, has been a focus of intense research in the last couple of years.

The growth and competition of species is a phenomenon omnipresent in nature [23]. These interactions lead to changes in local and global densities of species which in turn are an essential parameter in active systems and the formation of order. Active motion and coherently moving patterns on the other hand distribute particles differently through a system than e.g. diffusion. It is therefore a central question of this thesis if and how active particles, flocking and collective behavior can influence cooperation, competition and the general outcome of such games.

On the other hand, starting from the perspective of active matter, we will examine the question of how the interplay between different species can change the formation of order in a multi-species system. Does the game inhibit or promote pattern formation? If it does, what are the underlying mechanisms? Do the emerging pattern shapes, sizes or order formations change with different game parameters?

# Chapter 2

# Introduction to Active Matter

## 2.1 The State of Active Matter

Actively moving constituents are a feature seen in many different systems. While many organisms are capable of self-propelled and directed motion, there have been studies regarding the movements of inanimate object such as granular rods [43] or moving machines like robots [56], which can exhibit similar collective motion patterns compared to self-propelled living organisms such as birds or fish. This collective behavior originates from an interaction between the different particles in the system and can be expressed in many different forms. While flocks of white stork can fly long distances in parallel travel to then change their patterns to a swirling motion catching an updraft [31], wildebeest tend to align in linear formations when traveling the Serengeti [46]. Fish schools seem to move and change direction in unison when predators appear [30] and insects like pharaoh ants start to exhibit order in larger numbers [5] (examples in fig. 2.1 [1]). All of these behaviors bring some kind of evolutionary benefit with them. The storks can better sense the thermal updraft by travelling in flocks and observing their peers, wildebeest find the most efficient or safe routes between different feeding grounds, fish can better detect and avoid predators and ants organize themselves to fulfill their tasks more efficiently. In all of these examples the individual becomes part of a bigger swarm or flock, which displays properties not seen in the single constituents.

(a) (b) (c)

FIGURE 2.1: Display of Collective Behaviour: Swarms and Herds in Nature. (*a*) Large fish school (*b*) A flock of starlings (*c*) Migrating herd of wildebeest

[1] Photos by Matthew T Rader, James Wainscoat and The Citizen

The tools commonly used in statistical, especially non-equilibrium statistical physics, have proven very useful in the study of such systems. This might come as no surprise, because the field of statistical physics often times infers macroscopic observables from systems consisting of many constituents. Applied to the example of self-propelled particles this can mean measuring different kinds of order or collective behavior in the system.

## 2.2 Self-Propelled Models

The description of self-propelled particles has been an active field of research for the last decades [58] [42] [55]. While coherent motion is a very distinct system feature, achieving it can be realized by a multitude of models. Different implementations of interactions between particles, different single-particle properties or the influence of the environment the particles move in can all lead to collective behavior.

There are a multitude of models for implementing self-propelled systems and the related formation of ordered motion. Many implementations, from leader-follower models [25] to interactions with the $n$ nearest neighbors [3] over so-called wet and dry systems [32], where the substrate the particles move on either assists in momentum conservation in the system or not, have been studied.

In this thesis we will discuss two approaches operating on different length scales, an agent based approach following a generalized Vicsek model [57] as the main one and a kinetic Boltzmann approach leading to hydrodynamic equations to verify and discuss the results of the agent based approach..

The Vicsek model is chosen because it is a very basic and well analyzed model [9] [8] [11] of self-propelled particles interacting. It consists of particles moving through space with equal absolute velocity $v_0$ which adjust their individual directions to the average of other particles nearby. This *polar* alignment is not perfect and disturbed by variable noise. Depending on the density of particles and the amount of noise present in the system, the formation of order can be observed [57]. Order is expressed through travelling wave states near the onset of order while for higher densities and lower noise the system moves uniformly. Variations on the initial Vicsek model revealed the robustness of this approach in describing pattern formation of self-propelled particles [8].

Self-propelled systems can also be studied analytically via a *hydrodynamic* approach. Central aspect of these models is to encode the dynamics of self-propelled agents in a generalized Navier-Stokes equation [54] [6]. Like in the case of agent based models, depending on model parameters, the system forms ordered states [55] [34]. In the early days of active matter, this description was usually based on symmetry and conservation arguments to arrive at the hydrodynamic equations and macroscopic observations [54] [53]. This leads to the problem that even though one envisions individual particles driving the dynamics, the parameters in the resulting equations cannot be related to the underlying microscopic model. One way to close this gap was found by deriving the macroscopic equations directly from microscopical quantities through coarse graining of the microscopic dynamics in a kinetic Boltzmann approach [6] [1] [4].

While we will use the hydrodynamic treatment as a comparison and derive it as well, the main focus of this thesis will lie on an agent based simulation to imitate

biological systems as closely as possible. This agent based approach will be introduced after a brief introduction to the game theoretical model we utilize. We will implement the agent based model as a gerneralized Vicsek model [57] consisting of two individual species, where cross species interaction is mediated through a game theoretical interaction, which will be presented in the following chapter. We will then focus on analyzing the results of the agent based simulations and compare it to previous studies. After this, starting from a Boltzmann ansatz, the derivation of the hydrodynamic equations is explained briefly. We will use this to draw comparisons between the agent based and hydrodynamic model, focusing on similarities between the two while pointing out differences and their possible reasons. For a more detailed treatment of the hydrodynamic approach on its own, especially the results when simulating the generalized Navier Stokes equations numerically, see [33].

# Chapter 3

# The Game Theoretical Model

Game theory, which became a focus point of research during the late 1940's and 1950's and has been an active field of research ever since [26]. Even though there have been earlier examples of works which one would consider to belong to the field of game theory today [37], the birth of the field can maybe be dated to 1947 and the book *Theory of Games and Economic Behavior* by von Neumann and Morgenstern [27] [26], after which a myriad of books and papers followed in the years after.

Game Theory tries to mathematically model decision making and strategic thinking in many different fields such as economics, computer sciences, social sciences, physics and biology [35] [36] [14] [21] [2]. The examples of game theoretical models are plentiful, ranging from the description of bacterial populations and their interaction [17] over the competition between different companies [48], to even diplomatic consideration between different countries [44]. The field has produced ten Nobel Prizes [26] until 2014 and influences almost every area of life. This is because it offers a framework to model interactions between two or more parties and tries to find rules, guidelines of behavior or strategies to improve the outcome of said interactions.

The term game in this context describes a set of rules under which the protagonists, called players, interact with each other and try to maximize their outcomes or minimize their losses. The players, also referred to as agents, are, in classical game theory, assumed to be rational and can adopt different strategies to win the game.

## 3.1 The Cooperator-Defector Game

The cooperator-defector game is a simple and very famous game theoretical model often studied in introductory courses to the field [29]. The game consists of two rational players, which can either individually choose to play the role of a cooperator or a defector. Depending on what they and their opponent chose to play, both of them get a payout after the game. If both choose two play a cooperator, both get the reward $\mathcal{R}$. If one player decides to defect and the other cooperates, the defector gets the temptation payout $\mathcal{T}$, whereas the cooperator gets the suckers payoff $\mathcal{S}$. If both players defect, both of them get punishment $\mathcal{P}$. The relative values of these payouts make it more or less profitable to play a certain strategy and therefore change the dynamics of the game. The most famous version of this game is the so-called prisoner's dilemma [2] [38] [28] in which the reward $\mathcal{R}$ is smaller than the temptation $\mathcal{T}$ and the punishment $\mathcal{P}$ is bigger than the suckers payoff $\mathcal{S}$. It gets its name from the scenario that the two players in the game are criminals, which are apprehended

| | | Opponent $\mathcal{C}$ | Opponent $\mathcal{D}$ |
|---|---|---|---|
| Player | $\mathcal{C}$ | $\mathcal{R}$ | $\mathcal{S}$ |
| Player | $\mathcal{D}$ | $\mathcal{T}$ | $\mathcal{P}$ |

FIGURE 3.1: Payout matrix

and interrogated by police at the same time about a crime they committed together. If both of them keep quiet, they will both get a short prison sentence ($\mathcal{R}$). If one of them betrays his accomplice and talks to the police, the betrayer will walk free ($\mathcal{T}$) while the other will get the maximum sentence ($\mathcal{S}$). But if both of them talk, both will get a medium prison sentence ($\mathcal{P}$). Because the two prisoners can not talk to each other to ensure cooperation and they are both rational players it is always preferable for them to defect and talk to avoid the maximum sentence $\mathcal{S}$. The case where both players defect and get $\mathcal{P}$ is the outcome where neither player can benefit by changing his own strategy. This case is called the Nash equilibrium. The dilemma stems from the fact that if $\mathcal{P} < \mathcal{R}$, both players could get better payouts if they would cooperate, but then both players would also have an incentive to defect to get $\mathcal{T}(> \mathcal{R})$ again. There are multiple ideas and extensions to this game to ensure or incentivize mutual cooperation [2] [21] [14], but in the basic version of the game this dilemma leads to the fact that the Nash equilibrium performs worse than other outcomes [29].

## 3.2 Evolutionary Game Theory

A central assumption of classical game theory is the player's rationality. In areas like microbial biology however, this cannot be expected anymore. A proposed solution to this problem is evolutionary game theory. Here, the assumption of rationality is dropped and replaced by an iterative approach, where the game is played over many generations of various players, which hand down their strategies to the next generation [47] [23]. Because the strategies a rational player would choose usually perform better than other, after many generations, these strategies should be dominant in the game. This is especially useful in biology to see how behavior evolves and the dynamics of the system emerge.

### 3.2.1 Mean Field Limit and Replicator Equations

In the case of the cooperator-defector game we introduce the parameters $a$ and $b$ for the density of cooperators and defectors in a spatially extended system. We define the overall density $a + b = \rho$ and assume for the beginning that the system is homogeneous in space. This mean-field approach is equivalent to the statement that the dynamics of the game are much slower than the mixing of the system through e.g.

diffusion. We also define the fitness of the species in analogy to [17] as

$$\begin{aligned} f_A &= F + \mathcal{R}a + \mathcal{S}b \\ f_B &= F + \mathcal{T}a + \mathcal{P}b \end{aligned} \tag{3.1}$$

with base fitness $F$. We can now define the dynamic equations, with help of eq. 3.1, as

$$\partial_t a \equiv (f_A - f_B)\, ba \tag{3.2a}$$
$$\partial_t b \equiv (f_B - f_A)\, ab. \tag{3.2b}$$

The equations are a form of so-called replicator equations [17] and encode the dynamics of the game. The interpretation of these equations is as follows: The fitness difference indicates the relative strength of the species, while the $ab$ term encodes the probability of a cooperator and defector meeting and interaction with each other. With this it is easy to see that $\rho$ is constant

$$\partial_t \rho = \partial_t a + \partial_t b = \partial_t a - \partial_t a = 0. \tag{3.3}$$

We now introduce the parameters $\tau_A = \mathcal{S} - \mathcal{P}$ and $\tau_B = \mathcal{T} - \mathcal{R}$ and write

$$\begin{aligned} \partial_t a &= (\tau_A b - \tau_B a)\, ab \\ \partial_t b &= (\tau_B a - \tau_A b)\, ab. \end{aligned} \tag{3.4}$$

We only need the two parameters $\tau_A$ and $\tau_b$ instead of the four absolute payouts $\mathcal{R}$, $\mathcal{S}$, $\mathcal{T}$, $\mathcal{P}$ to completely encode the interaction, because only the differences matter. This can be understood as the fact that there are only two decisions to make: If a player meets a cooperator (defector), is it favorable for him to choose the same strategy? A negative $\tau_B$ ($\tau_A$) means it is.

### 3.2.2 Fixed Point Structure and the Four Games

We have seen that the overall density $\rho$ is time independent, only the relative amount of cooperators $a$ and defectors $b$ aren't. Now we will have look at the fixed points and flow of the four different possible game structures. Because $\partial_t a = -\partial_t b$ we only have to analyze one of the two equations and can write $\partial_t a$ as

$$\partial_t a = (\tau_A b - \tau_B a)\, ab = (\tau_A (1-a) - \tau_B a)\, a (1-a), \tag{3.5}$$

where it is easy to see the three fixed points ($\partial_t a = 0$)

$$a_0 = 0,\ a_1 = 1 \text{ and } a_\tau = \frac{\tau_A}{\tau_A + \tau_B}. \tag{3.6}$$

#### Prisoner's Dilemma

As above, the prisoner's dilemma is the case where $\mathcal{R} < \mathcal{T}$ and $\mathcal{S} < \mathcal{P}$, which means $\tau_A < 0$ and $\tau_B > 0$. This results in the fixed point structure of a stable one at $a = 0$ and an unstable one at $a = 1$. The third fixed point $a_\tau$ lies outside the physically meaningful region $a \in [0, 1]$, because we think of $a$ as a density and $a + b = 1$ at all times. Therefore every possible initial state of the system flows to $a = 0$, which

means that in the end all players will be defectors, in agreement with our previous analysis of two rational players in the classical game.

$$\partial_a \begin{cases} \leq 0, & \text{if } a \in [0,1] \\ > 0, & \text{otherwise} \end{cases}$$

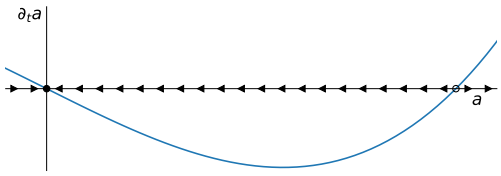


**Harmony**

The opposite case to the prisoner's dilemma is the game of harmony, where $\tau_A > 0$ and $\tau_B < 0$. Mutual cooperation is the ideal case while defecting brings no benefits, therefore the fixed point at $a = 1$ is stable and all meaningful initial states flow towards it.

$$\partial_a \begin{cases} \geq 0, & \text{if } a \in [0,1] \\ < 0, & \text{otherwise} \end{cases}$$

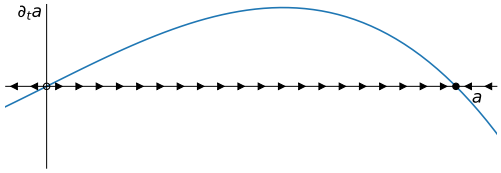


**Coordination**

A more interesting structure with three fixed points in the valid regime can be observed in the case of coordination, where both $\tau_A < 0$ and $\tau_B < 0$. Here it is always beneficial to be opportunistic and select the strategy the overwhelming majority plays. A typical example for this game would be choosing the side of the road to drive on. It doesn't matter which side is chosen as long as everyone follows the same rules. Here both fixed points $a_0$ and $a_1$ are stable, while $a_\tau$ is unstable and corresponds to the case that each side promises the same opportunities and any movement in either direction will eventually lead to $a_0$ or $a_1$. If $\tau_A = \tau_B$, the game would be symmetric and $a_\tau = \frac{1}{2}$, which means the best strategy is to do whatever the majority does. In contrast, if e.g. $|\tau_A| > |\tau_B|$, the fixed point is shifted in direction of $a_1$. This can be understood as the fact that the cooperators are "weaker" than the defectors and therefore need a higher initial density to compensate for that and be the dominant species is the end.

$$\partial_a \begin{cases} > 0, & \text{if } a < 0 \\ \leq 0, & \text{if } a \in \left[0, \frac{\tau_A}{\tau_A+\tau_B}\right] \\ > 0, & \text{if } a \in \left(\frac{\tau_A}{\tau_A+\tau_B}, 1, \right) \\ \leq 0, & \text{if } a \geq 1 \end{cases}$$

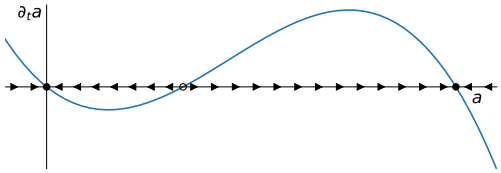


**Snowdrift Game**

Similar to the coordination game, the snowdrift game has three valid fixed points as well. The name is derived from a scenario where two drivers are stuck on a road which is blocked by a snowdrift. To be able to continue their journey, one of the drivers has to get out of his car and remove the snow, which takes some effort but enables both to get to their destination in the end. So if the other driver is already

removing the pile it is the best decision to sit tight in the warm car and wait until the road is cleared. But if the other driver does nothing, it is better to remove the snow than staying stuck. It is therefore always the best decision to play the strategy the opponent didn't choose. In terms of the parameters this corresponds to $\tau_A > 0$ as well as $\tau_B > 0$. The fixed points $a_0$ and $a_1$ are unstable, while $a_\tau$ is stable.

$$\partial_a \begin{cases} < 0, & \text{if } a < 0 \\ \geq 0, & \text{if } a \in \left[0, \frac{\tau_A}{\tau_A+\tau_B}\right] \\ < 0, & \text{if } a \in \left(\frac{\tau_A}{\tau_A+\tau_B}, 1,\right) \\ \geq 0, & \text{if } a \geq 1 \end{cases}$$

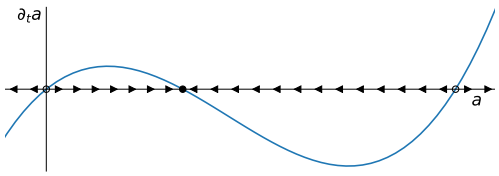


The framework we will develop in the coming chapters will be valid for all four games, but we will restrict the simulations and analysis of our equations to the case of the snowdrift game, because it is the only case with a stable fixed point with co-existing species. To investigate how the combination of the game with active matter influences this fixed point is one of the central questions of this thesis.

# Chapter 4

# The Agent Based Approach

## 4.1 The Microscopic Agent Based Model

In the field of statistical physics we usually observe or predict macroscopic system variables, e.g. order parameters, energy and/or temperature, which stem from many combined microscopical quantities. An agent based simulation is a powerful tool to get insight into how microscopical interactions can influence macroscopic dynamics and observables. Because it directly simulates the dynamics at particle level there is no error or information loss apart from averaging through approximations when we calculate macroscopic quantities. We introduce an agent based model similar to Chaté et al. [9] [8] and Bertin et al. [7], a Vicsek model [57] with diffusion. The Vicsek model is a minimal model with very few assumptions and simple interactions, while still exhibiting phenomenologically rich results. It is widely used in active matter simulations and has been studied intensely for the past twenty years [9] [40] [8] [6]. To put it into context with the different models mentioned in chapter 2, this is a model of a dry system with multiparticle metric collisions and polar particles aligning only in polar fashion. There are no leaders and we do not have direct repulsion or attraction between particles.

In detail, this model consists consists of $N$ particles on a two-dimensional quadratic plane of area $L \times L$. Each particle is either of species $A$ or $B$, has a position vector $\mathbf{r}_i$ and moves with fixed velocity $v_0$ according to its velocity vector $\mathbf{v} = v_0\mathbf{e}(\theta) = v_0 \begin{pmatrix} \cos(\theta) \\ \sin(\theta) \end{pmatrix}$. $\theta$ is the angle enclosed with the $x$-axis. The time $t$ is discrete in this model in steps of $dt$. Particles move ballistically up to random diffusion events and active matter interactions, which change the direction of $\mathbf{v}$. The position update each time step $dt$ is given by $\mathbf{r}_j^{t+dt} = \mathbf{r}_j^t + \mathbf{v}_j^t dt$. While the velocity $v_0$ is fixed, each particle updates its direction to the average direction of all particles of the same species in its active matter vicinity $\mathcal{A}_j^t$ at time $t$. $\mathcal{A}_j^t$ is defined as the disk around $\mathbf{r}_j^t$ with radius $d_0$, the active matter interaction range. This directional average is then disturbed by some noise $\eta$. If the vicinity is empty except for particle $j$ itself, a diffusion event happens with probability $p_{diff}$, which changes the direction by a value of $\eta_0$. $\eta_0$ is a stochastic variable which follows a flat distribution of range $(-h_0\pi, h_0\pi]$, $h_0 \in [0, 1]$. The standard deviation is then given by $\sigma_0 = h_0 \frac{\pi}{\sqrt{3}}$. The new direction at time $t + dt$

is therefore calculated by

$$\theta_j^{t+dt} = \begin{cases} \arg\left(\sum_{k\in\mathcal{A}_j^t} e^{i\theta_k t}\right) + \eta_j^t & \text{if } \mathcal{A}_j^t \neq \{j\} \\ \theta_j^t + \eta_{0,j}^t & \text{with probability } p_{diff}dt \text{ and if } \mathcal{A}_j^t = \{j\} \\ \theta_j^t & \text{else} \end{cases} \tag{4.1}$$

with the stochastic active matter noise variable $\eta$, which is given by a flat distribution in the range $(-h\pi, h\pi]$, $h \in [0,1]$ and standard deviation $\sigma = h\frac{\pi}{\sqrt{3}}$. Noises are uncorrelated to each other, in time and independent for each particle.

As mentioned, polar alignment requires polar particles, meaning particles with a head and tail or at least a direction to break the otherwise symmetric interaction of point-like particles with interaction radius $d_0$. In our case this is the movement direction $\mathbf{e}(\theta)$, which defines the "head" of our particle.

These properties, diffusion and alignment both, violate momentum conservation and we therefore assume that the plane on which the particles move absorbs or supplies the missing momentum.

In contrast to previous works we introduce two species and an interaction for particles to be able to change their species, if it is beneficial for them. If a particle switches species, it can lose its directional information and fly in a random direction afterwards until it aligns with partners of its new species again. We call this effect *Switch Randomization*, which can be either turned on or off to probe the relevance of directional information transfer on order formation. This can be understood in the context of two different systems: No randomization could refer to a system where an existing particle just changes its species (by e.g. changing some species defining properties like toggling the production of a resource), while a randomized system could describe an interaction where the old particle dies and a new particle of the other species pops into existence with random direction. We will usually refer to both of these options as "*species switch*" regardless of the underlying cause.

Every particle has a fitness level $f_j^t$ at time $t$. This is given by a base fitness $F$ and a value calculated from the number all other particles in its game theory vicinity $\mathcal{G}_j^t$, where $\mathcal{G}_j^t$ is the disk around particle $j$ with radius $d_{gt}$. The fitness is then calculated by

$$f_{A,j}^t = F + \frac{N_{A,j}^t}{N_j^t}\mathcal{R} + \frac{N_{B,j}^t}{N_j^t}\mathcal{S} = F + a_j^t\mathcal{R} + b_j^t\mathcal{S} \quad \text{if } j \text{ is of species } A \tag{4.2a}$$

$$f_{B,j}^t = F + \frac{N_{A,j}^t}{N_j^t}\mathcal{T} + \frac{N_{B,j}^t}{N_j^t}\mathcal{P} = F + a_j^t\mathcal{T} + b_j^t\mathcal{P} \quad \text{if } j \text{ is of species } B \tag{4.2b}$$

where $N_{A,j}^t$ is the number of particles of species $A \in \mathcal{G}_j^t$, $N_{B,j}^t$ the number of particles of species $B \in \mathcal{G}_j^t$ and $N_j^t = N_{A,j}^t + N_{B,j}^t$. $a_j^t$ and $b_j^t$ are the relative densities $N_{A,j}^t/N_j^t$ and $N_{B,j}^t/N_j^t$. A particle changes its species with probability $p_j^t$ if it would be beneficial to it, i.e. it would attain a greater fitness value by switching its species. $p_j^t$ is

given by

$$p_j^t = \begin{cases} (f_{B,j}^t - f_{A,j}^t)dt & \text{if } j \text{ is of species } A \text{ and } f_{B,j}^t - f_{A,j}^t > 0 \\ (f_{A,j}^t - f_{B,j}^t)dt & \text{if } j \text{ is of species } B \text{ and } f_{A,j}^t - f_{B,j}^t > 0 \end{cases} \tag{4.3}$$

This means switching species is more probable if the fitness gain would be greater and less likely if there is only a marginal difference in fitness. If we introduce the variables $\tau \equiv \tau_A = \mathcal{S} - \mathcal{P}$ and $\lambda \equiv \tau_B/\tau_A = \frac{\mathbf{T}-\mathcal{R}}{\mathcal{S}-\mathcal{P}}$ we can substitute and reframe our conditions in terms of relative fitness levels as

$$\begin{aligned} f_{B,j}^t - f_{A,j}^t =& F + a_j^t\mathcal{T} + b_j^t\mathcal{P} - F - a_j^t\mathcal{R} - b_j^t\mathcal{S} \\ =& a_j^t\tau_B - b_j^t\tau_A = \tau(a_j^t\lambda - b_j^t) \end{aligned} \tag{4.4}$$

and therefore the switch probability as

$$p_j^t = \begin{cases} \tau(a_j^t\lambda - b_j^t)dt & \text{if } j \text{ is of species } A \text{ and } \tau(a_j^t\lambda - b_j^t) > 0 \\ \tau(b_j^t - a_j^t\lambda)dt & \text{if } j \text{ is of species } B \text{ and } \tau(a_j^t\lambda - b_j^t) < 0 \end{cases} \tag{4.5}$$

$\tau$ can be interpreted as the game strength and $\lambda$ gives the relative strength of species $B$ in comparison to $A$. It is sufficient to assume $\tau \geq 0$ and limit $\lambda \in [0, 1]$, because we restrict our analysis to the snowdrift game only (see Chapter 3), where $\tau_A, \tau_B \geq 0$ and because of symmetry reasons we can assume w.l.o.g. $\tau_A \geq \tau_B$.

We expect the snowdrift game to be the most interesting implementation of the cooperator/defector game because it exhibits a stable fixed point of coexisting species, while the other games have absorbing states of only one surviving species. In nature, one could think of a system consisting of e.g. a colony of microbes able to produce a common resource which benefits themselves and other particles in their vicinity, while other microbes do not produce the resource and only profit from it [19]. The balance between these two species, resource producing (cooperators) and exploiting (defectors), is driven by the availability of this resource and therefore the particles producing it. This balance can change by e.g. particles switching on and off the production of this common good and results in a snowdrift game scenario [17]. A variable biofilm production as an example of two distinct species can be observed in Bacillus subtilis [45], where the non-producing species now also exhibits self-propelled motion, while the other remains stationary. We add a new variation, namely self-propelled motion for both species and study the effects flocking and swarming on a system of multiple interaction species.

To measure order in the system we introduce the directional order parameter

$$\varphi_A^t = \frac{1}{N_A^t}\left|\sum_{k=1}^{N_A^t} \exp\left(i\theta_k^t\right)\right| \qquad \varphi_B^t = \frac{1}{N_B^t}\left|\sum_{k=1}^{N_B^t} \exp\left(i\theta_k^t\right)\right| \tag{4.6}$$

for species $A$ and $B$, respectively and their temporal averages $\langle\varphi_A\rangle$ and $\langle\varphi_B\rangle$

$$\langle\varphi_A\rangle = \frac{1}{T}\sum_{t=1}^{T}\varphi_A^t \qquad \langle\varphi_B\rangle = \frac{1}{T}\sum_{t=1}^{T}\varphi_B^t \tag{4.7}$$

$\varphi_A^t$, $\varphi_B^t$, $\langle\varphi_A\rangle$ and $\langle\varphi_B\rangle$ can vary between 0 and 1, where 0 means no order in the system and 1 refers to perfect alignment of all particles.

## 4.2 Implementation

Even with the enormous computing power of modern machines it is crucial to find an efficient way to implement a simulation, because still the resource requirements of many-particle simulations quickly reach the limits of todays computers. Especially in statistical physics, where we want to avoid finite size effects in our macroscopic observables, the need to generate and simulate a great amount of particles is essential. If we are able to implement the simulation in a way that uses as little resources as possible and scales well with the system size and particle number, we can simulate many more particles in a reasonable time frame. The main concepts utilized to implement this will be shortly explained in the following.

There are two ways to reduce the simulation runtime: On the one hand coding the simulations efficiently to reduce the amount of calculations needed to evaluate the required variables. This is especially important in parts of the simulations which are executed repeatedly. On the other hand we can reduce the runtime by parallelizing the computation. To achieve this it is necessary to set up the simulation in a way that tasks can be run independently from each other on different CPU cores at the same time.

The simulation is set up, as described in section 4.1, as a system of particles in a box of size $L \times L$. Each particle has the properties position $\mathbf{r}$, direction $\mathbf{v}$ ($|v| = 1$), species $S = \{A, B\}$ and fitness $f$. The simulation is set up in discrete time steps. A time step $dt$ has multiple components. First, the game theoretical interaction is evaluated and the particle species is updated. In the next step the active matter interaction is processed and the particle directions are adjusted as well as alignment noise $\eta$ or diffusive noise $\eta_0$ are added. After this the particle positions are updated and as a last step a snapshot of the system can be saved into a hdf5 database for later analysis. These steps are repeated $sim\_steps = T/dt$ times, where T is the total time of the simulation. To better understand how these individual tasks are implemented, we take a look at the basic concepts of parallel computing and programming.

### 4.2.1 Parallel Programming

While normal computer programs are usually serial, parallel programming utilizes the fact that certain tasks in a program can be executed independently from each other and therefore evaluated simultaneously. One possible implementation of this is to take a multi core processor and while the main program only runs on one core, as soon as parts of the program which can be evaluated in parallel are reached, an algorithm distributes the different tasks in so-called threads to multiple cores to be evaluated there. After the parallel computation is finished, the threads and their results are reunited with the main thread and the serial computation continues (see fig. 4.1). While it would most of the time be beneficial to parallelize the whole code, this is usually not possible. Tasks have to be mutually exclusive in their dependencies to be parallelizable [39]. In our case we used parallelization to evaluate the interactions between particles and the update of their position each time step.

Even though parallel programming has a lot of advantages and benefits, there are some drawbacks as well. First of all the parallelization has to be explicitly set up in the code, because the process of auto-parallelization, where e.g. the compiler would

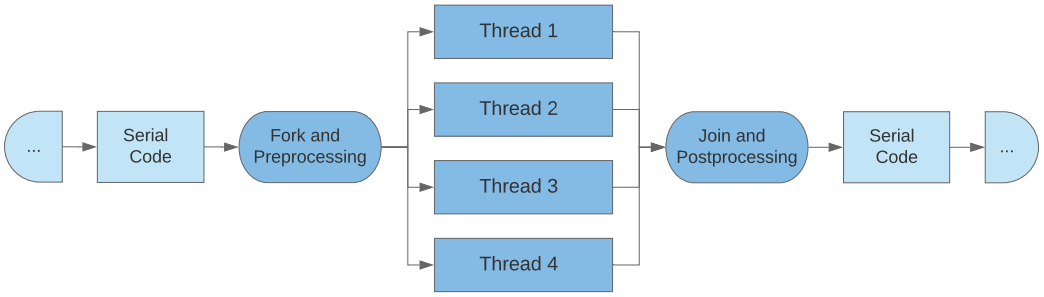


FIGURE 4.1: A parallel section of a program embedded into serial parts before and after it. A very simple example of a section like this in the simulation would be a code block where the array of all particles is passed to a function and then a parallelized section is initialized in which the position of the particles is updated in parallel by adding their velocity multiplied by time step $dt$ to their current position. If we for example pass 80 particles to a function which sets up 4 threads, thread 1 could then evaluate particles 1-20, thread 2 particles 21-40, etc. After the position update the function would terminate the tasks and return the now updated particle array back to the caller.

parallelize the program afterwards, has had very limited success to this day. Secondly there are challenges and problems which are inherit to parallel programming and don't happen in serial computing. The most important of these issues are so-called race conditions. These can happen when two parallel tasks access the same variable and make changes to it. If we e.g. take a variable $var1$ and two threads $thrd1$ and $thrd2$, which both have the task to add some value to $var1$, this can result in a race condition. If, for example, $var1 = 3$ in the beginning and both $thrd1$ and $thrd2$ want to increment it by 2. Naturally we should get the result $var1 = 7$ in the end. But, because of the way values are stored and edited in a computer, this is not necessarily the answer we get, if, e.g.: $thrd1$ reads $var1$ with a value of 3 at time $t_1$, after which $thrd2$ also reads $var1$ at time $t_2$ with a value of three. Meanwhile $thrd1$ executes the add 2 operation internally to get a result of 5. Then, at $t_3$, $thrd2$ does the addition to get 5 as well, because it read out $var1 = 3$ at $t_2$. $thrd1$, at the same time writes to $var1$ and sets it to 5. Finally, at $t_4$, $thrd2$ also writes $var1 = 5$ and the parallel computation finishes, but the result is not the one we expected. This read/write overlap is called a race condition and can only happen if the computation is not evaluated serially. A visualization of this problem can be found in fig. 4.2. To avoid this behavior, parallel programming uses locks on variables. The way these work is that threads lock the variable they're accessing to have exclusive read/write permissions. Other threads which want to access locked variables have to halt their computation and wait for the lock to be lifted when the first thread is finished with accessing the variable (see fig. 4.3). While this ensures the right result it slows down the computation because the threads have to check for locks and even stop their computation if they find one. They also have to apply and lift locks on variables they are editing. When writing code which is to be executed in parallel, the programmer always has to pay attention which variables have to be locked to avoid race conditions. Always locking variables negates most of the benefits parallel programming brings, while not locking crucial variables can lead to wrong results.

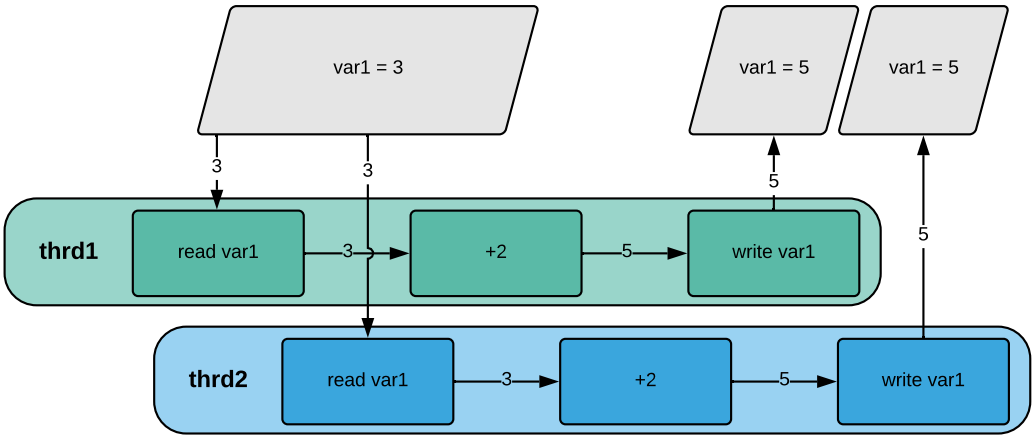


FIGURE 4.2: A race condition occurs while reading and writing *var*1 in parallel. The wrong result is the fault of overlapping access to the same variable by threads *thrd*1 and *thrd*2.

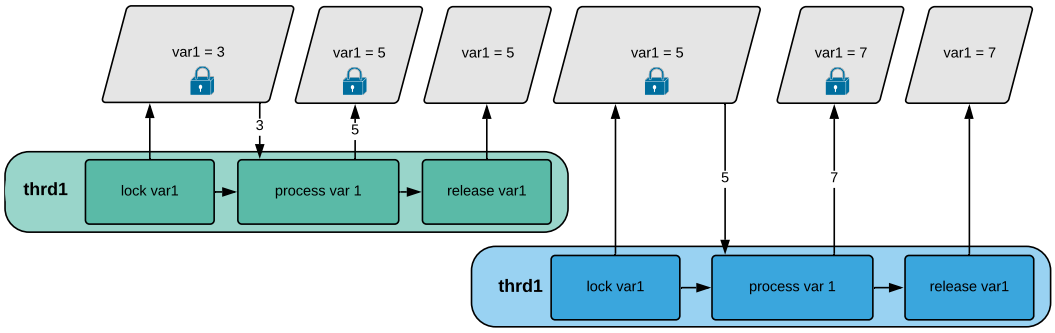


FIGURE 4.3: The race condition is resolved by locking the variable before marking changes to it. This process can slow down computation, because now *thrd*2 has to wait for *thrd*1 to finish.

### 4.2.2 The Box Algorithm

In the worst case the computation time of the simulation scales quadratic with the particle number $N$. This stems from the fact that to evaluate the interaction between particles we have to check their distances to see if they are smaller than their respective interaction radius and therefore interaction partners. These checks scale with $N^2$ if we have to compare every particle with every other particle. Even though this is a mathematical fact and our worst case performance will always be of quadratic order, we can take measures to speed up computation in most cases.

The most important method to both reduce the computational effort, and additionally set the system up to be parallelizable, is the partition of the system into small boxes to evaluate the interactions [20]. The active matter interaction will serve as an example for how the box algorithm is set up and works. The game theoretical interaction can then be treated in a similar fashion. If we look at a particle $j$ at time $t$, it interacts with all particles in its vicinity $\mathcal{A}_j^t$. Finding these interaction partners means one has to check the distances between particles. To avoid checking every

particle against every other particle in the system at each step in time we partition the system into boxes of optimal length

$$B_0 = d_0 + 2\, v_0\, dt\, s \tag{4.8}$$

with $d_0$ the active matter interaction radius, particle velocity $v_0$, time step $dt$ and step parameter $s \in \mathbb{N}$, which is the number of time steps boxes can be reused before they need to be updated. The algorithm works the following way: When the whole system is initialized, the boxes and their boundaries are fixed by the real box length $B = B_0 + h$, where $0 \leq h < B_0/m$, such that $m = \lfloor L/B_0 \rfloor \in \mathbb{N}$ boxes fit exactly into $L$. For now we set $s = 0$ for simplicity and convenience. Now we can assign each particle $j$ to a box according to its position. Because the box size is always $\geq d_0$, all particles in vicinity $\mathcal{A}_j^t$ have to lie in same box as $j$ or adjacent boxes. With this we only have to compare adjacent boxes and their particles and not all $N$ particles in the system anymore. While this does not reduce the computational effort if all particles are very close to each other, if we e.g. assume a homogeneous distribution the number of particles which have to be compared is reduced by a factor of $(3B)^{-2}L^2$. We also have to compare each box only to its left and upper neighbors, because we iterate over all boxes in the the system and the comparison with the lower right boxes will be taken care of as soon as these are iterated over. As soon as we completed this for all boxes, which can be done in parallel, and found all interaction partners, we can perform the interactions. The same steps with the respective radii can also be used for the game theoretical interaction. After this, the boxes will be reset, filled again and the steps can be repeated for a new time step. Because it is an additional

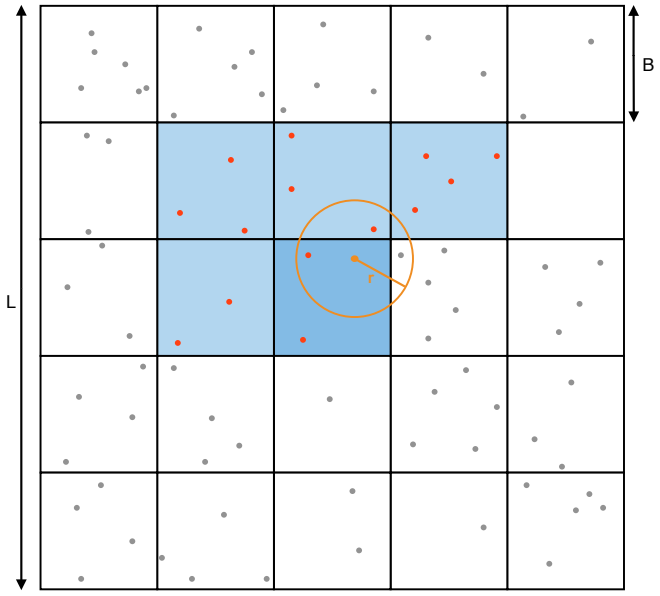


FIGURE 4.4: Box algorithm example: The system is divided into 25 boxes of length B. Particle $j$ (orange dot) interacts with all other particles in its vicinity $\mathcal{A}_j^t$ (orange circle), where the box algorithm in this time step only compares it to the upper left boxes(light blue) and the particles assigned to them(red). All other particles (grey) are invisible to the active box where particle $j$ resides in. The particle which lies in $\mathcal{A}_j^t$ but in the box right to $j$ will be added to $j$'s interaction partner when this box is active.

effort to make and fill the boxes it is sometimes beneficial to reuse the boxes multiple time steps. This is where the parameter $s$ comes into play. Particles move a maximal distance of $2v_0dt$ towards each other per time step. Therefore, if we increase the box size by $2v_0dt \cdot s$ we make sure that no two particles in non-adjacent boxes can be closer than the interaction radius in the next $s$ time steps. The tradeoff of the increased box size is of course that we have to make more comparisons each time step between particles which cannot be interaction partners. Choosing a small non zero $s$ can speed up computation in cases of low density or when the interaction radius is large compared to the particle velocity $v_0$ and time step $dt$.

The use of this algorithm is only possible because we are dealing with local interactions and not global ones. We therefore know that two particles further apart than $B_0$ can never interact with each other in the next time steps. We utilize this to cut down the number of comparisons between particles and achieve a block of code ideal for parallelization.

## 4.3 Results of the Simulation

### 4.3.1 Isotropy, Active Matter Waves and Coherent Motion

To be able to better classify results and get an understanding of the novelties the combination of active matter and game theory offers, it is useful to look at the base case of a pure active matter simulation. This means that we switch off the game theoretical interaction and can therefore study differences and similarities of the two cases: With and without game. While there are 17 free parameters in the system and it is far from feasible to test every combination we mainly focus on and vary a few essential ones: The density $\rho = NL^{-2}$, the alignment noise standard deviation $\sigma$, which we tie to the diffusive noise standard deviation $\sigma_0$, so $\sigma = \sigma_0$, the absolute game strength $\tau$ and the relative game strength between species $\lambda$.

The first thing we want to study are the different phases of order in the system. According to previous agent based simulations, we expect them for certain density and noise combinations [9] [8]. Without game we can observe three phases: In the low density, high noise regime we see isotropic movement and the density remains homogeneous throughout the system. The inverse case, the high density, low noise regime yields coherent motion of a system with many clusters in an arbitrary, but uniform direction. The intermediate case, where the onset of order happens, is the most interesting though: Above a threshold density $\rho_t$ for a given noise we can observe that the particles form wave patterns which travel through the system (fig. 4.5a). These waves then get broader with increasing density until we reach the ordered phase where no wave is visible anymore in a continuous manner. We define the density above which we can not distinguish the wave from the background anymore as $\rho_{dh}$. All these results are in perfect agreement with previous agent based active matter simulations [7] [9] [57].

In the next step we switch on the game theory interaction and get a similar picture of different unordered or ordered phases: Depending on the parameters, especially $\tau$ and $\lambda$, we now get up to five different phases in the system. In the case of $\lambda = 1$, which means both species are equally strong, we recover the three phases we have already seen in the pure active matter scenario of homogeneous isotropy, waves and homogeneous coherent motion. With respect to the overall density $\rho$ we observe that the onset of order happens later, which is to be expected because the active matter interaction only works inner-species and therefore the number of particles that can be interacted with is reduced. Naively one could assume that the threshold density $\rho_t$ for the balanced game case is twice as large as for the case without game because the distribution of particles should be 50/50. But because the directional information can be destroyed when a particle switches species due to switch randomization, which acts as an additional noise in the system when a particle switches its species back and forth, the threshold density lies even higher.

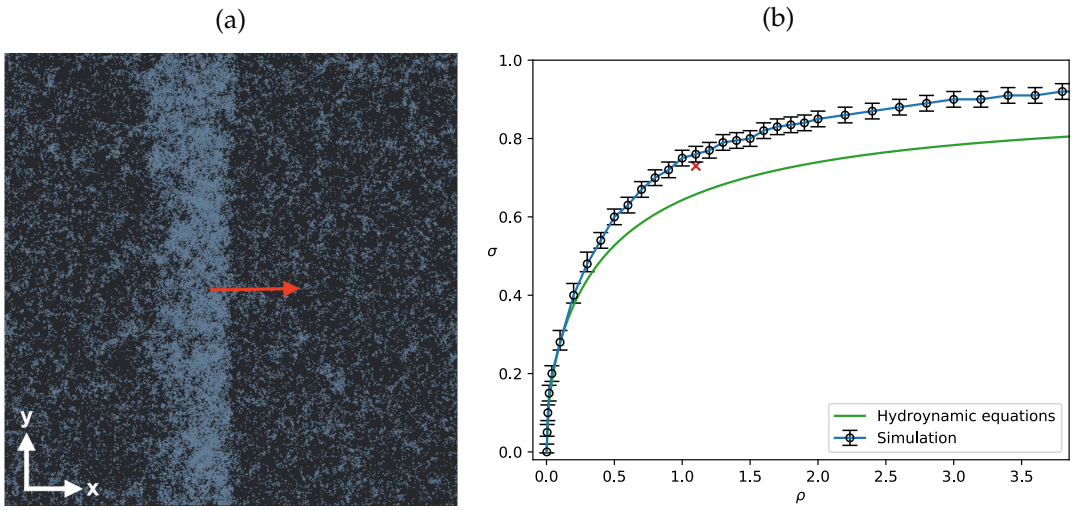


FIGURE 4.5: Agent Based Simulation without Game (*a*) Snapshot of the simulation in a wave state with $\rho = 1.1$, $\sigma = 0.73$. The arrow indicates the direction of movement the wave travels. (*b*) $\rho/\sigma$ plot. The plot points with error bars mark the transition to order $\sigma_t(\rho)$ in the simulation. The dashed line is a plot of $\sigma_{crit}(\rho)$, the expected transition to order given by the hydrodynamic equations, which we will treat in chapter 6. The cross marks the position of simulation (a) in the parameter plane

Within the tested parameter regime the game theory interaction is much faster than the active matter interaction, meaning that the fixed points of relative densities of species $A$ and $B$ are reached long before there is an onset of order. This reduces the effective noise introduced by switch randomization of particles because these events become rarer. A linear fit to simulation data puts the increase this effective noise induces in $\sigma$ at the density $\rho = 1.5$ at $\approx 0.05\lambda$.

From now on we will fix $\rho = 1.5$ and use $\sigma$ as the variable to differentiate the different order regimes. This corresponds to taking a vertical slice in figs. 4.6 while fixing $\sigma$ and varying $\rho$ would mean slicing horizontally. In the parameter regime we choose here, both approaches yield phenomenologically equal results. We choose to fix $\rho$ here to suppress finite size effects for small $\rho$ and lengthy simulations for large $\rho$.

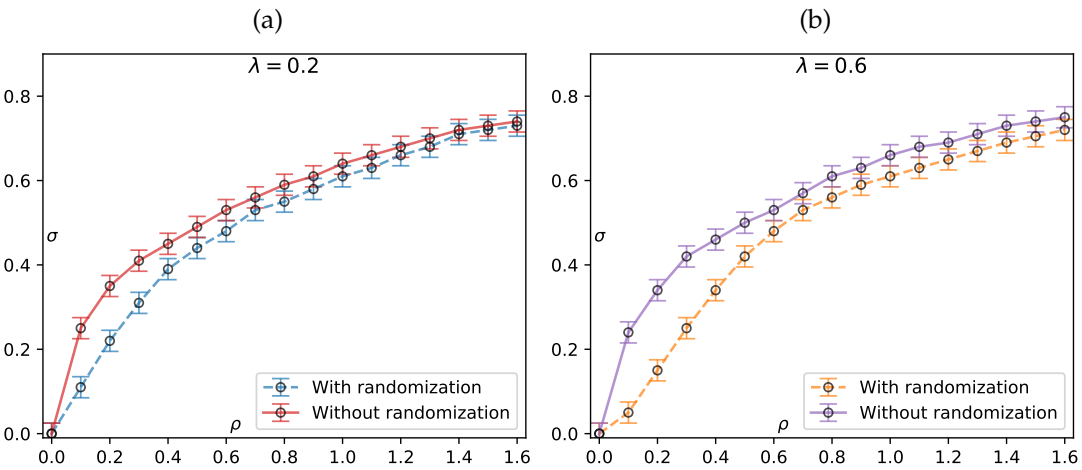

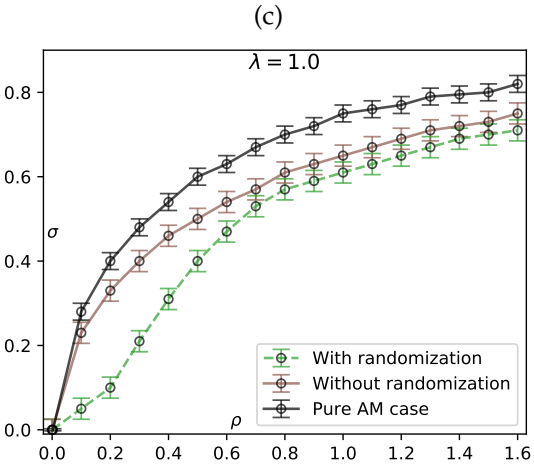


FIGURE 4.6: Transition to Order for Different Values of $\lambda$. $(a)$ $\sigma_{t,A}$ against the overall density $\rho$ with $\lambda = 0.2$. Comparison between system with (dashed line) and without switch randomization (solid line). While the difference in $\sigma_{t,A}$ is very significant for small and scarce systems, it almost vanishes for higher values of $\rho$. $(b)\lambda = 0.6$ $(c)$ $\lambda = 1.0$ The data for the black solid line is taken from fig. 4.5b to compare the cases of one species and two species which interact via the game.

### The Five Phases

If we choose $\lambda < 1$, we observe up to 5 phases, depending on the values of $\tau$ and $\lambda$. For small $\lambda \lesssim 0.3$, the first case we want to look at, the phases we observe with increasing density (or decreasing noise) are:

| | Species $A$ | Species $B$ | Phase Name | Phase Identifiers |
|---|---|---|---|---|
| I) | homogeneous isotropic | homogeneous isotropic | Isotropic Homogeneous Phase (IHP) | $\langle\varphi_A\rangle \approx 0, \langle\varphi_B\rangle \approx 0$ $\langle\nu_A\rangle < 0.3, \langle\nu_B\rangle < 0.3$ |
| II) | waves | induced waves | Wave Phase I (WP1) | $\langle\varphi_A\rangle \gtrsim 0.25, \langle\varphi_B\rangle \approx 0$ $\langle\nu_A\rangle \gtrsim 0.3, \langle\nu_B\rangle < 0.3$ |
| III) | clustered ordered | clustered isotropic | Ordered Phase I (OP1) | $\langle\varphi_A\rangle \gtrsim 0.5, \langle\varphi_B\rangle \gtrsim 0.25$ $\langle\nu_A\rangle < 0.3, \langle\nu_B\rangle < 0.3$ |
| IV) | induced waves | waves | Wave Phase II (WP2) | $\langle\varphi_A\rangle \gtrsim 0.5, \langle\varphi_B\rangle \gtrsim 0.25$ $\langle\nu_A\rangle < 0.3, \langle\nu_B\rangle \gtrsim 0.3$ |
| V) | clustered ordered | clustered ordered | Ordered Phase II (OP2) | $\langle\varphi_A\rangle \approx 1, \langle\varphi_B\rangle \gtrsim 0.7$ $\langle\nu_A\rangle < 0.3, \langle\nu_B\rangle < 0.3$ |

TABLE 4.1: The Five Phases

These combinations exist because the transition density for each species is dependent on $\lambda$. We introduce the parameter

$$\nu_A^t = 2\sqrt{\frac{1}{L}\sum_{c=1}^{L}\left(\varphi_{A,c}^t - \langle\varphi_{A,c}\rangle\right)^2} \tag{4.9}$$

to classify the phases. The system is partitioned into $L$ channels either along the $x-$ or $y-$axis depending on the direction of order (see figs. 4.7-4.11). The order parameter $\varphi_{A,c}^t$ is calculated for each channel $c$. $\nu_A^t$ is defined as twice the standard deviation

of $\varphi^t_{A,c}$. The factor 2 is introduced so that $\nu^t_A \in [0,1]$ and $\langle \nu_A \rangle$ is the temporal average of $\nu^t_A$. It measures the differences in directional order in the system and can therefore be used to judge if there are waves present in the system (high values of $\nu^t_A$) or if the order is uniform (low values of $\nu^t_A$). $\nu^t_B$ for species $B$ is defined accordingly.

The densities of species $A$ and $B$ are on average $a = \frac{\rho}{1+\lambda}$ and $b = \frac{\rho\lambda}{1+\lambda}$.

We can then classify and describe the five different phases for fixed $\rho$ in detail:

( I ) If we start in a high noise regime, both species are isotropic, so $\varphi_A, \varphi_B \approx 0$. The system is homogeneous and movement looks diffusive. We refer to this phase as Isotropic Homogeneous Phase (IHP). It is very similar to the isotropic phase we have already seen in the pure active matter simulation.

(II ) If we now decrease the noise and pass the threshold $\sigma_{t,A}$, species $A$ starts to form plane waves. Species $B$ should still be isotropic from an active matter perspective, because $\sigma > \sigma_{t,B}$. But even though we don't see a directional order $\varphi_B$, we still observe a wave pattern in $B$ (fig. 4.8). This happens because the increased density of species $A$ inside the wave induces an increase in species $B$ in this location as well. We refer to this phase as Wave Phase I (WP1).

(III) If we now further decrease the noise, order with high $\varphi_A$ emerges in species $A$. The spatial variations are larger than in the IHP, but the distribution is more homogeneous than in WP1. We observe loose clusters of species $A$. Species $B$ is also clustered but still isotropic in this phase, which is called Ordered Phase I (OP1). The explanation for this phenomenon lies in the small value of $\lambda$. In this phase we are in the regime of $\sigma_{dh,A} > \sigma > \sigma_{t,B}$, meaning species $A$ would be ordered and homogeneous even in a pure active matter scenario, while species $B$ would still be isotropic and homogeneous, so $\sigma > \sigma_{t,b}$. The observation we make here is therefore very similar to the case with no game theoretical interaction. This can be explained by the fact that because both species are spatially nearly homogeneous compared to the wave phases. This results in the game not having much influence apart from enforcing the overall ratio $\delta \equiv N_B/N_A$ everywhere.

(IV) The next phase we reach with lower noise is more interesting again. It is called Wave Phase II (WP2), because we now reached $\sigma_{t,B} > \sigma$ and species $B$ starts to form plane wave patterns on its own. A very interesting observation here is that now also species $A$ forms waves again, even though from an active matter standpoint it should be homogeneously ordered. This is again the result of the game interaction where the increased density of $B$ inside the wave raises the amount of $A$ as well while outside the wave the opposite happens. The difference to WP1 is that now both $\varphi_A$ and $\varphi_B$ are nonzero, so we have order in both species. There is also a completely new observation in this phase, namely the formation of species-distinct bands inside the wave. This phenomenon and its causes will be examined in section 4.3.2.

( V ) The last phase emerges with even smaller noise. It consists of clustered, ordered motion in both species and corresponds to the ordered phase we already know from the pure active matter case. Like in OP1, the game doesn't have much influence apart from enforcing $\delta$, but compared to OP1 $\delta$ is larger now and we observe clustering of the species $A$ and $B$. We call this phase Ordered Phase II (OP2).

The presence of the five distinct phases is due to the fact that the transitions $\sigma_{t,a}$, $\sigma_{dh,a}$, $\sigma_{t,b}$ and $\sigma_{dh,b}$ are all dependent on $\lambda$. For small enough $\lambda \leq 0.3$ we are in the regime where $\sigma_{dh,a} > \sigma_{t,b}$, which means species $A$ can be in an ordered and clustered phase already without the presence of waves, while species $B$ is not able to form waves on its own yet. The five phases only appear in systems with switch randomization, as the direction transfer between the species induces order in both species as soon as one species starts to exhibit coherent motion.

In contrast to a well mixed scenario ($\langle\varphi\rangle \approx 0$ and $v_0 dt \gg d_{gt}$) we observe $\delta > \lambda$ for $\lambda < 1$. This effect is stronger for WP2 and OP2, where we observe the species separation. It therefore seems plausible that these two effects are related (see section 4.3.2). It is also interesting to note that the wave structure in WP1, where only $A$ shows directional order, is weaker compared to WP2 or a similar case without game. This leads to the conclusion that the game inhibits wave and pattern formation in this particular case. A simulation of the hydrodynamic equations revealed hysteresis effects (see chapter 7) for the four phase transitions. It would be interesting to see if these also appear in the agent based simulation, but would require further work and analysis as the the current way the simulation is implemented makes it hard to check for these effects.

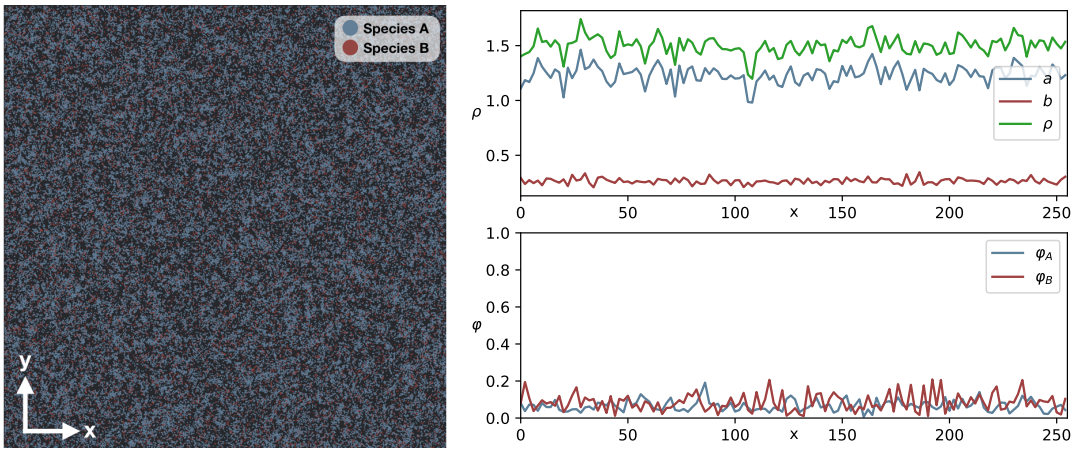


FIGURE 4.7: The Isotropic Homogeneous Phase (IHP) with $\sigma = 1.0$, $\langle \varphi_A \rangle = 0.007$, $\langle \varphi_B \rangle = 0.007$, $\nu_A = 0.06$ and $\nu_B = 0.09$. All simulations underlying figs. 4.7-4.11 with parameters $\rho = 1.5$, $\tau = 0.4$, $\lambda = 0.2$, $d_{gt} = 10$, $L = 256$. Snapshot of the system on the left and profile view with local densities in upper and local order parameters in lower plot on the right.

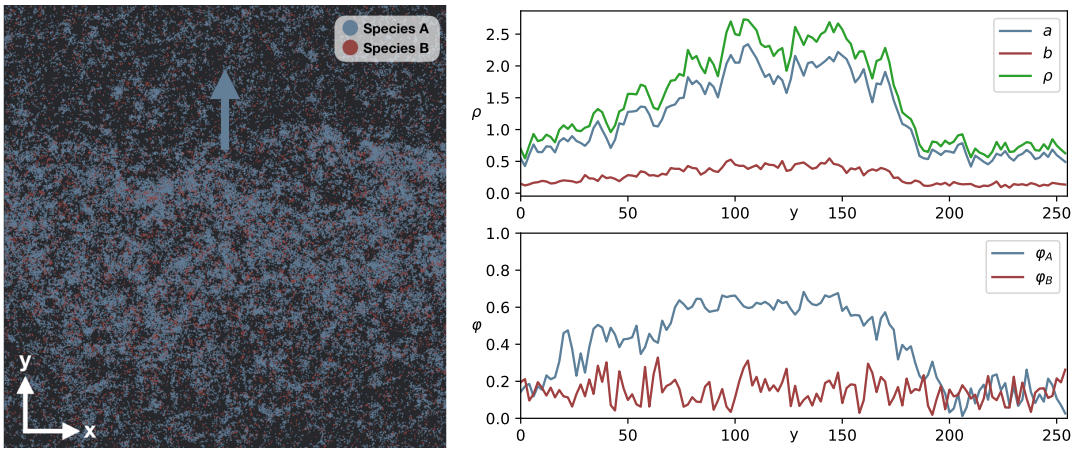


FIGURE 4.8: The First Wave Phase (WPI) with $\sigma = 0.65$. The blue arrow indicates the direction of order of species $A$. $\langle \varphi_A \rangle = 0.37$, $\langle \varphi_B \rangle = 0.4$, $\nu_A = 0.06$ and $\nu_B = 0.15$

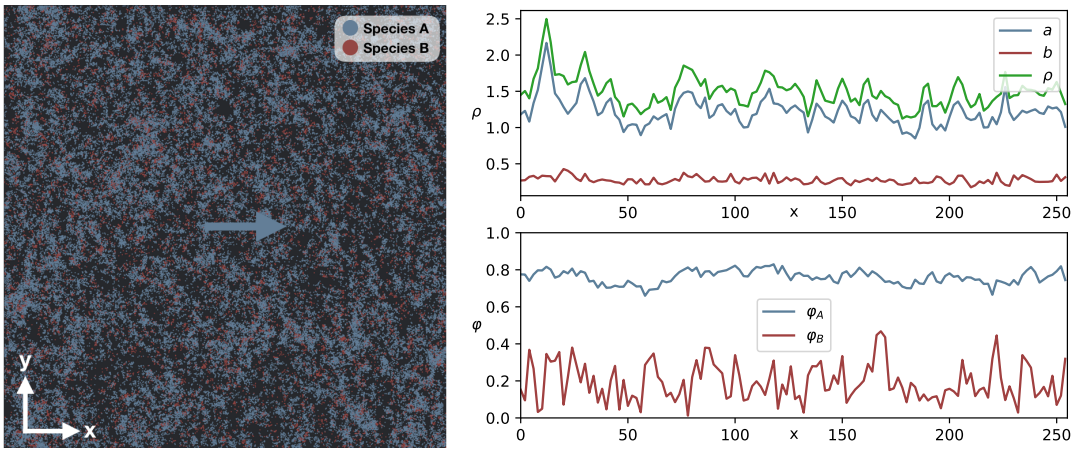


FIGURE 4.9: The First Ordered Phase (OP1) with $\sigma = 0.55$ $\langle \varphi_A \rangle = 0.61$, $\langle \varphi_B \rangle = 0.11$, $\nu_A = 0.06$ and $\nu_B = 0.2$

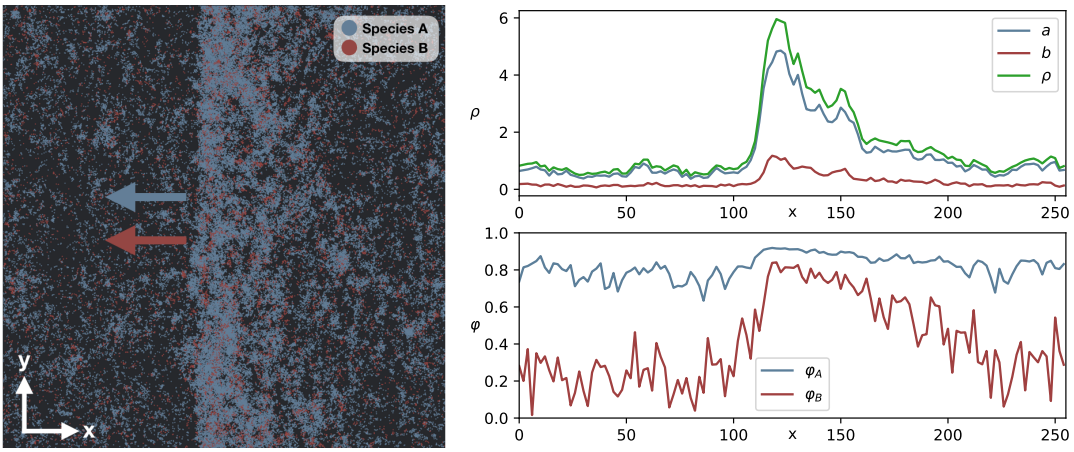


FIGURE 4.10: The Second Wave Phase (WP2) with $\sigma = 0.40$. The red arrow indicates the direction of order of species $B$. $\langle \varphi_A \rangle = 0.79$, $\langle \varphi_B \rangle = 0.47$, $\nu_A = 0.12$ and $\nu_B = 0.45$

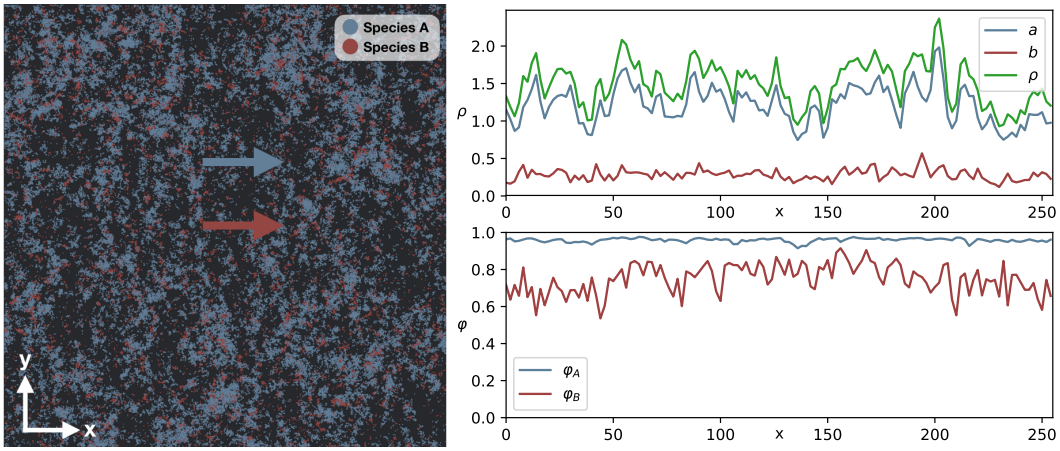


FIGURE 4.11: The Second Ordered Phase (OP2) with $\sigma = 0.15$, $\langle \varphi_A \rangle = 0.95$, $\nu_A = 0.01$ and $\nu_B = 0.16$

### Merged Wave Phase

If we set $\lambda$ to an intermediate value $0.3 \lesssim \lambda < 1$, the WP1 and WP2 phases merge and OP1 vanishes. We now observe directional order in both species inside the new merged wave phase. Beginning from $\lambda \approx 0.3$, we start seeing that in the regime where WP1 would lie, the game interaction increases $b$ so much inside the wave, that the induced wave in species $B$ also begins to display a nonzero order parameter $\varphi_B$. This means that locally $\rho > \rho_{t,B}$, so the isotropic state becomes unstable and order emerges, contrary to the case with the same parameters but without game. Because we now get order in both species as soon as order emerges in one, OP1 disappears.

The transition between WP1 and WP2 becomes fluent and the phases impossible to distinguish because of the induced ordered wave in $B$ even in higher noise regimes. That this phase is indeed composed out of two underlying phases can be seen by the comparison with simulations without game and also by the fact that the joined wave phases are occurring in a wide range of $\sigma$, with $\sigma_{t,A}$ as the bound towards the IHP and $\sigma_{dh,B}$ to OP2.

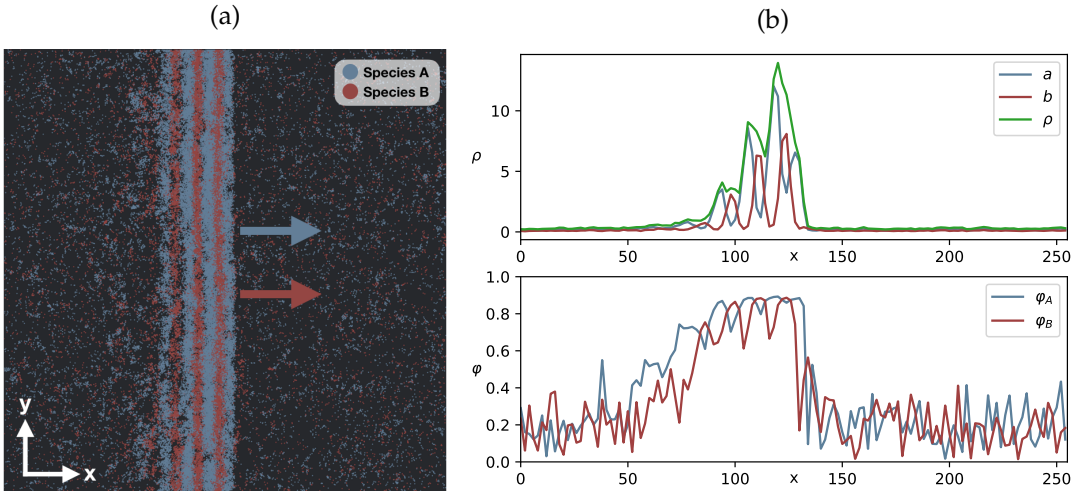


FIGURE 4.12: Snapshot and wave profile of merged wave phase with $\lambda = 0.5$, $\rho = 0.45$, $\tau = 0.4$, $L = 256$ and $d_{gt} = 10$ (*a*) The system snapshot displays a very even wave front with a more diffuse tail travelling through the system from left to right. The species distinct bands are clearly visible inside the wave (*b*) Wave profile in $x$ averaged over $y$-axis. The system was partitioned into 256 channels along the $x$-axis, all particles in the channels counted and then the channel density (upper plot) and directional order (lower plot) evaluated. We see a clear correlation between wave and order, while the scarce background seems isotropic.

The wave itself and the species separated bands get a lot more prominent for increasing $\lambda$ (fig. 4.12). We therefore conclude that a more equal game stabilizes the patterns. Before we further analyze the patterns inside the wave we will try to understand their formation and origin.

### 4.3.2 Game Theoretical Pattern Formation

We now want to turn to the phenomenon of separating species, as seen in WP2 and OP2, and the ratio increase. If we switch off the active matter interaction, so only diffusive movement and game theoretical interactions are present, we can observe the species forming spot- or band- like patterns (fig. 4.13 and fig. 4.17) under certain conditions. These patterns emerge with increasing absolute game strength $\tau$ for given velocity $v_0$ and noise $\sigma$. The size of the patterns depends on the game theory interaction radius $d_{gt}$ and the relative game strength $\lambda$. While we would expect the ratio of species $A$ to $B$, $\delta$, to be $\lambda$ in the well mixed case, with the emergence of the patterns $\delta$ increases if $\lambda < 1$ (fig. 4.19).

#### One Dimensional Case and Model

To better understand this phenomenon we model the system in 1d and observe the same behavior. Particles move only on a line and diffusion is implemented as a flip in movement direction occurring with probability $p$ each time step $dt$. With slow ($v_0 dt \ll d_{gt}$) or completely switched off movement the patterns emerge quickly and become static. We now have alternating stripes of species $A$ and $B$, where we can analyze the fitness value of every single point in the system. We assume the line to

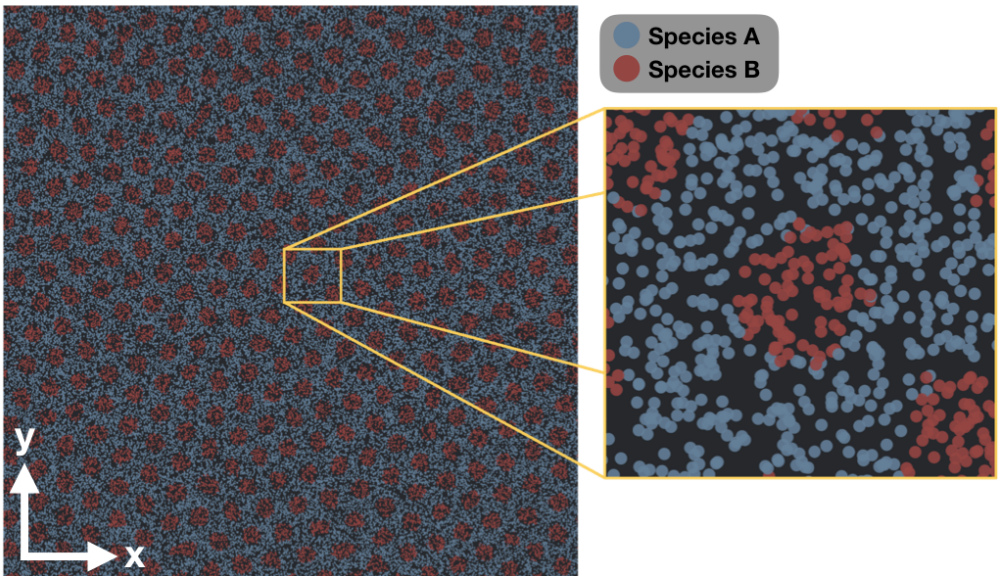


FIGURE 4.13: The Spot Order in 2d. Spot Order in a system with $\rho = 1.5$, $\tau = 1.0$, $\lambda = 0.4$, $v_0 = 0.016$ and $\sigma_0 = 0.5$ with magnified spot on the right

be continuous and that a section of the line has a weight according to its length $l$ in the fitness evaluation. The lengths of sections of species $A$ and $B$ are defined as $x_A$ and $x_B$, respectively.

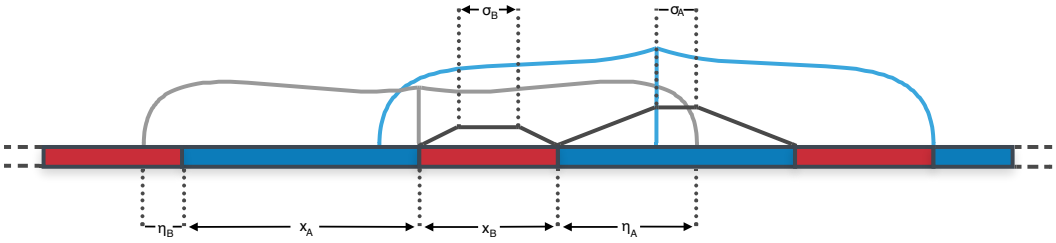


FIGURE 4.14: Formation of Species Separated Patterns in One Dimension: The braces of length $2d_{gt}$ mark the vicinities $\mathcal{G}$ of the particles at the center of the brace, $x_A$ and $x_B$ are the lengths of the sections of species $A$ and $B$. $\eta_A \equiv d_{gt} - x_B$, $\eta_B \equiv d_{gt} - x_A$, $\sigma_A$ and $\sigma_B$ are helper variables to calculate the optimal lengths of $x_A$ and $x_B$, which maximize the fitness. The dark grey trapezoidal lines indicate the fitness values of particles at this point.

We want to find the system configuration and therefore the lengths $x_A$ and $x_B$ which maximize the fitness in the system. After sufficient time has passed the system is in the static case, which is equivalent to the statement that the fitness is non-negative everywhere in the system. If we look at a particle at the boundary point $\mathcal{B}$ of the species and its vicinity $\mathcal{G}$, which is indicated by the grey brace in fig. 4.14, we see that the ratio of species $A$ to $B$ in $\mathcal{G}$ is

$$\delta_{\mathcal{B}} = \frac{x_A + \eta_A}{x_B + \eta_B} \tag{4.10}$$

Because $f_A = -f_B$ per definition, we can infer that the fitness level on the boundary has to be zero which is only the case when $\delta_{\mathcal{B}} = \lambda$. We can therefore write the

following equations:

$$d_{gt} = x_A + \eta_B \tag{4.11a}$$
$$d_{gt} = x_B + \eta_A \tag{4.11b}$$
$$x_B + \eta_B = \lambda(x_A + \eta_A) \tag{4.11c}$$

where we used the fitness equation $f_A = \tau(a - \lambda b) = 0$ to deduce the last equation. We can solve this system of equations in terms of $x_A$ and write

$$x_B = \frac{\lambda - 1}{\lambda + 1} d_{gt} + x_A \tag{4.12a}$$
$$\eta_A = \frac{2}{\lambda + 1} d_{gt} - x_A \tag{4.12b}$$
$$\eta_B = d_{gt} - x_A \tag{4.12c}$$

If we now want to deduce the fitness of other points than the boundary, we can simply start at a boundary point and slide the brace, and therefore the corresponding base point in fig. 4.14, e.g. right and observe how the ratio $\delta$ changes. We can see that up to the point where either end of the brace reaches a boundary point (see blue brace in fig. 4.14), the fitness (dark grey trapezoidal lines) linearly increases. After that, there is a fitness plateau until the other end of the brace reaches a boundary point. From here on the fitness linearly decreases until the center of the brace reaches the next boundary point. For the other species the reasoning is analogue.

The width of the fitness plateau is marked by $\sigma_A$ and $\sigma_B$, respectively. Depending on the value of $\lambda$, there are two distinct cases: Either the right edge of the brace hits a boundary point first when sliding to the right (case $I$), or the left edge reaches a boundary point first (case $II$). We will evaluate case $I$ first. The equation for $\sigma_A$ is therefore

$$\sigma_A = x_A - 2(x_B - \eta_B) = x_A - 2(x_A - \eta_A) = -x_A + 2\eta_A \tag{4.13}$$

The fitness contribution of $x_A$ can then be written as

$$f_A = f_A^{max} \frac{x_A + \sigma_A}{2} \tag{4.14}$$

with the maximal fitness value

$$f_A^{max} = \tau \frac{2x_B - \lambda(x_A + \sigma_A)}{2d_{gt}} \tag{4.15}$$

which is assumed at the plateau and where we used $f_A = \tau(a - \lambda b)$ again with $a$ and $b$ the relative parts of species $A$ and $B$ in the brace of size $2d_{gt}$. If we plug in (4.12a-c), we can, after some calculation, write the fitness in $A$ as

$$f_A = \frac{\tau}{d_{gt}} \left( -(\lambda + 1)x_A^2 + 3d_{gt}x_A - \frac{2}{\lambda + 1} d_{gt}^2 \right) \tag{4.16}$$

If we look at case $II$ next, we can write

$$\sigma_A = x_A - 2\eta_A \tag{4.17}$$

with the same equation for $f_A$, but differently looking peak fitness

$$f_A^{max} = \tau \frac{2x_B - \sigma_A - \lambda x_A}{2d_{gt}} \tag{4.18}$$

But if we plug in (4.12a-c) again, we get the same value for $f_A$ in the end as in (4.16). The same would be true for $f_B$ and $\sigma_B$, but calculations show that, because we assumed w.l.o.g. $\lambda \leq 1$, only one case exists for $\sigma_B$ anyway, as the other becomes relevant only for $\lambda \gtrsim 1.64$. This leads to the conclusion that both cases lead to the same optimal value for $x_A$ and $x_B$ in the end. For $\sigma_B$ and $f_B$ we can therefore write

$$\sigma_B = x_B - 2\eta_B \tag{4.19}$$

$$f_B = f_B^{max} \frac{x_B + \sigma_B}{2} \tag{4.20}$$

with the maximal fitness in $B$ of

$$f_B^{max} = \tau \frac{\lambda(2x_A - \sigma_B) - x_B}{2d_{gt}} \tag{4.21}$$

If we now plug in (4.21) into (4.20), we can, with the help of (4.12a-c), write

$$f_B = \frac{\tau}{d_{gt}} \left( -(\lambda+1)x_A^2 + (\lambda+2)d_{gt}x_A - d_{gt}^2 \right) \tag{4.22}$$

We can now define the average fitness per unit length

$$f = \frac{f_A + f_B}{x_A + x_B} = \frac{\tau}{d_{gt}} \frac{-2(\lambda+1)x_A^2 + (\lambda+5)d_{gt}x_A - \frac{\lambda+3}{\lambda+1}d_{gt}^2}{2x_A + \frac{\lambda-1}{\lambda+1}} \tag{4.23}$$

The optimal length of $x_A$ is now the value which maximizes (4.23):

$$x_A^{opt} = \frac{1}{\sqrt{2}} d_{gt} + \frac{1}{2}\frac{1-\lambda}{1+\lambda} d_{gt} \tag{4.24}$$

With the use of (4.12a) we can then write

$$x_B^{opt} = \frac{1}{\sqrt{2}} d_{gt} - \frac{1}{2}\frac{1-\lambda}{1+\lambda} d_{gt} \tag{4.25}$$

This also means the length $x_A + x_B = \sqrt{2}d_{gt}$ is invariant for different $\lambda$.

We can now make an estimate for $\delta$

$$\delta = \frac{x_B}{x_A} = \frac{\frac{1}{\sqrt{2}} + \frac{1}{2}\frac{1-\lambda}{1+\lambda}}{\frac{1}{\sqrt{2}} - \frac{1}{2}\frac{1-\lambda}{1+\lambda}} = \frac{\sqrt{2} - 1 + \left(\sqrt{2}+1\right)\lambda}{\sqrt{2} + 1 + \left(\sqrt{2}-1\right)\lambda} \tag{4.26}$$

This prediction is only valid in the regime where $\eta_A \geq 0$ and $\eta_B \geq 0$. If we write them in terms of $x_A$ we get

$$\eta_A = \frac{2}{\lambda+1} - x_A \tag{4.27a}$$

$$\eta_B = 1 - x_A \tag{4.27b}$$

It is easy to see that $\eta_A > \eta_B$ for $\lambda < 1$, so the variable of interest is $\eta_B$. If we now plug $x_A^{opt}$ into (4.27b) we get $\eta_B = 0$ for

$$\lambda_{crit} = \frac{\sqrt{2} - a}{3 - \sqrt{2}} \approx 0.2612 \tag{4.28}$$

If $\lambda < \lambda_{crit}$ the separated order breaks down because there is no net positive fitness anymore for particles in $x_B$. This can also be seen in the simulation, as evident by fig. 4.15. If $\lambda > \lambda_{crit}$, the predictions match the results of our simulations perfectly apart from small deviations caused by the periodic boundary conditions. If the system length $L$ is chosen as a multiple of $\sqrt{2}d_{gt}$, the discrepancies between theory and simulation vanish.

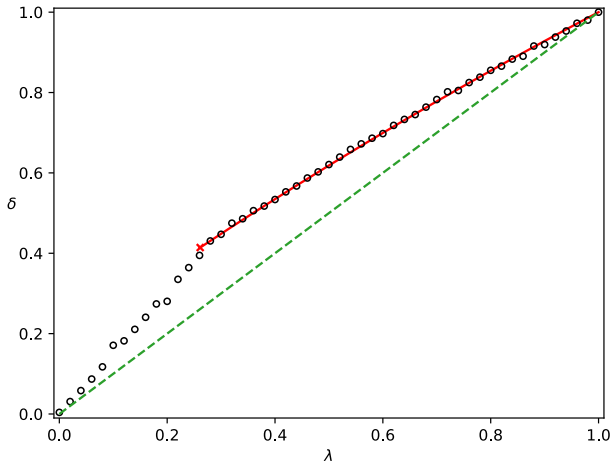


FIGURE 4.15: The Effects of Species Phase Separation on the Ratio $\delta$. The circles mark the realised ratio $\delta$ for a given $\lambda$ in the simulation. The red line is the calculated $\delta$ by the prediction (4.26) and matches the simulation perfectly until $\lambda_{crit}$ (red cross). The dashed line is the ratio in the well-mixed case. Parameters: $L = 100$, $d_{gt} = \sqrt{2}L/10$, $\tau = 1$


FIGURE 4.16: Species Order Phase Separation in 1d Simulation. The in fig. 4.14 predicted patterns, seen in the simulation. Position in $x$-axis, fitness in $y$-axis.

### Two Dimensional Case

For our two dimensional system the reasoning is similar as for one dimension regarding the heightened average fitness in an ordered state. The patterns which appear are circles (fig. 4.13) or bands (fig. 4.17) and calculations to evaluate the optimal size of these patterns are more complicated than in the one dimensional case. For $\lambda \lesssim 0.60$ the patterns appearing are circles with radius $r$, while for $\lambda > 0.60$ the circles merge and form band structures in the system which bear a fitness advantage. The transition between spots and bands seems to be continuous, as there are still spots visible for higher values of $\lambda$. The increase in $\delta$ for both the spots and the bands can be seen in 4.19.

For $\lambda \leq 0.6$ we rely on the simulations to measure the spot size by two methods: A diameter measurement and averaging over many spots estimates the spot width $x_B$ directly. The second method utilizes the fact that we can measure the relative

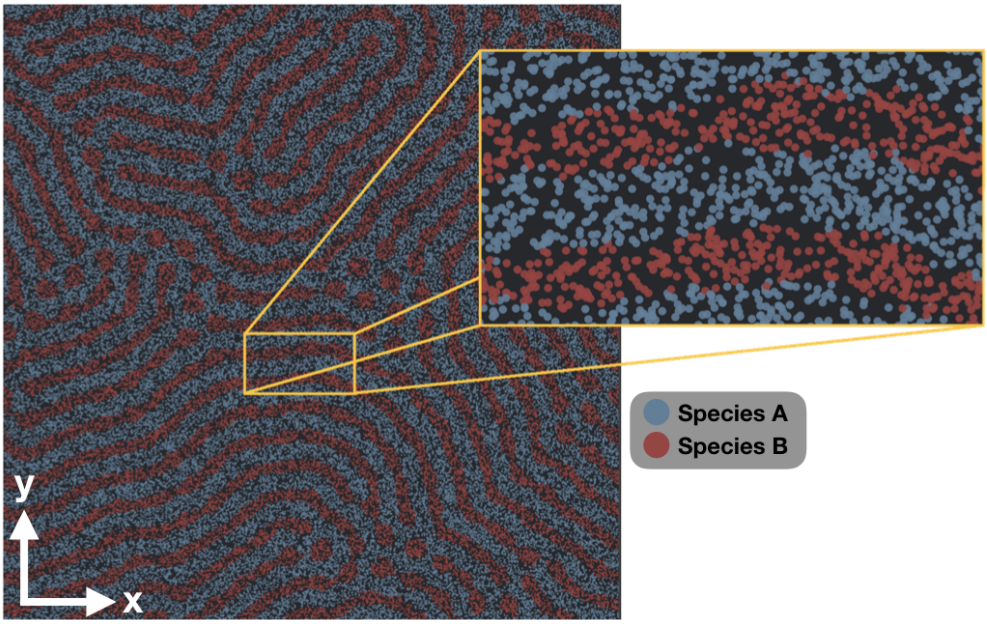


FIGURE 4.17: The Band Order in 2d. Band Order in a system with $\rho = 1.5$, $\tau = 1.0$, $\lambda = 0.66$, $v_0 = 0.016$ and $\sigma_0 = 0.5$ with magnified bands on the right.

amount $a$ and $b$. We assume $\rho$ to be spatially homogeneous, which is a reasonable assumption because the particles are initialized with random positions and move diffusively through the system with no active matter interaction between them. We can therefore estimate $x_B$ as

$$x_B = L\sqrt{\frac{b}{N_{Spots}\pi}} \tag{4.29}$$

with $N_{Spots}$ the number of spots in the system. We assumed the spots to be perfect circles with area $A = (x_B/2)^2\pi$, so $bL^2 = N_{Spots}A$. Both methods were used to get more reliable measurements.

Analogue to the one dimensional case we find a linear dependency of $x_B$ on $d_{gt}$, so the number of spots $N_{Spots}$ in the system scales with $d_{gt}^{-2}$, while the realized ratio $\delta$ is independent of $d_{gt}$ (fig. 4.18a).

As soon as the spots become unstable and the bands emerge, we see a rise in $\Delta = \delta - \lambda$, the absolute deviation from the mean field limit. The width $x_B$ of the bands has been measured directly on multiple positions in the system and then been averaged. This average seems to scale linear with $d_{gt}$ as well, while $\delta$ independent of $d_{gt}$ (fig. 4.18b).

These findings ought to be expected, because we only have two length scales in our system without active matter interaction: The particle movement velocity $v_0$ times $dt$ and the game theoretical interaction radius $d_{gt}$. In absence of movement the only remaining length scale is $d_{gt}$ and all other parameters in the system should adjust accordingly. We attribute deviations int the measurements to finite size effects, especially for small $d_{gt}$.

Fig. 4.19 shows the measured ratio $\delta$ against the relative game strength $\lambda$ for two dimensional systems, analogue to fig. 4.15 for the one dimensional case.

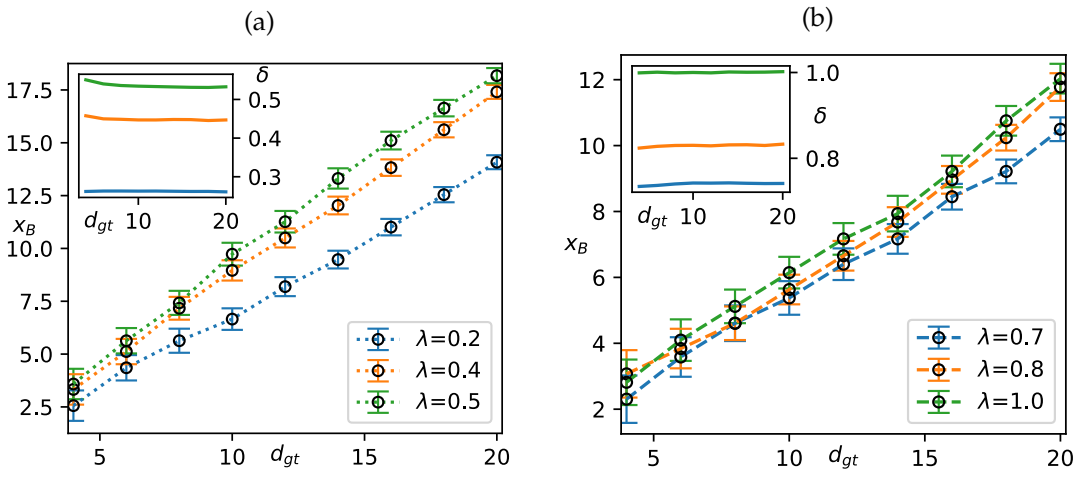


FIGURE 4.18: Spot and Band Width in Comparison to $d_{gt}$. (*a*) Average spot widths for different $\lambda$. We can see a linear growth of $x_B$ with $d_{gt}$ as in the 1d case. The width grows faster for higher $\lambda$. Inset: $\delta$ ratios in comparison to $d_{gt}$ for the same values of $\lambda$. (*b*) Band width against $d_{gt}$. We again observe a linear relation. In comparison to the spots we observe slower growth. Inset: $\delta$ is again constant for different $d_{gt}$

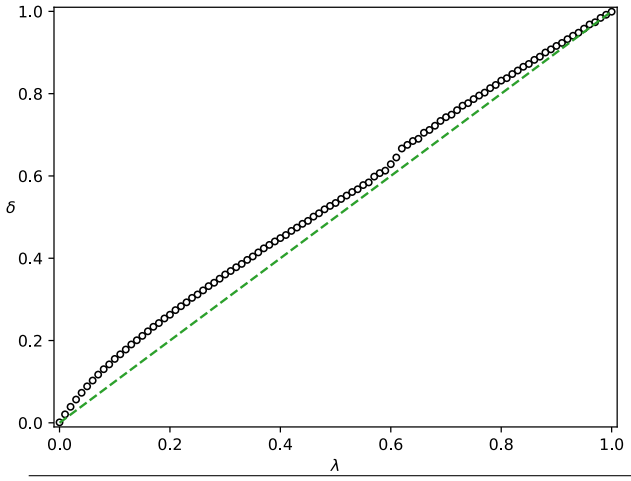


FIGURE 4.19: The Effects of Spot Order Phase Separation on the Ratio $\delta$. The circles mark the realised ratio $\delta$ for a given $\lambda$ in the simulation. The dashed line is the ratio in the well-mixed case. The merge of spots into bands is clearly visible in the ratio $\delta$ at about $\lambda = 0.6$. Parameters: $L = 256$, $d_{gt} = 10$, $\tau = 1$

### Spot Order vs. Diffusion

The game theoretical patterns appear and vanish in a continuous fashion with the interplay between the game strength $\tau$ and the diffusive movement. We fix $\sigma_0 = 0.5$, so the movement strength is controlled by the value of $v_0$.

The species separated patterns vanish when the movement of the particles is so fast that the game interaction is not able to compensate for the mixing any longer. This means we are in the mean-field limit now and the ratio $\delta$ equals the relative game strength $\lambda$. $d_{gt}$, the game theoretical interaction range of each particle is an important control parameter as well, because for larger values of $d_{gt}$ particles have to travel further to escape the interaction with other particles. For larger $d_{gt}$ we also observe, in analogy to the on dimensional case, increasing pattern size. In a system without active matter interaction we could also use $d_{gt}$ as a measure for the system, as it is the only relevant length scale in this case. But because we want to take into account the possibility of a combined system and the influence of the interplay between $d_{gt}$

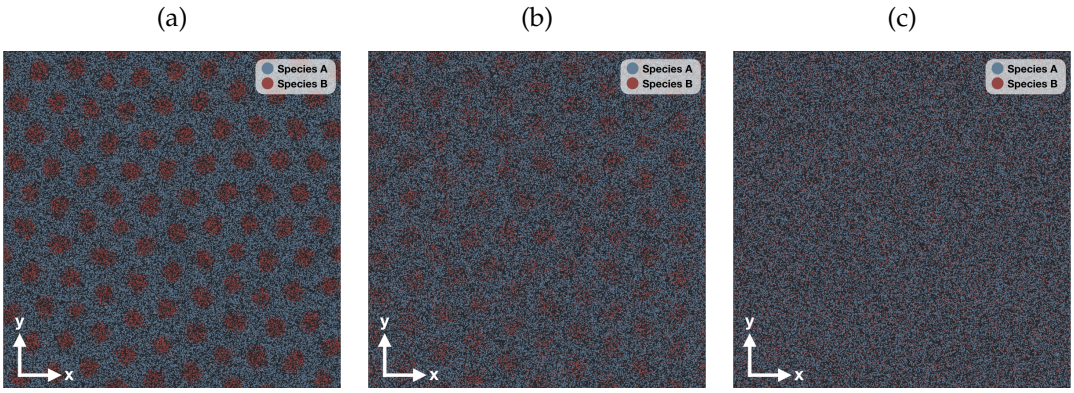


FIGURE 4.20: Gradual Disappearance of Spots for Increasing Diffusion. Parameters: $\tau = 0.1$, $\lambda = 0.3$, $d_{gt} = 20$, $\rho = 1.5$ and $\sigma_0 = 0.5$ (*a*) Clearly visible spots for $v_0 = 0.04$. (*b*) The spots get more diffuse, $v_0 = 0.12$. (*c*) No visible spots anymore at $v_0 = 0.2$.

and $d_0$ we use $d_{gt}$ as a control parameter. Fig. 4.20 shows the system for $\lambda = 0.3$, $\tau = 0.1$ and $v_0 \in [0, 0.2]$, where we can see the gradual disappearance of the spots. The same behavior occurs for the band structure as well. To measure the influence of pattern formation we analyzed the difference between $\lambda$ and $\delta$, $\Delta \equiv \delta - \lambda$ for various values of $\lambda$ and $d_{gt}$ (fig. 4.21).

In regimes where diffusion outweighs the game and we would not see patterns for non-active particles, the patterns reappear when we switch on the active matter interaction and collective motion occurs. The reason for this is that the high directional order decreases the relative movement of particles compared to each other. This then leads to the game theoretical interaction being able to restabilize the species separation in regions with high $\varphi$ again.

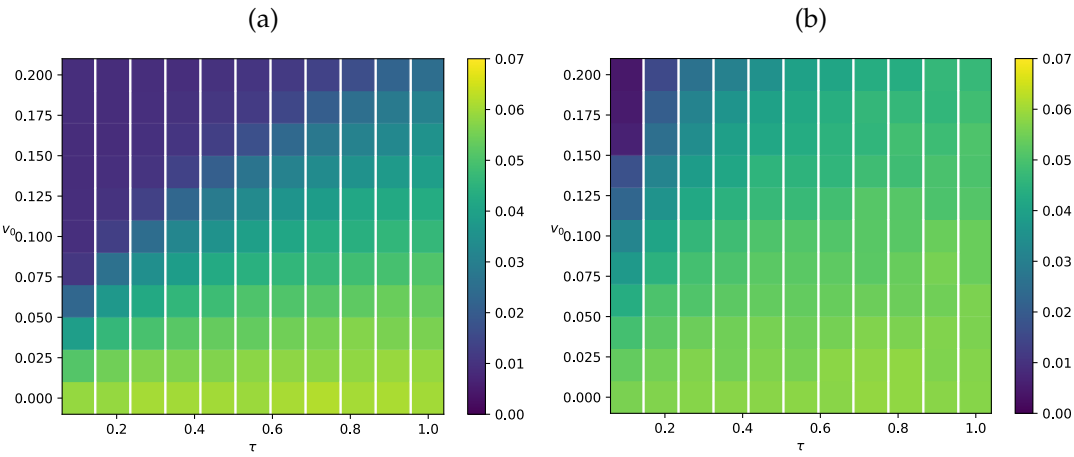

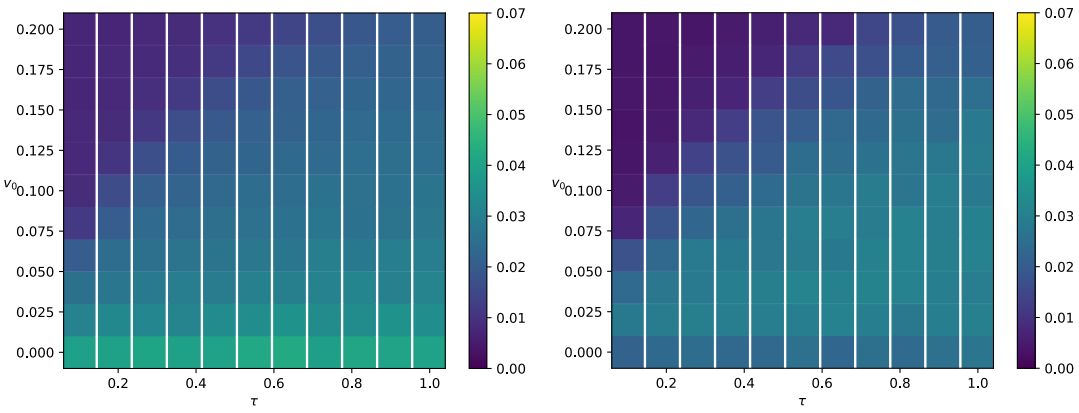


FIGURE 4.21: Species Separation Induced Ratio Shift $\Delta$ for Different Values of $\tau$, $v_0$ (*a*) $\lambda = 0.3$, $d_{gt} = 10$ (*b*) $\lambda = 0.3$, $d_{gt} = 20$ (*c*) $\lambda = 0.5$, $d_{gt} = 10$ (*d*) $\lambda = 0.8$, $d_{gt} = 10$

### 4.3.3 Polar Order Stabilized Species Separation

While we have seen bands in the case without particle alignment only for $\lambda > 0.6$, we observe them in the combined system (fig. 4.22) as soon as the merged wave phase appears ($\lambda \gtrsim 0.3$).

This effect is caused by the alignment that reduces the relative motion between particles stronger in travelling direction than perpendicular to it. The explanation for this lies in the way the noise $\sigma$ is incorporated: While there is an alignment in movement direction every time step $dt$, the noise mainly displaces the particles sideways. The spots are therefore stretched along the axis perpendicular to $\mathbf{w}$ and $\mathbf{u}$ to the point where the spots get so much they eventually form bands.

If switch randomization is implemented, particles loose their alignment when switching species and therefore fall behind inside the wave and get "*caught*" by the next cluster of their own species, where they align again. This contributes to the separation of species inside a wave, so switch randomization enhances the band formation inside waves.

## 4.4 Central Results of the Agent Based Approach

We implemented an agent based approach to an active system with two species to probe for effects of a combination of active matter and a cooperator/defector game. In contrast to previous active matter simulations [9] [8] [7] we use two active species whose densities can vary locally and also globally in exchange with each other.

While both species align individually, they adapt their densities according to a cooperator/defector game in a snowdrift game scenario. We probed for the effects the game has on the formation of order in the system and how the self-propelled motion and pattern formation influences the game theoretical fixed points.

After confirming results of previous studies [9] [7] for a single species we turned to the combined model of two species and observed a shift in the onset of order

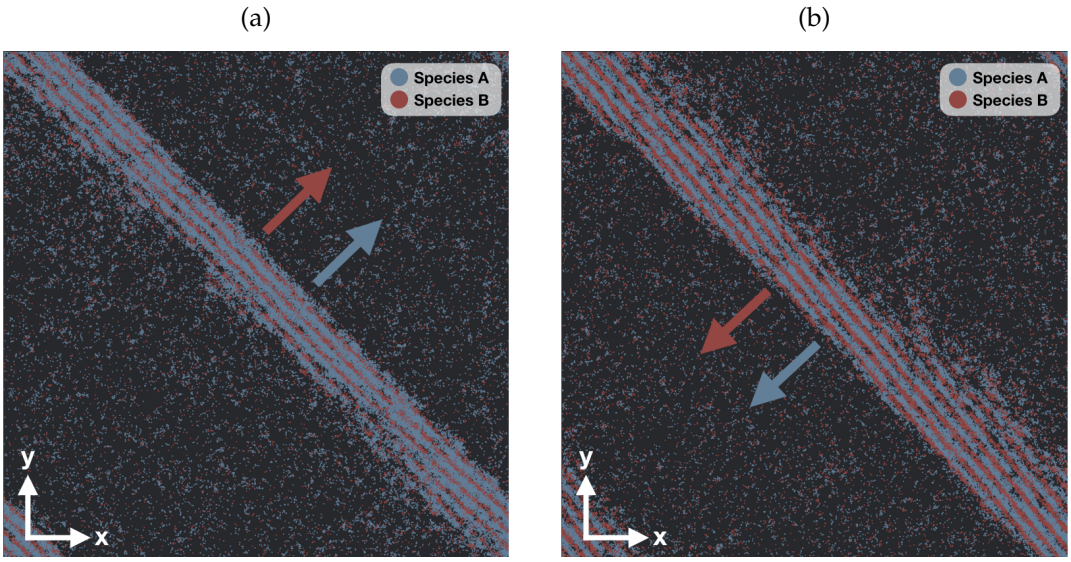


FIGURE 4.22: Wave Bands for Different $\lambda$ (*a*) 0.3 and (*b*) 0.6. Bands get more prominent for higher values of $\lambda$

towards higher density values. This effect is enhanced if the particles cannot transfer directional information upon switching species.

For very uneven games with one much stronger species, we observed up to five different phases by varying the noise in the system: An isotropic homogeneous phase where neither species moves coherent, two wave phases, where either one (Wave Phase I) or both species (Wave Phase II) display directional order inside the wave. And two ordered phases, where there is ordered motion in the whole system for either one (Ordered Phase II) or both species (Ordered Phase II). For more equal games the first ordered phase vanishes and both wave phases merge into one.

With increasing order we observe species separation into either clusters (spots) or bands. This effect is rooted in the continuous game theoretical interaction and while it can also be observed without active matter interaction if diffusive movement is slow compared to the strength of the game, it is restabilized in regimes with high directional order.

While there have been studies probing spatially extended cooperator/defector games [22] [50] on a lattice, the separation of species has not been observed before in a spatially continuous snowdrift game to our knowledge. In contrast to previous lattice models we observe a decreasing ratio of cooperators for all values of relative game strength between cooperators and defectors. We developed a one dimensional model for the formation and fitness advantage this species separation induces for particles in separated systems and confirmed it with further simulations.

In the next chapter we want to compare the results of our agent based simulation with an analytic approach using the Boltzmann equation for active matter to link microscopic and macroscopic parameters and arrive at a hydrodynamic description of our system. For this alternative approach to our system of two interacting active species we will define a microscopic model first and derive hydrodynamic equations describing it. These equations, their fixed points and stability will be analyzed analytically and numerically. We will draw comparisons to the agent based simulations,

confirm results and conclusions we drew in this chapter and point out differences and their most likely reasons. A more in-depth study of the following Boltzmann and hydrodynamic approach on its own can be found in [33].

# Chapter 5

# The Kinetic Boltzmann Approach

## 5.1 The Microscopic Model

To be able to better put the results we derived through the agent based approach into context, we consider the model of two interacting active species from a different viewpoint and on a different length scale. We will outline a kinetic Boltzmann approach leading to a hydrodynamic description and compare numerical simulations of these equations to the results we discussed last chapter.

In analogy to Bertin, Droz and Grégoire [6], we define our model consisting of a two dimensional plane with coordinates $x$ and $y$, which is populated by two species of point-like, active particles. Each particle has a position $\mathbf{r}_j$ and moves through space with velocity $\mathbf{v}_j = v_0\mathbf{e}(\theta_j)$ with the absolute value $v_0$ identical for all particles, but adjustable and individual direction $\theta_j$. The direction $\theta_j$ is given as an angle in relation to the $x$-axis in the periodic range of $(-\pi, \pi]$. Furthermore the particles are subject to stochastic diffusion with diffusion probability $\lambda$ per unit time. This diffusion manifests as a direction change $\eta$, where the new direction $\theta' = \theta + \eta$, adjusted for the periodicity of the angle. The noise $\eta$ arises from a Gaussian distribution $P_0(\eta)$ with standard deviation $\sigma_0$.

Because our aim is to study the collective behavior of particles, we need to introduce an interaction between particles. A collision between two particles is defined as the event when their respective interaction radii $d_0$ overlap. We assume only binary collisions here in contrast to the multiparticle collisions we used for the agent based approach. We need to make this assumption in order to be able to corse-grain the model and derive the Boltzmann equation for active matter. There is still a debate if and how this difference in collision implementation influences the dynamics [49] [6] [24]. It would be subject of further research to see how much of the observed discrepancies between agent based and hydrodynamic results are due to this difference in implementation.

The probability of two particles colliding with each other is proportional to their cross-section $R$, which can be derived from geometric observations. In the reference frame of particle 1, the relative velocity of its potential collision partner, particle 2, is

$$\mathbf{v}_{rel} = v_0(\mathbf{e}(\theta_2) - \mathbf{e}(\theta_1)). \tag{5.1}$$

The two particles collide in a time step $dt$ if particle 2 is somewhere in the area $C$ given by fig. 5.1. The area can then be evaluated to

$$C = \int_0^\pi d\vartheta \, 2d_0 v_{rel} dt = 2\pi d_0 v_{rel} dt. \tag{5.2}$$

Together with (5.1), this then leads to the cross section

$$R(\theta_1, \theta_2) = 2\pi d_0 v_0 |\mathbf{e}(\theta_2) - \mathbf{e}(\theta_1)|. \tag{5.3}$$

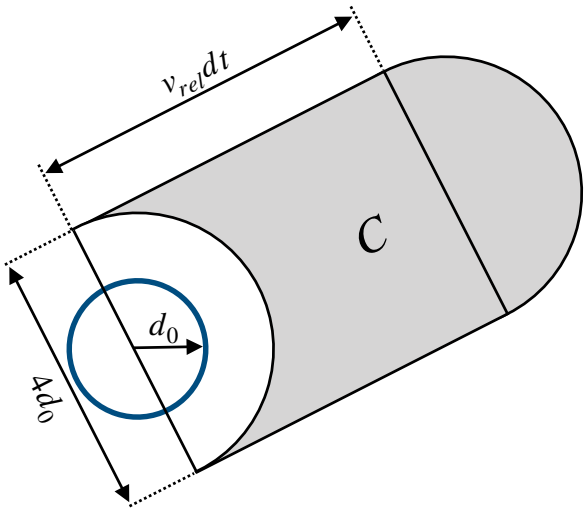


FIGURE 5.1: Geometric cross section for binary collision in the rest frame of particle 1. The blue circle indicate the interaction radius of particle 1, while particle 2 has to lie somewhere in the grey area $R$ in order to collide with particle 1 in the next time step dt. $v_{rel}$ is the absolute value of $\mathbf{v}_{rel}$, while the orientation of the area gives the direction of $\mathbf{v}_{rel}$. The area $R$ can then be calculated either by integral or geometric considerations to be of size $2\pi d_0 v_{rel} dt$.

When two particles of the same species collide, they align with each other by averaging their directions $\theta_1$ and $\theta_2$ to both move approximately in direction $\bar{\theta}$, apart from collision noise:

$$\theta_1' = \bar{\theta} + \eta_1 \qquad \theta_2' = \bar{\theta} + \eta_2 \tag{5.4}$$

with

$$\bar{\theta} = arg\left(e^{i\theta_1} + e^{i\theta_2}\right) \tag{5.5}$$

and $\eta_1$, $\eta_2$ independent noise variables derived from the Gaussian distribution $P(\eta)$ with standard deviation $\sigma$, which can differ from $\theta_0$. These variables $\sigma$, $\sigma_0$ and distributions $P(\eta)$ and $P_0(\eta)$ are referred to as the collision and diffusion noise, respectively.

Because we want to study the interplay between two active species, we need to introduce a second interaction, which enables the species to influence each other. This is realized by a game theoretical interaction like we have seen in chapter 3. If one particle of species A and one particle of species B meet, they play a game with each other, whereby the fitness of each particle changes according to the game parameters $\tau_A$ and $\tau_B$. If it would be advantageous from a fitness standpoint for a particle to switch its species, it does so with probability corresponding to the expected fitness gain.

## 5.2 The Boltzmann Equation

Now that we have a definition of our model, we need to describe it mathematically. Starting from Hamiltonian dynamics, the Boltzmann equation can be derived from a many particle Hamiltonian and the BBGKY-hierarchy [18]. To achieve this, we need to coarsen the microscopic model. While it is also possible to start from a macroscopic hydrodynamic description of our system, we choose to use the Boltzmann equation for the reason that it can be derived from our microscopic model and used to arrive at the hydrodynamic description through a series of transformations and approximations. It can therefore be seen as an intermediary and a connection between the microscopic and macroscopic model [40]. Because of this property it has been a focus of research for active matter systems in the past years and been applied to a variety of systems [24] [15] [52] [6] [7] [41].

To use this approach, we introduce the ballistic length $d_{bal}$, which is the average distance the particles travel in a straight line without diffusion, and the average distance between particles $d_{pp}$. The coarsening requires the assumption that the ballistic length is much larger than the interaction radius, so $d_{bal} \gg d_0$. We further need to assume that the mean distance between particles is much larger than the interaction radius, $d_{pp} \gg d_0$. These assumptions assure that we can view the interactions as single events and there is no memory effect carrying over from one collision to the next.

The Boltzmann equation is then a function of the one-particle density $f(\mathbf{r}, \mathbf{p}, t)$ in the phase space, where $f$ is normalized such that

$$N(t) = \int f(\mathbf{r}, \mathbf{p}, t) d\mathbf{r} d\mathbf{p} \tag{5.6}$$

is the number of particles in the phase space volume integrated over. $f$ can therefore be viewed as a probability density function of particles at position $\mathbf{r}$ with momentum $\mathbf{p}$ at time $t$. Because the particles in our model all have the same absolute momentum $|\mathbf{p}|$, we can make a substitution, introduce $\theta$ and integrate out the absolute momentum, so that $f(\mathbf{r}, \theta, t)$ is the probability density of particles at position $\mathbf{r}$, pointing in direction $\theta$ at time $t$.

We can then write the Boltzmann equation for our system of self-propelled particles (for now still without game theoretical interaction and only one species) as

$$\partial_t f(\mathbf{r}, \theta, t) + v_0 \mathbf{e}(\theta) \partial_{\mathbf{r}} f(\mathbf{r}, \theta, t) = I_{dif}[f] + I_{col}[f, f]. \tag{5.7}$$

with partial time derivative of $f$ and a second term on the left hand side and the diffusion and collision terms on the right hand side. With no diffusion or interaction in the system the right hand side would be zero and the dynamics be governed by the term $v_0 \mathbf{e}(\theta) \partial_{\mathbf{r}} f(\mathbf{r}, \theta, t)$. It is easy to see that this so-called streaming term conveys the flow in the system: The gradient of the one particle density $f(\mathbf{r}, \theta, t)$ gives the direction and amount of the maximal spatial change in $f$ and $\mathbf{e}(\theta)$ the direction of movement. This means that in absence of interactions the change of $f$ in time is just the current movement in the system.

With diffusion and collisions, which are implemented through the framework of master equations consisting of gain and loss terms to $f(\mathbf{r}, \theta, t)$. We start with the

diffusion term in our case is given by

$$I_{dif}[f] = -\lambda f(\theta) + \lambda \int_{-\pi}^{\pi} d\theta' \int_{-\infty}^{\infty} d\eta f(\theta') P_0(\eta) \delta_{2\pi}(\theta' - \theta + \eta), \tag{5.8}$$

where we suppressed $\mathbf{r}$ and $t$ in the notation of $f$, which will be done often to simplify notation, when parameters are not relevant at the moment. The first term of (5.8) represents the loss term of all and can be interpreted as the subtraction of all particles which had direction $\theta$ before but scattered with probability $\lambda$ to a different direction and are therefore no longer part of $f(\theta)$. The second term, also called gain term is the integral over all possible configurations which had direction $\theta'$ before and point now, after the diffusion event of probability $\lambda$, in direction $\theta$ because of the addition of noise

$$P_0(\eta) = \frac{1}{\sqrt{2\pi\sigma_0^2}} \exp\left[-\frac{\eta^2}{2\sigma_0^2}\right]. \tag{5.9}$$

The collision term reads

$$\begin{aligned} I_{col}[f,g] = &- f(\theta) \int_{\theta-\pi}^{\theta+\pi} d\theta' R(\theta,\theta') g(\theta') + \int_{-\pi}^{\pi} d\theta_1 \int_{\theta_1-\pi}^{\theta_1+\pi} d\theta_2 f(\theta_1) g(\theta_2) R(\theta_1,\theta_2) \\ &\times \int_{-\infty}^{\infty} P(\eta) \delta_{2\pi}\left(\theta - \frac{\theta_1+\theta_2}{2} - \eta\right). \end{aligned} \tag{5.10}$$

Again, the first part represents a loss term and the second a gain term. We have to remove all particles from $f(\theta)$ which pointed in direction of $\theta$ and collided with any other particle pointing in direction $\theta'$. This happens with a probability given by the cross section

$$R(\theta,\theta') = 2v_0 d_0 |\mathbf{e}(\theta) - \mathbf{e}(\theta')| = 4v_0 d_0 \left| \sin\left(\frac{\theta-\theta'}{2}\right) \right| \tag{5.11}$$

that has been derived in (5.3). The gain term on the other hand adds all particles which pointed in direction $\theta_1$ before and now, after collision with a particle with direction $\theta_2$ and addition of the $2\pi$ periodic noise

$$P(\eta) = \frac{1}{\sqrt{2\pi\sigma^2}} \exp\left[-\frac{\eta^2}{2\sigma^2}\right], \tag{5.12}$$

point in direction $\theta$. The cross section $R$ again represents the probability of the collision happening in the first place.

Put together this equation captures, with the assumptions we made before about a dilute system and molecular chaos, the dynamics of our microscopic system. It is a highly complicated integro-differential equation which can usually not be solved by analytic methods.

## 5.3 The Combined Model

Now that we have established the pure active matter Boltzmann equation, we want to modify it to incorporate two species $A$ and $B$ and an interaction term to couple the two. To achieve this we introduce the species specific functions $\alpha(\mathbf{r},\theta,t)$ and $\beta(\mathbf{r},\theta,t)$ and a game theory interaction term $I_{gt}$. The two resulting coupled Boltzmann equations are

$$\begin{aligned}\partial_t\alpha\left(\mathbf{r},\theta,t\right)+v_0\mathbf{e}(\theta)\partial_{\mathbf{r}}\alpha\left(\mathbf{r},\theta,t\right)&=I_{dif}\left[\alpha\right]+I_{col}\left[\alpha,\alpha\right]+I_{gt}^{A}\left[\alpha,\beta\right]\\ \partial_t\beta\left(\mathbf{r},\theta,t\right)+v_0\mathbf{e}(\theta)\partial_{\mathbf{r}}\beta\left(\mathbf{r},\theta,t\right)&=I_{dif}\left[\beta\right]+I_{col}\left[\beta,\beta\right]+I_{gt}^{B}\left[\beta,\alpha\right]\end{aligned} \tag{5.13}$$

with the game theoretical interaction terms

$$\begin{aligned}&I_{gt}^{A}\left[\alpha,\beta\right]=(\tau_A b-\tau_B a)b\alpha \;\text{ and }\; I_{gt}^{B}\left[\beta,\alpha\right]=(\tau_B a-\tau_A b)a\beta\\ &\text{where }\; a(\mathbf{r},t)=\int_{-\pi}^{\pi}d\theta\;\alpha\left(\mathbf{r},\theta,t\right)\;\text{ and }\; b(\mathbf{r},t)=\int_{-\pi}^{\pi}d\theta\;\beta\left(\mathbf{r},\theta,t\right)\end{aligned} \tag{5.14}$$

in complete analogy to chapter 3.2, but now with spacial dependencies in the sense that we no longer work in the mean field limit and the combined density $\rho(\mathbf{r}) = \alpha(\mathbf{r}) + \beta(\mathbf{r})$ can therefore vary locally. There is no inter-species alignment term $I_{col}[\alpha,\beta]$ which means the only interaction between species is of game theoretical nature. It acts as an intermediary between the two species and can change their local and overall densities $\alpha$ and $\beta$ through the opposing gain and loss terms.

## 5.4 Fourier Transformed Boltzmann equation

The set of coupled Boltzmann equations 5.13 we have is very complicated and not completely solvable. While it would be possible to directly simulate the equations numerically, we choose the approach to approximate the equations and arrive at a hydrodynamic description of our model which can be analyzed and interpreted easier than the complete equations. We do this to derive the slow hydrodynamic fields, which have an illustrative counterpart and interpretation in nature. Additionally, we can draw comparisons to the Navier Stokes equation.

After a derivation, which can be found in Appendix A.1 and a rescaling which effectively sets $\lambda = v_0 = d_0 = 1$, we arrive at the Fourier representation of the Boltzmann equation

$$\begin{aligned}\partial_t\hat{\alpha}_k+\frac{1}{2}\left(\nabla\hat{\alpha}_{k-1}+\nabla^*\hat{\alpha}_{k+1}\right)&=(\hat{P}_{0,k}-1)\hat{\alpha}_k+\sum_p\hat{\alpha}_{k-p}\hat{\alpha}_p A_{p,k}+(\tau_A\hat{\beta}_0-\tau_B\hat{\alpha}_0)\hat{\beta}_0\hat{\alpha}_k\\ \partial_t\hat{\beta}_k+\frac{1}{2}\left(\nabla\hat{\beta}_{k-1}+\nabla^*\hat{\beta}_{k+1}\right)&=(\hat{P}_{0,k}-1)\hat{\beta}_k+\sum_p\hat{\beta}_{k-p}\hat{\beta}_p A_{p,k}-(\tau_A\hat{\beta}_0-\tau_B\hat{\alpha}_0)\hat{\alpha}_0\hat{\beta}_k.\end{aligned} \tag{5.15}$$

with

$$\hat{\alpha}_k(\mathbf{r},t)=\int_{-\pi}^{\pi}d\theta\;e^{ik\theta}\alpha\left(\mathbf{r},\theta,t\right), \tag{5.16}$$

$\beta_k$ defined analogue and

$$A_{p,k} \equiv \int \frac{d\vartheta}{2\pi} R(|\vartheta|) \left( \hat{P}_k \cos\left( (\tfrac{k}{2} - p)\vartheta \right) - \cos(p\vartheta) \right). \tag{5.17}$$

$\hat{P}_k$ and $\hat{P}_{0,k}$ are the Fourier transformation of the noise distributions and $\nabla \equiv \partial_x + i\partial_y$.

### 5.4.1 The Continuity Equation

If we have a closer look at the definition of the Fourier series and take species $A$ as an example, we can see that

$$\hat{\alpha}_0(\mathbf{r}, t) = \int d\theta \; e^{i\theta 0} \alpha(\mathbf{r}, \theta, t) = \int d\theta \; \alpha(\mathbf{r}, \theta, t) = a(\mathbf{r}, t) \tag{5.18}$$

which corresponds to the spatial density of species $A$. The same is true for $B$ and if we add them together we can define the overall density

$$\rho = \hat{\alpha}_0 + \hat{\beta}_0 = a + b \tag{5.19}$$

with $a$ and $b$ from (5.14). Furthermore, if we now turn to

$$\begin{aligned} \hat{\alpha}_1(\mathbf{r}, t) &= \int d\theta \; e^{i\theta} \alpha(\mathbf{r}, \theta, t) = \int d\theta \; \cos(\theta) \alpha(\mathbf{r}, \theta, t) + i \int d\theta \; \sin(\theta) \alpha(\mathbf{r}, \theta, t) \\ &= \int d\theta \; e_x(\theta) \alpha(\mathbf{r}, \theta, t) + i \int d\theta \; e_y(\theta) \alpha(\mathbf{r}, \theta, t) \equiv w_x(\mathbf{r}, t) + i w_y(\mathbf{r}, t) \end{aligned} \tag{5.20}$$

which can be identified with the momentum field

$$\mathbf{w}(\mathbf{r}, t) = \int d\theta \; \mathbf{e}(\theta) \alpha(\mathbf{r}, \theta, t) = \begin{pmatrix} w_x(\mathbf{r},t) \\ w_y(\mathbf{r},t) \end{pmatrix} \tag{5.21}$$

of species $A$. This field indicates the flow of species $A$ because of the fact that $\alpha(\mathbf{r}, \theta, t)$ is the function which gives a value for the amount of particles at location $\mathbf{r}$ pointing in direction $\theta$ at time $t$. When we weight this with the (because of the rescaling) normalized velocity vector $\mathbf{e}(\theta)$ and integrate over $\theta$, we get the averaged direction the field is flowing at this point in time and space weighted with the local density $\alpha$.

The same reasoning leads to the flow field of species $B$ which can be written as

$$\mathbf{u}(\mathbf{r}, t) = \int d\theta \; \mathbf{e}(\theta) \beta(\mathbf{r}, \theta, t) = \begin{pmatrix} u_x(\mathbf{r},t) \\ u_y(\mathbf{r},t) \end{pmatrix}. \tag{5.22}$$

These are the only two modes of the Fourier representation that have a direct interpretation and correspondence to macroscopic observables in our system. They are called slow fields because they vary on macroscopic time scales only and are an important part of the hydrodynamic treatment in the next chapter, where we derive generalized Navier Stokes equations for these observables.

Dividing $\mathbf{w}(\mathbf{r})$ by $\rho(\mathbf{r})$ gives the polar order field, which can take on values from 0 to 1 and indicates the directional order at $\mathbf{r}$.

If we now take the time derivative of the overall density $\rho$, we can expand it with help of (5.19) and (5.15)

$$\begin{aligned}\partial_t \rho = \partial_t \hat{\alpha}_0 + \partial_t \hat{\beta}_0 = &-\frac{1}{2}\left(\nabla \hat{\alpha}_1^* + \nabla^* \hat{\alpha}_1 + \nabla \hat{\beta}_1^* + \nabla^* \hat{\beta}_1\right) + (P_{0,0} - 1)(\hat{\alpha}_0 + \hat{\alpha}_0) \\ &+ \sum_p \hat{\alpha}_p^* \hat{\alpha}_p A_{p,0} + \sum_p \hat{\beta}_p^* \hat{\beta}_p A_{p,0}\end{aligned} \tag{5.23}$$

where we used the fact that because $\alpha(\mathbf{r}, \theta, t)$ is a real-valued function, its Fourier components fulfill the relation $\hat{\alpha}_{-k}(\mathbf{r}, t) = \hat{\alpha}_k^*(\mathbf{r}, t)$. Also, because $P_0$ is a probability density its 0-th Fourier component $P_{0,0} = \int_{-\infty}^{\infty} P_0 = 1$ and all components $A_{0,k}$ are zero, which can be easily seen from its definition in (5.17) only the term with the spatial derivatives is non-zero and we can write

$$\begin{aligned}= &-\frac{1}{2}((\partial_x + i\partial_y)(w_x - iw_y) + (\partial_x - i\partial_y)(w_x + iw_y) \\ &\quad + (\partial_x + i\partial_y)(u_x - iu_y) + (\partial_x - i\partial_y)(u_x + iu_y)) \\ = &-\left(\partial_x(w_x + u_x) + \partial_y(w_y + u_y)\right) = -\partial_{\mathbf{r}} \cdot (\mathbf{w} + \mathbf{u}) = -\partial_{\mathbf{r}} \cdot (\rho \mathbf{v})\end{aligned} \tag{5.24}$$

where we defined the velocity field $\mathbf{v} \equiv (\mathbf{w} + \mathbf{u})/\rho$. So in the end we arrive at the continuity equation

$$\partial_t \rho + \partial_{\mathbf{r}} \cdot (\rho \mathbf{v}) = 0 \tag{5.25}$$

from which we can follow that the spatial integral of $\rho$ is constant in time, so the overall number of particles in the system is conserved.

### 5.4.2 The Isotropic Solution

For convenience and better understanding, we want to make a change of variables: We introduce the absolute and relative game strength $\tau$ and $\lambda$ as

$$\tau = \tau_A \tag{5.26a}$$

$$\lambda = \frac{\tau_B}{\tau_A} \tag{5.26b}$$

so we can write the game theoretical interaction term as

$$\pm\left(\tau_A \beta_0 - \tau_B \alpha_0\right) \alpha_0 \beta_0 = \pm\tau\left(\beta_0 - \lambda \alpha_0\right) \alpha_0 \beta_0. \tag{5.27}$$

Even though the derived equations until now and in the following are applicable to alle four cases of the cooperator-defector game, from now on we want to restrict ourselves to the case of the snowdrift game with $\tau_A, \tau_B > 0$ again in analogy to chapter 4 and to be able to draw comparisons. Because $\tau_A, \tau_B > 0$ and the fact that we can choose $\tau_A \geq \tau_B$ without loss of generality using the interchangeability of $A$ and $B$ in our underlying equations, we can easily see that $\tau > 0$ and $\lambda \in [0, 1]$. This is why we can refer to $\tau$ as the absolute game strength as it indicates the rate and therefore the strength with which the game theoretical interaction takes place, while $\lambda$ is the relative game strength of $B$ compared to $A$.

With these new parameters we want to try to solve the previously derived Boltzmann equations. Even though there is no general solution available, we can easily see one particular solution: The isotropic solution in which $\alpha(\mathbf{r}, \theta, t) = \alpha(t)$ and

$\beta(\mathbf{r},\theta,t) = \beta(t)$:

$$\begin{aligned} \alpha(\mathbf{r},\theta,t) =& \alpha(t) \Rightarrow \hat{\alpha}_0(t) = 2\pi\alpha(t)\,, \quad \hat{\alpha}_k = 0\ \forall k \neq 0 \\ \beta(\mathbf{r},\theta,t) =& \beta(t) \Rightarrow \hat{\beta}_0(t) = 2\pi\alpha(t)\,, \quad \hat{\beta}_k = 0\ \forall k \neq 0 \end{aligned} \tag{5.28}$$

which follows directly from the definition of the Fourier series (A.2). From now on we will drop the hats over $\hat{\alpha}_k$ and $\hat{\beta}_k$ to clean up the notation which shouldn't lead to any ambiguity because now we exclusively work in Fourier space. With this the only two remaining equations are

$$\begin{aligned} \partial_t\alpha_0 =& \tau(\beta_0 - \lambda\alpha_0)\alpha_0\beta_0 \\ \partial_t\beta_0 =& \tau(\lambda\alpha_0 - \beta_0)\alpha_0\beta_0 = -\partial_t\alpha_0. \end{aligned} \tag{5.29}$$

The spatial derivatives evaluate to zero because there is no dependency on $\mathbf{r}$ anymore. The term with the Fourier transformed noise vanishes again because of the normalization of the probability density. We can now easily find the fixed points of these equations by setting the left hand side of the equations to zero:

$$\alpha_0^{fp} = \begin{cases} 0 \\ \rho \\ \rho\frac{1}{1+\lambda} \end{cases} \qquad \beta_0^{fp} = \begin{cases} \rho & (I) \\ 0 & (II) \\ \rho\frac{\lambda}{1+\lambda} & (III) \end{cases} \tag{5.30}$$

Checking the linear stability of these fixed points, we see that fixed points $(I)$ and $(II)$ are always unstable, while fixed point $(III)$ is stable below critical density

$$\begin{aligned} \rho_{crit,\alpha} =& \frac{1-P_{0,1}}{A_{1,1}+A_{0,1}}\,(1+\lambda) \quad \Rightarrow \quad \alpha_{crit,0} = \frac{1-P_{0,1}}{A_{1,1}+A_{0,1}} \\ \rho_{crit,\beta} =& \frac{1-P_{0,1}}{A_{1,1}+A_{0,1}}\left(1+\lambda^{-1}\right) \quad \Rightarrow \quad \beta_{crit,0} = \frac{1-P_{0,1}}{A_{1,1}+A_{0,1}}, \end{aligned} \tag{5.31}$$

while it is unstable above it. This is true as long as $\rho_{crit} \geq 0$. A negative $\rho_{crit}$ indicates that the fixed point is always stable (see Appendix A.2 for details). $\rho_{crit,\alpha}$ is the global density at which the first Fourier mode of species $A$ becomes critical and $\alpha_{crit,0}$ is then the density of species $A$ at which the mode becomes critical. So for values of $\rho < \rho_{crit}$ fixed point (III) remains stable, while above this threshold none of the homogeneous, isotropic fixed points is stable any longer. To get insight into what happens in this case, we need to approximate the equations. This is done in the next chapter by a scaling ansatz, imposing a cut-off and closing the equations to arrive at a hydrodynamic description.

# Chapter 6

# Hydrodynamic Equations and Linear Stability Analysis

## 6.1 The Hydrodynamic Equations

The system of equations (5.15) is not closed and we will need to make assumptions and approximations before solving the resulting hydrodynamic equations. The standard way to do this is by making a scaling ansatz and imposing a cutoff [6] [7]. The approximation relies on the fact that we work in a regime close to the isotropic solution and therefore $\alpha(\mathbf{r}, \theta, t)$ and $\beta(\mathbf{r}, \theta, t)$ only slightly depend on $\theta$. This can be reframed as the fact that the momentum fields $w$ and $u$ are small in comparison to the individual particle velocity. We have also seen that the instability of the homogeneous fixed point occurs first for the mode $k = 1$.

Imposing the scaling ansatz and cut-off (see Appendix A.3 for details), we arrive at the hydrodynamic description:

$$\partial_t \alpha_0 = -\tfrac{1}{2}(\nabla \alpha_1^* + \nabla^* \alpha_1) + \tau(\beta_0 - \lambda\alpha_0)\beta_0\alpha_0 \tag{6.1a}$$

$$\partial_t \beta_0 = -\tfrac{1}{2}(\nabla \beta_1^* + \nabla^* \beta_1) - \tau(\beta_0 - \lambda\alpha_0)\beta_0\alpha_0 \tag{6.1b}$$

$$\begin{aligned}\partial_t \alpha_1 =&(\mu_A(\alpha_0, \beta_0) - \xi_A(\alpha_0)|\alpha_1|^2)\alpha_1 + \nu_A(\alpha_0)\nabla^*\nabla\alpha_1 - \tfrac{1}{2}\nabla\alpha_0 \\ &- \gamma_A(\alpha_0)\alpha_1\nabla^*\alpha_1 - \kappa_A(\alpha_0)\alpha_1^*\nabla\alpha_1\end{aligned} \tag{6.1c}$$

$$\begin{aligned}\partial_t \beta_1 =&(\mu_B(\alpha_0, \beta_0) - \xi_B(\beta_0)|\beta_1|^2)\beta_1 + \nu_B(\beta_0)\nabla^*\nabla\beta_1 - \tfrac{1}{2}\nabla\beta_0 \\ &- \gamma_B(\beta_0)\beta_1\nabla^*\beta_1 - \kappa_B(\beta_0)\beta_1^*\nabla\beta_1\end{aligned} \tag{6.1d}$$

with parameters

$$\begin{aligned}
\nu_A =& -\tfrac{1}{4}\left[P_{0,2} - 1 + (A_{0,2} + A_{2,2})\alpha_0\right]^{-1} \\
\nu_B =& -\tfrac{1}{4}\left[P_{0,2} - 1 + (A_{0,2} + A_{2,2})\beta_0\right]^{-1} \\
\mu_A =& P_{0,1} - 1 + (A_{0,1} + A_{1,1})\alpha_0 + \tau(\beta_0 - \lambda\alpha_0)\beta_0 \\
\mu_B =& P_{0,1} - 1 + (A_{0,1} + A_{1,1})\beta_0 - \tau(\beta_0 - \lambda\alpha_0)\alpha_0 \\
\gamma_A =& 4\nu_A A_{1,2} \qquad \kappa_A = 2\nu_A(A_{2,1} + A_{-1,1}) \qquad \xi_A = -4(A_{2,1} + A_{-1,1})\nu_A A_{1,2} \\
\gamma_B =& 4\nu_B A_{1,2} \qquad \kappa_B = 2\nu_B(A_{2,1} + A_{-1,1}) \qquad \xi_B = -4(A_{2,1} + A_{-1,1})\nu_B A_{1,2}.
\end{aligned}$$

While the equation for the densities $\alpha_0$ and $\beta_0$ are still exact equations and independent of our truncation scheme, the momentum equations are an approximation with the first non-trivial cutoff imposed to close the infinite system of equations (5.15).

Equations (6.1c) and (6.1d) can be viewed as generalized Navier Stokes equations. Because both equations, (6.1c) and (6.1d), are very similar, we restrict our analysis to (6.1c), but the reasoning for (6.1d) is analogue. While the left-hand side only only consists of the time derivative of $\alpha_1$, which is complex but has a one-to-one correspondence to the momentum field and is strongly related to the polar order field (see section 5.4.1), the right hand side encodes the dynamics of this change. The first two terms with prefactors $\mu_A$ and $\xi_A$ are active matter based and have no correspondence in the Navier Stokes equations. They indicate the flocking and ordering of particles depending on the noise and alignment properties. In contrast to the one species system Bertin et al. [6] treated, these properties depend not only on the density of their own species, but also on the density of the second one. This is encoded in the factor $\mu_A(\alpha_0, \beta_0)$. The third term is the viscous damping, with the only difference to the Navier Stokes equation being the $\alpha_0$ dependency of $\nu_A$. The forth term can be rewritten together with party of the las two terms to form the pressure gradient, again with the only difference to the classical Navier Stokes equation lying in the density dependency of a prefactor. The remaining parts of the last two terms convey the non-linear coupling of the flow field to itself. In contrast to the Navier Stokes equation the active matter hydrodynamic equations are not Galilei invariant anymore. The reason for this lies in the fact that particles always move with velocity $v_0$ relative to the stationary surface they travel on we therefore restrict our frame of reference, which destroys Galilei invariance.

Because the density equations (6.1a-b) are still exact and we have already shown the conservation of the density $\rho$ taken over the whole system, this is also valid for our hydrodynamic equations. This means while locally neither $\alpha_0(\mathbf{r})$, $\beta_0(\mathbf{r})$ nor $\rho(\mathbf{r})$ are conserved and even globally the amount of species $A$ and $B$ can vary, the overall density density conservation guarantees that we can use the average of $\rho$ as a control parameter to describe the system.

## 6.2 Homogeneous Solutions

With our simplified system of equations (6.1a-d) we can find solutions by assuming that our fields are spatially homogeneous, therefore all spatial derivatives vanish and we remain with

$$\partial_t \alpha_0 = \tau(\beta_0 - \lambda\alpha_0)\beta_0\alpha_0 \tag{6.2a}$$

$$\partial_t \alpha_1 = (\mu_A - \xi_\alpha|\alpha_1|^2)\alpha_1 \tag{6.2b}$$

$$\partial_t \beta_0 = -\tau(\beta_0 - \lambda\alpha_0)\alpha_0\beta_0 \tag{6.2c}$$

$$\partial_t \beta_1 = (\mu_B - \xi_\beta|\beta_1|^2)\beta_1. \tag{6.2d}$$

The overall density $\rho = \alpha_0 + \beta_0$ is still conserved, as can be easily seen by adding (6.2a) to (6.2c):

$$\partial_t \rho = \partial_t \alpha_0 + \partial_t \beta_0 = 0 \tag{6.3}$$

If we now set the left hand side of (6.2a-d) to zero, we can find the fixed points of these equations

$$a \equiv \alpha_0^{fp} = \begin{cases} 0 \\ \rho \\ \rho\frac{1}{1+\lambda} \end{cases} \qquad b \equiv \beta_0^{fp} = \begin{cases} \rho \\ 0 \\ \rho\frac{\lambda}{1+\lambda} \end{cases}$$
$$w \equiv \alpha_1^{fp} = \begin{cases} 0 \\ \sqrt{\frac{\mu_A}{\xi_A}}e^{i\phi_A} \end{cases} \qquad u \equiv \beta_1^{fp} = \begin{cases} 0 \\ \sqrt{\frac{\mu_B}{\xi_B}}e^{i\phi_B} \end{cases} \tag{6.4}$$

$\phi_A, \phi_B \in [0, 2\pi]$ are complex phases which indicate the direction the species is travelling via the relations $w = w_x + iw_y$ and $u = u_x + iu_y$. The symmetries of these equations and therefore the fixed points enable us to only consider the behavior of species $A$ as representative for the whole system. The three different density fixed points together with the zero velocity fixed point we recognize from our analysis of the full Fourier transformed Boltzmann equations. For our purposes only the fixed point $a = \rho\frac{1}{1+\lambda}$ is relevant, because the others are, as we have already shown, unstable. This is also evident from our agent based simulation as we only see mixed states of both species $A$ and $B$ present with a ratio $\delta = b/a \simeq \lambda$.

We also have a new solution with non-zero momentum $\sqrt{\mu_A/\xi_A}$ which becomes valid if both $\mu_A > 0$ and $\xi_A > 0$. For small noise values both factors are positive and $\mu_A$ is the first to switch sign with either increasing noise or decreasing density. To reduce the number of free parameters we set $\sigma = \sigma_0$, which can be understood as setting the diffusion noise equal to the alignment noise. This does not alter the phenomenological outcome [7]. For noise values $\sigma > \sqrt{2\ln(3/2)} \approx 0.901$ we get $\mu_A < 0$ regardless of the density $a$ (see Appendix A.5) and the non-zero momentum fixed point vanishes. For even higher noise $\sigma > \sqrt{2\ln(5/2)} \approx 1.35$, $\xi_A$ becomes negative and the fixed point reappears theoretically. This regime is not physically sensible anymore because it would refer to the fact that with higher noise the hydrodynamic velocity field would become more ordered and grow without boundary for certain density values. This solution is an artefact of our approximation and can therefore be neglected.

It can be shown that noise and density can both be control parameters of the system [7] and it doesn't make a phenomenological difference if we use $\sigma$ or $\rho$, as long as we are in the regime of $0 < \sigma < \sqrt{2\ln(3/2)}$. In the future we will only work in this regime, so $\xi_A > 0$ and $\mu_A$ can, for large enough densities, take on positive values. This critical density, which guarantees the existence of the non-zero momentum fixed point, can be obtained by plugging in the density fixed point

$$a = \rho\frac{1}{1+\lambda} \qquad b = \rho\frac{\lambda}{1+\lambda} \tag{6.5}$$

into $\mu_A$

$$\mu_A(a, b) = P_{0,1} - 1 + (A_{0,1} + A_{1,1})\rho\frac{1}{1+\lambda} \tag{6.6}$$

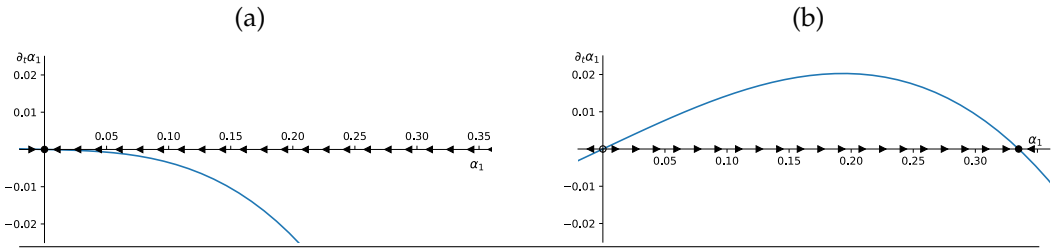


FIGURE 6.1: Fixed point and flow structure of the zero and non zero velocity cases. (*a*) The momentum field $\alpha_1$ plotted against its temporal derivative $\partial\alpha_1$, for $\rho = 0.4$, $\lambda = 1$. The arrows indicate the flow towards the only stable fixed point at $\alpha_1 = 0$. (*b*) Same as (a), but now $\rho = 1$. The zero velocity fixed point becomes unstable in this scenario and the flow points towards the stable fixed point $w$.

and setting it equal to zero. With the same calculations for species $B$ the critical densities then read

$$\rho_{crit,\alpha} = \frac{1 - P_{0,1}}{A_{0,1} + A_{1,1}} (1 + \lambda) \tag{6.7a}$$

$$\rho_{crit,\beta} = \frac{1 - P_{0,1}}{A_{0,1} + A_{1,1}} \left(1 + \lambda^{-1}\right). \tag{6.7b}$$

A visualization of the two relevant cases and their flow for species $A$ with the density either $\rho < \rho_{crit,\alpha}$ ($\hat{=}\mu_A < 0$) and $\rho > \rho_{crit,\alpha}$ ($\hat{=}\mu_A > 0$) can be found in fig. 6.1a and fig. 6.1b, respectively.

Here it is easy to see, that for low densities the zero velocity fixed point is stable but for high densities it becomes unstable and the non-zero velocity fixed point is stable. This leads to the bifurcation structure of fig. 6.2, where the fixed points $w$ and $u$ in relation to the density $\rho$ are shown. The four different figures refer to four different values of $\lambda$. The larger $\lambda$ gets, the more the bifurcation points get shifted apart, $\rho_{crit,\alpha}$ to the left and $\rho_{crit,\beta}$ to the right. The dotted lines along the $\rho$-axis, originating at the bifurcation points indicate the unstable region of the zero velocity fixed point. The two green lines in fig. 6.2a indicate the slices where fig. 6.1a and fig. 6.1b lie.

## 6.3 Inhomogeneous Perturbations

Until now we only looked at homogeneous solutions for, and homogeneous perturbations to the hydrodynamic equations. While this is a good way to get insight into the dynamics at play, it fails to capture the whole picture. Even though there is no solution available to the full system of hydrodynamic equations, we can still analyze inhomogeneities by adding space-dependent perturbations to our homogeneous fixed points and check the stability and evolution of the resulting equations. We can then make the ansatz

$$\begin{aligned} \alpha_0(\mathbf{r}, t) &= a + \delta a(\mathbf{r}, t) & \beta_0(\mathbf{r}, t) &= b + \delta b(\mathbf{r}, t) \\ \alpha_1(\mathbf{r}, t) &= w + \delta w(\mathbf{r}, t) & \beta_1(\mathbf{r}, t) &= u + \delta u(\mathbf{r}, t) \end{aligned} \tag{6.8}$$

with $a$, $b$, $w$, $u$ the homogeneous fixed points of $\alpha_0$, $\beta_0$, $\alpha_1$, $\beta_1$, respectively and $\delta a$, $\delta b$, $\delta w$, $\delta u$ the inhomogeneous perturbations. We plug this into the hydrodynamic equations (6.1a-d) and expand to first order.

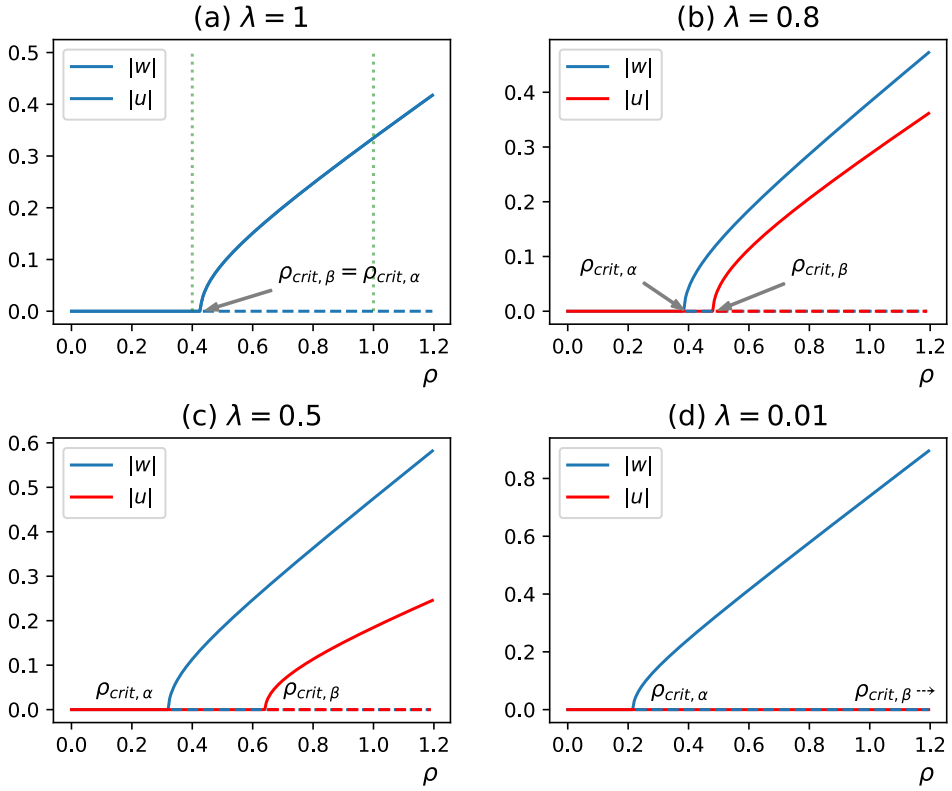


FIGURE 6.2: Bifurcation structure of $w$ and $u$ with $\sigma = \sigma_0 = 0.5$ (*a*) For $\lambda = 1$ the bifurcation for $w$ and $u$ overlap, as the species are equally strong. For $\rho < \rho_{crit,\alpha} = \rho_{crit,\beta}$, the velocities are $w = u = 0$. As soon as $\rho > \rho_{crit,\alpha} = \rho_{crit,\beta}$ we get the homogeneously stable solution $w = u = \sqrt{\mu_A/\xi_A} = \sqrt{\mu_B/\xi_B} > 0$. The zero branch gets unstable for $\rho > \rho_{crit,\alpha}$ (dashed line). The green lines mark the position of fig. 6.1a and fig. 6.1b. (*b*), (*c*),(*d*) With $\lambda < 1$ we get $\rho_{crit,\alpha} < \rho_{crit,\beta}$ as the two bifurcations split and drift apart with decreasing $\lambda$. We still have the regime of $w = u = 0$ for $\rho < \rho_{crit,\alpha}$ and $w = \sqrt{\mu_A/\xi_A}$, $u = \sqrt{\mu_B/\xi_B}$ for $\rho > \rho_{crit,\beta}$, but now get a new area where $u = 0$ still, but $w = \sqrt{\mu_A/\xi_A} > 0$ for $\rho_{crit,\alpha} < \rho < \rho_{crit,\beta}$.

To analyze the stability of the fixed points, we then employ a plane wave ansatz with wave vector $\mathbf{q}$, which leads to a Jacobian matrix whose eigenvalues indicate the stability. A more detailed derivation of this can be found in Appendix A.4 or in [33].

### 6.3.1 Stability: Eigenvalues of Jacobian Matrix without game

The Jacobian matrix for the ordered homogeneous as well as for the isotropic fixed point yields six eigenvalues $s_{1-6}$, which are dependent on the density $\rho$, the game parameters $\tau$ and $\lambda$, the wave vector of the perturbations $\mathbf{q}$ and noise $\sigma$. Without loss of generality we choose that the velocity of $A$ encoded in $w$ points in $x$-direction. We start with the case of $\tau = 0$, $\lambda = 1$, which corresponds to a switched off game with an equal distribution of species $A$ and $B$. This means the system decouples and we have two independent active matter species. These behave exactly alike and we can therefore just observe species $A$ for now. Because there is a correspondence between $\sigma$ and $\rho$ in active matter systems as mentioned before, we can fix $\sigma = 0.5$ and still get

a full picture of the dynamics in the system [7]. We are now left with the eigenvalues $s_{1-3}(\rho, \mathbf{q})$ as functions of the density and wave vector corresponding to species $A$. Analysis shows that positive eigenvalues and therefore instabilities occur first and strongest for $\mathbf{q} \parallel \binom{1}{0}$, when the inhomogeneity points in the same direction as the velocity. We can now track the largest eigenvalue $s(\rho, q)$ as a function of $\rho$ and the absolute value of $\mathbf{q}$, $q = |\mathbf{q}|$ (fig.: 6.3).

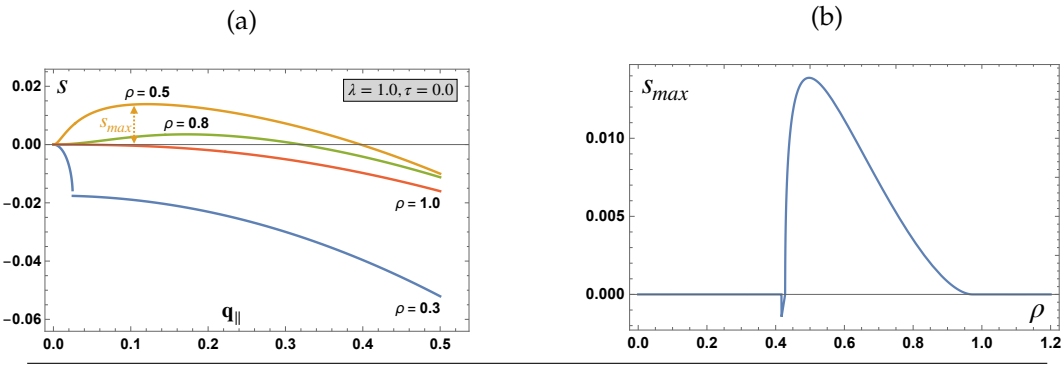


FIGURE 6.3: The maximum eigenvalue of the Jacobian matrix without game. $(a)$ $s(q)$ as a function of $q$ for different densities $\rho$. Densities below $\rho \lesssim 0.42$ correspond to the isotropic fixed point, while densities above show non-zero velocities. $(b)$ Maximal value of $s_{max}(\rho) = max_q s(\rho, q)$ over all $q$. Again, $\rho \lesssim 0.43$, shows no instability and corresponds to the isotropic regime, with the unstable order above until, for high densities, the system gets stable again

For $\rho$ between $\approx 0.43$ and $\approx 0.98$ we get $s_{max} > 0$ and therefore the system is unstable under inhomogeneous perturbations. Below and above these densities ($\rho_{crit}$ and $\rho_{dh}$) the system is stable in the isotropic and ordered regime, respectively. The unstable regime is where the transition from isotropic to ordered happens and can be associated with the onset of order in the system.

The eigenvector corresponding to $s_{max} > 0$ gives the direction of the instability and reads

$$\mathbf{v} = \begin{pmatrix} \delta a \\ \delta w \\ \delta w^* \end{pmatrix} = \begin{pmatrix} v_a \\ v_w \\ v_w \end{pmatrix} \tag{6.9}$$

with the factors dependent on the specific value of $\rho$. Because $\delta w = \delta w^*$ and the relation to the velocity field in position space $w = w_x + i w_y$ we can infer that the eigenvector $\mathbf{v}$ points in the same direction as the instability wave vector $\mathbf{q}$ and the velocity of the system.

If we account for the fact that the densities for each species are $\rho/2$, because $\lambda = 1$, these results are in perfect agreement with [7]. This comes to no surprise as the system without game reduces exactly to the one e.g. Bertin et al. analyzed. The main findings were:

- For low densities $\rho < \rho_{crit}$ there is no order in the system and the isotropic homogeneous solution is stable against homogeneous and inhomogeneous perturbations.
- For densities above $\rho_{crit}$ the homogeneous ordered solution is unstable against inhomogeneous perturbations and leads to the formation of wave-like patterns which travel through the system with isotropic regions in between. The instability is largest for perturbations parallel to the direction of motion.

- For very high densities the homogeneous ordered solution becomes stable again with velocity $\sqrt{\mu/\xi}$ against homogeneous and inhomogeneous perturbations.

Even though we did just recover results of previous analysis, it is still valuable to mention them for two reasons: We see that in the limit case of no game we recover the base model again and we can compare findings we make with this base model now.

We can also draw comparisons to the agent based simulation, where we see three phenomenologically different regions as well: For low densities and high noise there is no order in the system and we see an isotropic homogeneous state. After we cross the threshold density $\rho_{crit}$ or threshold noise $\sigma_t$ we observe waves in the system. This corresponds to the region of instability and positive eigenvalues in the hydrodynamic analysis. For even higher values of $\rho$, we see a clustered but uniformly moving system in the simulations, while the eigenvalues indicate a stabilization of the non-zero velocity fixed point.

### 6.3.2 Stability: Eigenvalues of Jacobian Matrix with game

In the next step we switch on the game by setting $\tau \neq 0$, while still keeping $\lambda = 1$ at first. The degeneracy in the eigenvalues vanishes and we get a single maximum eigenvalue $s$ (fig.: 6.4a). We find a regime with positive maximum eigenvalue $s_{max}$. This regime is independent of $\tau$, except for the limit of very small $\tau$ (fig.: 6.5a), which corresponds to the transition to no game again. Below the critical density of $\rho_{crit,\alpha} = \rho_{crit,\beta} \approx 0.43$ the system displays no order and the homogeneous isotropic fixed point is stable. Above $\rho_{dh,\alpha} = \rho_{dh,\beta} \approx 0.98$ the system becomes stable again in the ordered homogeneous state. In between we expect wave pattern formation, as the results mirror the case without game.

We want to study the case of $\lambda \neq 1$ next. The species are now unequally strong and therefore their ratios and critical densities differ. This results in interesting stability structures which depend on the values of $\lambda$ and $\tau$ not just quantitatively but also qualitatively (fig. 6.4b and fig. 6.5). Depending on the value of $\lambda$, we can observe an unstable band, which splits into bands two for small enough $\lambda \lesssim 0.55$ and correspondingly strong enough $\tau$. We therefore see up to five different regions, two of them unstable, three stable. We can identify the first stable region with the smallest values of $\rho$ with the isotropic state of both species and the region with the highest values of $\rho$ with the regime where both species are ordered. The two unstable bands correspond to the regions where $\rho_{crit,\alpha} < \rho < \rho_{dh,\alpha}$ for the lower band and $\rho_{crit,\beta} < \rho < \rho_{dh,\beta}$ for the upper. These regions are mutually exclusive for small enough values of $\lambda$ in the sense that $\rho_{dh,\alpha} < \rho_{crit,\beta}$, which explains the emergence of two unstable bands. The onset of order, equivalent with the first unstable region happens earlier for smaller values of $\lambda$. This is due to the fact that for small $\lambda$ the density $\rho_{crit,\alpha}$ decreases. The stable band in the middle is caused by the a state where species $A$ is already ordered while species $B$ is still isotropic. The game interaction stabilizes the system in this region, evident by the fact that for larger values of $\tau$ the stable band gets broader. The limit of $\tau \to 0$ always recovers the standard pure active matter system, as expected.

In summary, we see up to five regions:

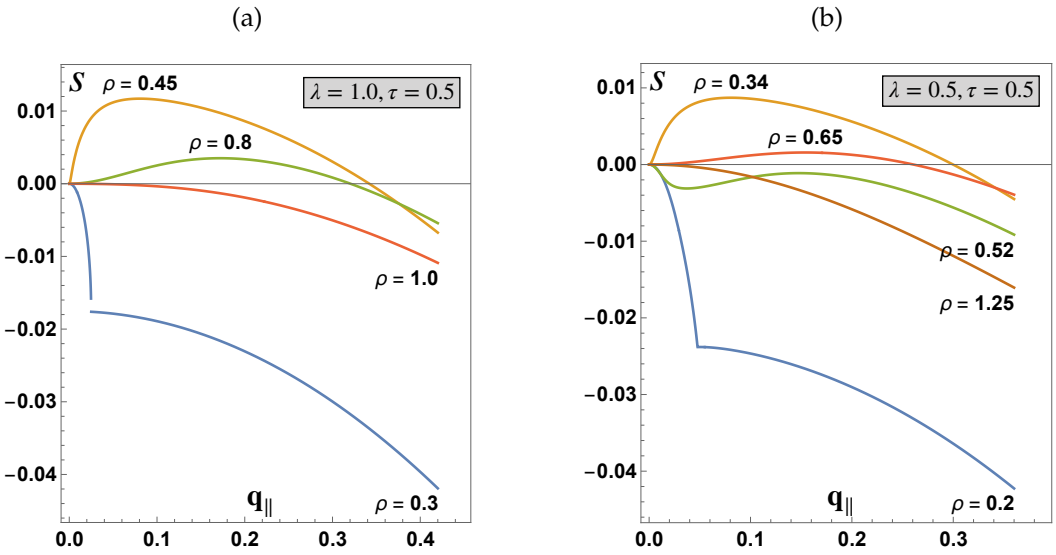


FIGURE 6.4: The maximum eigenvalue of the Jacobian matrix with game. $(a)$ $s(q)$ as a function of $q$ for different densities $\rho$ with $\lambda = 1.0$. Densities below $\rho \lesssim 0.42$ correspond to the isotropic fixed point, while densities above exhibit non-zero velocities. $\rho_{crit,\alpha} = \rho_{crit,\beta} \approx 0.43$, $\rho_{dh,\alpha} = \rho_{dh,\beta} \approx 0.98$ $(b)$ Like (a), but $\lambda = 0.5$ now. $\rho_{crit,\alpha} \approx 0.32$, $\rho_{dh,\alpha} \approx 0.51$, $\rho_{crit,\beta} \approx 0.64$ and $\rho_{dh,\beta} \approx 1.2$

( I ) Both species are isotropic and homogeneous

(II) The fixed point of $w > 0$ and $u = 0$ becomes unstable. Order begins to emerge in the system, presumably with wave pattern formation (in analogy to pure active matter case)

(III) Species $A$ is ordered and homogeneous, while species $B$ is still isotropic ($w > 0$, $u = 0$)

(IV) $w > 0$ and $u > 0$, though unstable, probably with wave pattern formation

( V ) Species $A$ and $B$ are both homogeneous and ordered

These five regions are the hydrodynamic equivalent to the five phases we have seen in the agent based simulation with a few distinct differences. It is generally difficult to make quantitative comparisons between the two approaches. This is evident by the fact that even for parameters which should have a one to one correspondence e.g. $\lambda$ we see the five phases only up to $\lambda \approx 0.3$ in the agent based simulations, while they are already visible in the hydrodynamic analysis at $\lambda \approx= 0.55$. This could be due to different model implementations e.g. the difference of binary versus multiparticle collisions or due to nonlinear effects not accounted for in the linear stability analysis. We also note that the Boltzmann and hydrodynamic descriptions are approximations and use assumptions which could be violated in the system and therefore lead to inexact results. We therefore mainly resort to qualitative comparisons between the two approaches.

A very clear difference between the agent based and the hydrodynamic results already evident here is that in OP2 we see uniformly moving, but spatially clustered particles. The hydrodynamic description on the other hand predicts a homogeneous distribution again. We also see species separated bands in OP2, which are incompatible with the spatial homogeneity of region (V).

We can't draw any conclusions about species separation in region (IV), as the fixed point is unstable, but we will see in chapter 7 that the spot or band order is a phenomenon of the agent based description only. This is due to the spatially extended implementation of the interactions in the simulations, while in the Boltzmann description interactions are completely local.

Apart from these differences, the agent based simulations and the hydrodynamic description agree overwhelmingly.

**Eigenvectors**

To analyze the direction the instability exhibits, we need to evaluate the eigenvector of $s_{max}$ again. We can write it in a general form as

$$\mathbf{v} = \begin{pmatrix} \delta a \\ \delta b \\ \delta w \\ \delta w^* \\ \delta u \\ \delta u^* \end{pmatrix} = \begin{pmatrix} v_a \\ v_b \\ v_w \\ v_w \\ v_u \\ v_u \end{pmatrix} \tag{6.10}$$

We therefore have the growing instability pointing parallel to the disturbance $\mathbf{q}$ and the macroscopic velocities.

For $\lambda = 1$ we the system is similar to the one without game except for one crucial fact:

While in the case of no game the velocities of the two species $w$ and $u$ pointed in uncorrelated directions, we now find $w \parallel u$ at the onset of order where $s_{max} > 0$. This coupling is enforced by the game theoretical interaction in an inhomogeneous regime where the densities approach the game theory fixed point locally. If these inhomogeneities now move through the system, they have to move in the same directions to still obey the ratio given by $\lambda$ locally. This directional alignment is a general phenomenon of the game theoretical interaction and independent of the value of $\lambda$. We have seen this already in the agent based simulations, where the motion of both species synchronizes as soon as the game theoretical interaction is switched on.

If we now set $\lambda \neq 1$, we always get a parameter regime where $w, u > 0$ and species $A$ would be stable at the ordered fixed point for the case without game, while the species $B$ fixed point would be unstable. This regime corresponds to the upper unstable band (for $\lambda \lesssim 0.55$, so that the bands are distinct) or at least the upper region of the unstable band (for $0.55 \lesssim \lambda < 1$). Even though species $A$ should be stable, the eigenvector indicates an instability in $w$. This means that the game induces an instability in the otherwise stable fixed point of species $A$.

A similar effect happens for the lower band (or lower region of the joined bands), where $w > 0$, $u = 0$ and the eigenvector of $s_{max}$ displays an instability in $w$-direction as well as in $u$-direction. This means that the game induces a motion in species $B$ even though it would not form order on its own as evident by the fact that $\rho < \rho_{crit,\beta}$.

We can therefore conclude that the coupling between the species through their game theoretical interaction induces a change in their active matter behavior. This can again be linked to results of the simulations, the induced waves in WP1 and WP2.

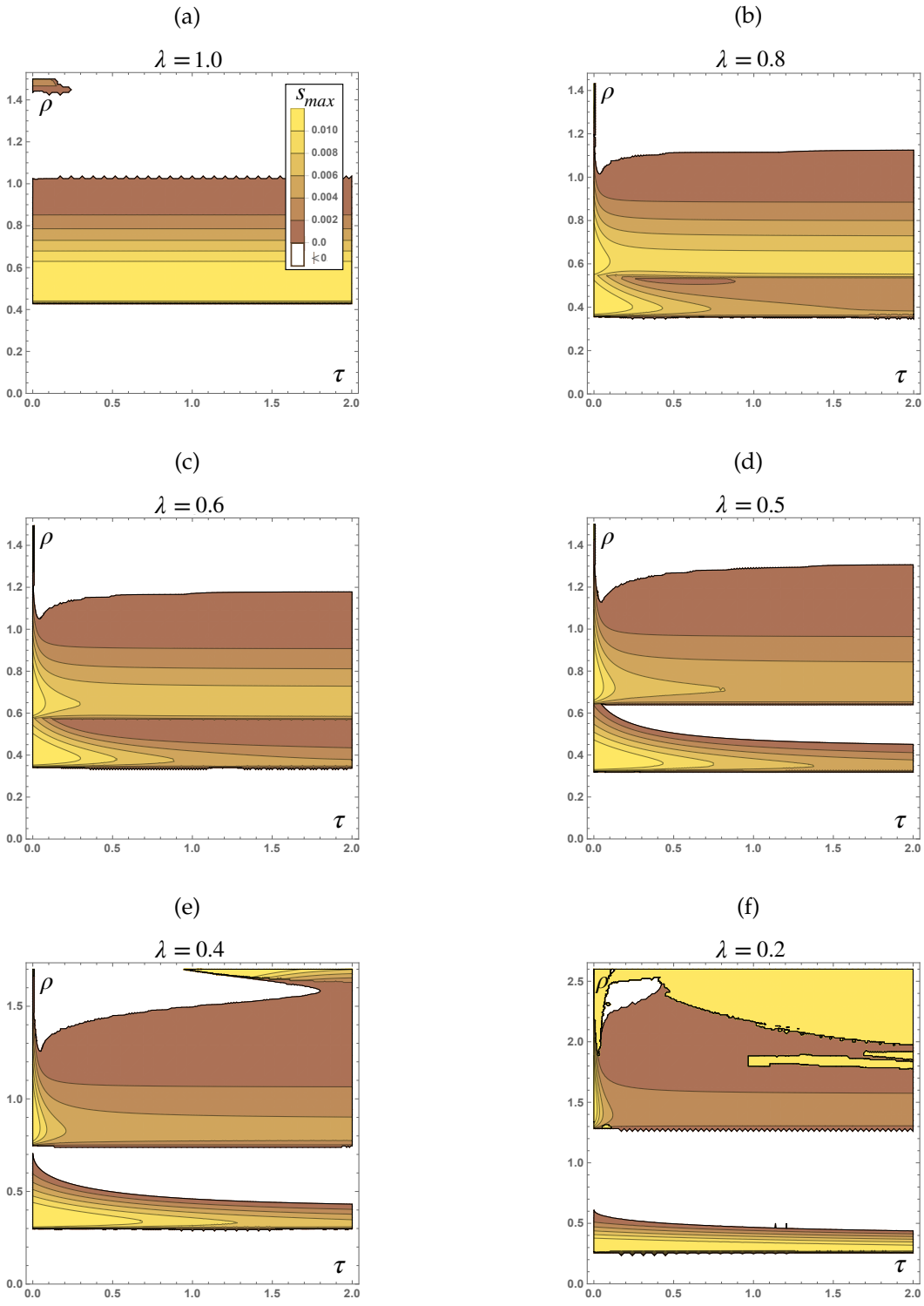


FIGURE 6.5: Maximal Eigenvalue $s_{max}$ as a function of $\rho$ and $\tau$ for six different values of $\lambda$. White areas indicate negative $s_{max}$, while the color coded regions correspond to $s_{max} > 0$ with darker colors referring to higher values of $s_{max}$ (*a*) $\lambda = 1$: $\tau$ has no influence on $s_{max}$, very similar to the case without game. (*b*), (*c*) $\lambda = 0.8$ and $\lambda = 0.6$: The unstable regions broadens, $\tau$ begins to show influence on $s_{max}$. (*d*) $\lambda = 0.5$: The stable band between the two instabilities emerges. (*e*), (*f*) $\lambda = 0.4$ and $\lambda = 0.2$: The stable band broadens

# Chapter 7

# Simulation and Analysis of the Hydrodynamic Equations

## 7.1 The Algorithm

We turn to a numerical simulation of the hydrodynamic equations (6.1a-d) in order to check the results of the agent based simulation. We start by making the system discrete and imposing a two dimensional grid with periodic boundary conditions. The spatial derivatives are then replaced by their finite difference approximations and time evolution is done via a 4th order Runge-Kutta method. For further details regarding the implementation and a more detailed discussion of the results presented in this chapter, see [33].

## 7.2 Results and Comparison to the Agent Based Simulation

### 7.2.1 The Five Phases and the Density Shift

Starting with the knowledge in mind that the linear stability analysis in section 6.3 revealed up to 5 different stability regions for our system, we try to study these numerically. We use $\rho$ as a system control parameter and keep $\sigma = \sigma_0 = 0.5$ fixed in contrast to the agent based approach, where the noise was the control parameter. The agent based simulation revealed the five phases IHP, WP1, OP1, WP2 and OP2 for small values of $\lambda$ (see section 4.3.1). These five phases also appear in the hydrodynamic simulation (wave phases see fig. 7.1 and fig. 7.2).

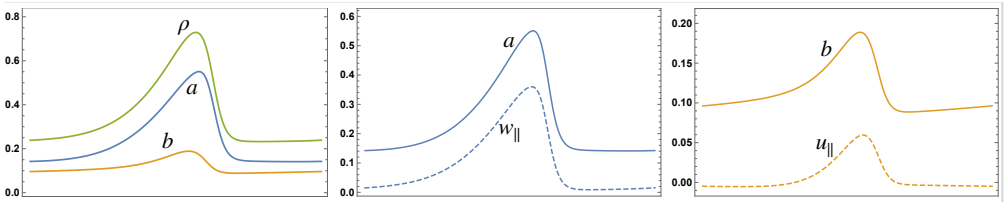


FIGURE 7.1: Wave profile for WP1 with $\rho = 0.35$, $\lambda = 0.4$ and $\tau = 1$. All plots show a spatial slice of the system with constant $y$ on the x-axis. The y-axis gives just the density for the left plot, density and velocity order for the right and middle column of plot. Species $A$ induces the wave in $B$.

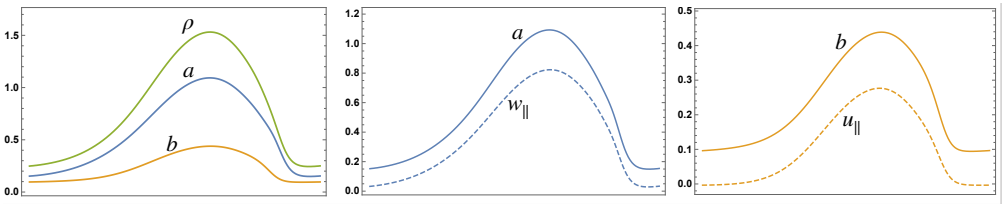


FIGURE 7.2: Wave profile for WP2 with $\rho = 0.80$, $\lambda = 0.4$ and $\tau = 1$. Species $B$ induces the wave in $A$.

For increasing $\lambda$ the phases start to blend into each other and OP1 vanishes. It can also happen that multiple waves of the same shape travelling with equal velocity form. W.l.o.g. we assume the waves to travel in x-direction. We can then only look at a slice of the system in x-direction, because the wave is symmetric along the y-axis. The shape of the wave is asymmetric with a very steep front and more shallow tail at the end. This tail gets broader with increasing values of $\rho$, similar to the agent based results, while the wave also gets higher (fig. 7.3).

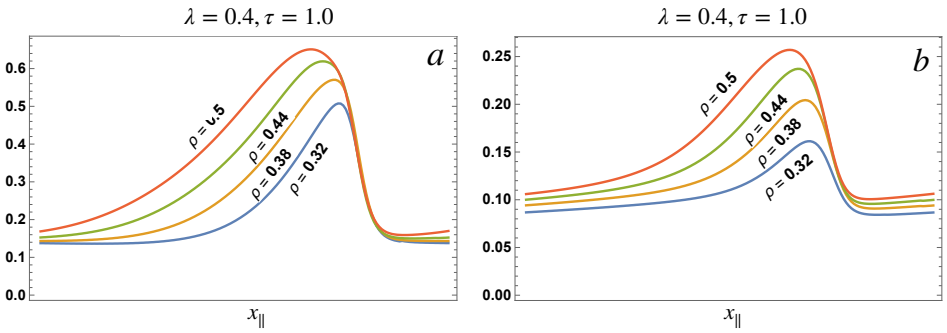


FIGURE 7.3: Wave increase with $\rho$. The system is in WP2, both waves increase and get broader with increasing $\rho$.

In contrast to the agent based simulation we do not observe species separating spatial patterns. This is due to the fact that the game theoretical interaction in the agent based simulation averages the relative amounts of particles over a circle with radius $d_{gt}$, while in the hydrodynamic simulation the densities are completely local variables. But in the wave phases WP1 and WP2 we still observe a density shift for a different reason: While the waves are travelling through the system, the game theoretical interaction takes time to adapt to the ever changing densities $a$ and $b$ and realize the optimal ratio $\lambda$ again. This results in a wave delay between the wave forming from the active matter interaction and the induced wave from the game. This effect gets stronger for smaller values of $\tau$, so when the game is weaker. This is line with expectations, because a weaker game takes longer to readjust the ratio of $a$ to $b$. This wave delay and also the fact that the waves and therefore their local deviations from the optimal ratio $\lambda$ are not symmetric, leads to a shift in the ratio $\delta = b/a$. This ratio shifts away from the fixed point and increases for WP1, while it decreases for WP2 (fig. 7.4).

The density shift increases for larger values of $\lambda$ and smaller values of $\tau$. It can even happen that this wave induced ratio shift inverses the outcome of the game in the sense that we get $\delta > 1$ while $\lambda < 1$, so the weaker species from a game perspective

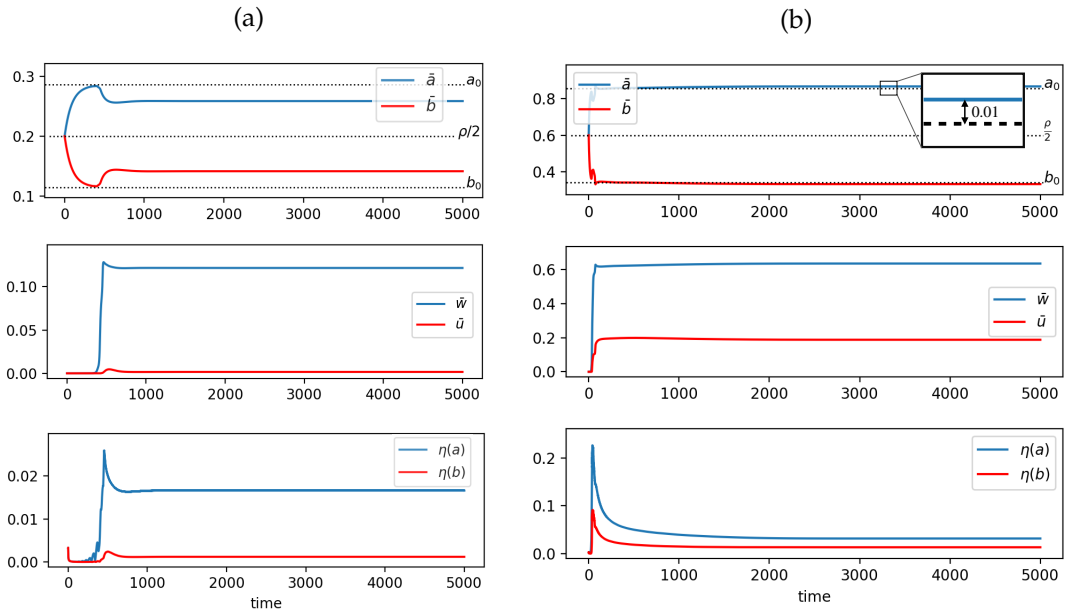


FIGURE 7.4: The wave induced density shift for $\lambda = 0.4$ and $\tau = 0.2$. All plots share their abscissa in units of simulation time T. First row: density, second row: velocity order, third row: inhomogeneity parameter $\eta$ ($a$) In WP1 the ratio $\delta = b/a$ increases as evident from the first plot. In comparison with the other two plots we can see that the density shift emerges as the waves appear. ($b$) For WP2 we get a density shift with wave formation as well, but smaller and in the other direction, so $\delta$ decreases.

comes out on top. For a more detailed explanation, an analytic ansatz and further discussion of these effects, see [33].

We couldn't reproduce this effect in the agent based simulation yet, due to the fact that we already observe a density shift from the spot order. Because of the species separation which occurs with the spot order and the extended area the agent based game averages over the effects stemming from the wave delay are suppressed. It would be interesting to see if the effect can be reproduced or confirmed through further agent based studies.

### 7.2.2 The Bifurcation Structure

While we have observed the five phases in both simulations and in the linear stability analysis, we can go further with the hydrodynamic simulation and check for hysteresis effects at the transitions between different phases. This is achieved by putting the system in different initial states and then slowly varying the parameters, especially the density $\rho$ to observe the parameter range of different phases. We measure the inhomogeneities in the system with parameters $\eta(a)$ and $\eta(b)$, the averages spatial variations over the system in $a$ and $b$, respectively. For $\eta = 0$ the system is in a homogeneous state, while $\eta > 0$ indicates pattern formation and inhomogeneities.

The pure active matter case with no game reveals hysteresis for both transitions (fig. 7.5a), in agreement with [40] [52].

If we switch on the game and start with parameters $\lambda = 0.4$, $\tau = 0.2$, we observe hysteresis effects at all transitions. This means the phases are bistable in the overlapping regions. If we for example start in WP1 and decrease $\rho$ quasi-statically, the

system remains inhomogeneous even below $\rho_{t,a}$, the density at which the IHP becomes unstable according to the linear stability analysis. The wave collapses after crossing $\rho_{i,a}$ (fig. 7.5b). The same behavior can be observed at all transitions with the phases stability extended beyond their point of linear stability. This happens due to the non-linear nature of the system and is an indicator for first order phase transitions [40] [52].

For increased $\tau$ the overlapping regions get wider and ultimately the branches of the two wave phases merge at $\tau \approx 1$ (fig. 7.5c). This corresponds to a state where OP1 can only be reached through the right initial conditions and not through a collapse of a wave phase anymore.

Alternatively, if we keep $\tau$ constant and sufficiently small and vary $\lambda$, we observe the branches getting wider and starting to overlap but not join as in the case for large $\tau$ before. We therefore have a tristable state in the system where both WP1 and WP2 as well as OP1 can be stable (fig. 7.5d). For a more detailed discussion see [33].

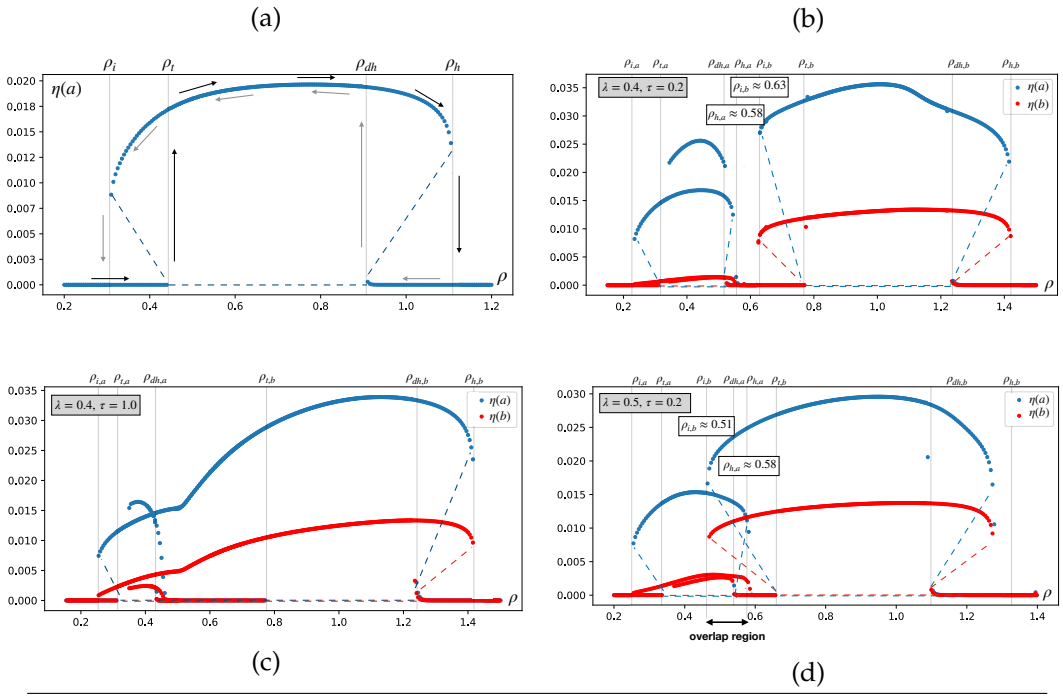


FIGURE 7.5: The different bifurcations and hysteresis effects in the system ($\rho$ against $\eta$). Solid lines mark stable branches and are generated from simulation data while dashed lines mark estimated unstable fixed points. (*a*) No game ($\tau = 0, a = b$). We see that both the transition from IHP to WP and from WP to OP show hysteresis effects. Following the arrows shows the flow in the system and the points where the system jumps to a different branch. (*b*) $\lambda = 0.4$, $\tau = 0.2$ The system shows hysteresis effects on all four transitions. The higher $\eta(a)$ in WP1 indicates multiple waves in the system and is the branch the system jumps to when decreasing $\rho$ starting in OP1. (*c*) Joined branches for $\lambda = 0.4$, $\tau = 1$. There is only one joined wave phase anymore consisting of a merge of WP1 and WP2. (*d*) Tristable states and overlapping wave phases for $\lambda = 0.5$, $\tau = 0.2$. Small $\tau$ prevent the branches from merging and we instead see multiple stable wave states in certain parameter regions.

# Chapter 8

# Summary and Outlook

We started this thesis with the open question of how an active matter system with multiple species interacting in a game theoretical scenario would behave. To probe this we developed a model of two active species interacting in a snowdrift game scenario. In contrast to previous active matter systems [57] [9], global densities of individual species are no longer conserved, while the different implementation of motility through self-propelled particles offers a distinction to earlier studies regarding spatially extended cooperator/defector games [22] [50].

In nature, there are many systems which involve both actively moving constituents that have to compete with other species for e.g. resources [12] [10] [13]. It is therefore an interesting question how such a combination can be modelled mathematically.

We chose a minimal model in order to keep results general while still observing phenomenologically rich behaviour. Starting with an agent based model, we implemented simulations on a continuous 2d surface populated by two species of active particles in a generalized Vicsek model [57]. Previous agent based simulations of one active species revealed pattern formation for Vicsek models with travelling wave states near the onset of order [9] [8].

For our system of two species we observe up to five different phases of isotropic, ordered or wave states in the system. If one species is much stronger than the other, resulting in a very high ratio of this species in the system, the onset of order for both species can be observed in distinct wave states for different noise values. Wave forming species induce waves in the other species as well through local game interactions. While in the first wave phase only the stronger species moves in an ordered fashion, the second wave phase displays order for both species. Located between the two wave states (when differentiating by noise/density values), we have found a state of uniform movement of the stronger species while the other species moves isotropically still. In the regimes above and below the wave states we find, similar to previous agent based simulations [9] a phase where the whole system moves uniformly or is completely isotropic, respectively.

For more equal games the ordered phase between the two wave phases vanishes and we observe a new, merged wave phase, where both species exhibit order as soon as the wave emerges. This wave is more distinct than the solo wave phases for more dissimilar games. A more equal game therefore stabilizes the active matter induced pattern formation.

We also observe species separated bands inside the system as soon as both species are ordered. This means that both the second wave phase and the uniformly ordered

phase have this property. For more equal games this effect gets stronger and can be observed best in the merged wave phase.

For very low motility the separation of species can also be observed for systems without active matter interaction. Depending on the relative game strengths we observe either the formation of species distinct spots or bands inside the system. We developed a 1d model to understand this phenomenon and probed the effect in 1d and 2d for its dependency on different parameters like motility, relative and absolute game strength. This separation of species also induces a shift in the ratio of species away from the well mixed fixed point towards a more equal distribution. While a similar effect has been observed to a degree in previous simulations of a snowdrift game on a lattice [22] [50], to our knowledge it was not studied in a continuous model before. Also, in distinction to lattice simulations, we observe the continuous formation of bands out of spots and the ratio shift is always in the direction of more equal outcomes in contrast to [22]. It would be subject to further studies to develop a 2d model for this effect, the formation of bands and prediction of spot and band sizes.

While these patterns vanish with increasing motility, they are restabilized in ordered systems of active matter, especially in the highly ordered wave bands of the merged wave phase.

To further verify results we achieved by the agent based simulations and point out differences where necessary, we also developed and implemented a model following a kinetic Boltzmann approach. This ansatz has proven useful more active matter in previous works [6] [7] [40]. We derived hydrodynamic equations and implemented a numeric simulations to compare results to the agent based approach. This approach, especially the numerical simulations and its results, is explained in more detail in [33] as a stand-alone model, while it has been used mainly as verification for the agent based approach in this thesis.

We could confirm the five phases for strongly uneven games, which merge again for disparities in the species ratios, similar to the agent based model. Through a study of the phase transitions we could observe hysteresis effects for all transitions. This could not yet be observed in the agent based approach due to implementation limitations. It would be task of further research to probe for hysteresis effects.

Because of differences in implementation, especially the local nature of the game interaction, the formation of spot and band order and the connected ratio shift could not be observed in the hydrodynamic approach. While we found a ratio shift also for the hydrodynamic simulations in wave phases, the effect is of different reason, namely in the interplay of the game theoretical interaction enforcing the ideal species ratio everywhere in the system while travelling wave bands constantly shift the ratio away from the game theoretical fixed point. If this effect is solely visible in the hydrodynamic simulations or hidden under the species separation induced ratio shift remains to be seen in further studies.

While this thesis only probed a few characteristics of this simple but phenomenologically rich system, we have seen interesting results stemming from the combination of active matter and evolutionary game theory. We believe there are still many results to be discovered and probed in systems like this which exceed the scope of this thesis but are possible starting points for further works in this direction.

# Appendix A

# Detailed Calculations

## A.1 Derivation of Fourier transformed Boltzmann terms

In chapter 5, we want to perform the Fourier transformation of

$$\partial_t \alpha\left(\mathbf{r},\theta,t\right) + v_0 \mathbf{e}(\theta)\partial_{\mathbf{r}}\alpha\left(\mathbf{r},\theta,t\right) = I_{dif}\left[\alpha\right] + I_{col}\left[\alpha,\alpha\right] + I_{gt}^{A}\left[\alpha,\beta\right] \tag{A.1}$$

in $\theta$ with Fourier representation

$$f\left(\mathbf{r},\theta,t\right) = \frac{1}{2\pi}\sum_{k=-\infty}^{\infty} e^{-ik\theta}\hat{f}_k(\mathbf{r},t) \;\text{ and }\; \hat{f}_k(\mathbf{r},t) = \int_{-\pi}^{\pi} d\theta\, e^{ik\theta} f\left(\mathbf{r},\theta,t\right), \tag{A.2}$$

$$\text{therefore } \int_{-\pi}^{\pi} e^{ik\theta} = 2\pi\delta_{k,0} \;\text{ and }\; \sum_{k=-\infty}^{\infty} e^{-ik\theta} = 2\pi\delta(\theta).$$

If we multiply every term in (A.1) by $e^{ik\theta}$ and integrate over $\theta$, we get the Fourier representation of the Boltzmann equation.

To simplify the notation, we suppress writing all dependencies of space and time, also, if not specified differently, all integrals have boundaries $-\pi$ to $\pi$ and sums run from $-\infty$ to $\infty$. For the first part we can easily write

- $\int d\theta\, e^{ik\theta}\partial_t\alpha(\theta) = \partial_t\hat{\alpha}_k$ .

Next, a little more involved, but also quite straightforward is the convection term. W.l.o.g. we choose $\mathbf{e}(\theta) = \begin{pmatrix}\cos(\theta)\\ \sin(\theta)\end{pmatrix}$ and write

- $$\begin{aligned}\int d\theta\, e^{ik\theta} v_0\mathbf{e}\cdot\partial_{\mathbf{r}}\alpha(\theta) &= v_0\int d\theta\, e^{ik\theta}(\cos(\theta)\partial_x + \sin(\theta)\partial_y)\alpha(\theta)\\ &= v_0\int d\theta\, e^{ik\theta}\tfrac{1}{2}\left(e^{i\theta}+e^{-i\theta}\right)\partial_x\alpha(\theta) + v_0\int d\theta\, e^{ik\theta}\tfrac{1}{2i}\left(e^{i\theta}-e^{-i\theta}\right)\partial_y\alpha(\theta)\\ &= \frac{v_0}{2}\partial_x\left(\hat{\alpha}_{k+1}+\hat{\alpha}_{k-1}\right) + \frac{v_0}{2i}\partial_y\left(\hat{\alpha}_{k+1}-\hat{\alpha}_{k-1}\right)\\ &= \frac{v_0}{2}\left((\partial_x - i\partial_y)\hat{\alpha}_{k+1} + (\partial_x + i\partial_y)\hat{\alpha}_{k-1}\right)\\ &= \frac{v_0}{2}\left(\nabla\hat{\alpha}_{k-1} + \nabla^*\hat{\alpha}_{k+1}\right),\end{aligned}$$

where we introduced the Fourier space derivatives $\nabla = \partial_x + i\partial_y$ and $\nabla^* = \partial_x - i\partial_y$.

Now we transform the terms $I_{dif}$, $I_{col}$ and $I_{gt}$:

- $$\begin{aligned}\int d\theta\, e^{ik\theta} I_{dif}\,[\alpha] &= -\int d\theta\, e^{ik\theta}\lambda\alpha(\theta) \\ &\quad + \int d\theta\, e^{ik\theta}\lambda \int d\theta' \int_{-\infty}^{\infty} d\eta\; P_0(\eta)\alpha(\theta')\delta_{2\pi}(\theta-\theta'-\eta) \\ &= -\lambda\hat{\alpha}_k + \lambda \int d\theta' \int_{-\infty}^{\infty} d\eta\; e^{ik(\theta'+\eta)} P_0(\eta)\alpha(\theta') \\ &= -\lambda\hat{\alpha}_k + \lambda\hat{\alpha}_k\hat{P}_{0,k} = \lambda(\hat{P}_{0,k}-1)\hat{\alpha}_k\end{aligned}$$

Here we used the Fourier transformation $\hat{f}_k = \int_{-\infty}^{\infty} dx\, \exp[ikx]\, f(x)$ to write the k-th Fourier mode of $P_0(\eta)$ as $\hat{P}_{0,k} = \exp(-k^2\sigma_0^2/2)$.

To get a more general understanding of the dynamics, the collision term will be evaluated for different collision partners and their dependent functions $\alpha$ and $\beta$. Furthermore we will split the calculation up into two parts $(I)$ and $(II)$ to get more manageable equations:

- $$\int d\theta\, e^{ik\theta} I_{col}\,[\alpha,\beta] = \overbrace{-\int d\theta\, e^{ik\theta}\alpha(\theta) \int_{\theta-\pi}^{\theta+\pi} d\theta'\; R(\theta,\theta')\beta(\theta')}^{(I)} + \underbrace{\int d\theta\, e^{ik\theta} \int d\theta_1 \int_{\theta_1-\pi}^{\theta_1+\pi} d\theta_2 \int_{-\infty}^{\infty} d\eta\; \alpha(\theta_1)\beta(\theta_2)R(\theta_1,\theta_2)P(\eta)\delta_{2\pi}\left(\theta - \tfrac{\theta_1+\theta_2}{2} - \eta\right)}_{(II)}$$

We use (A.2) to substitute in $\hat{\alpha}_k$ and $\hat{\beta}_k$

$$\begin{aligned}(I) &= -\frac{1}{(2\pi)^2}\int d\theta\, e^{ik\theta}\sum_q e^{-iq\theta}\hat{\alpha}_q \int_{\theta-\pi}^{\theta+\pi} d\theta' R(\theta,\theta')\sum_p e^{-ip\theta'}\hat{\beta}_p \\ &= -\frac{1}{(2\pi)^2}\int d\theta \int d\vartheta \sum_{q,p}\hat{\alpha}_q\hat{\beta}_p R(|\vartheta|)e^{i\theta(k-q-p)}e^{-ip\vartheta} \\ &= -\frac{1}{2\pi}\int d\vartheta\; \sum_{q,p}\hat{\alpha}_q\hat{\beta}_p R(|\vartheta|)\delta_{q,k-p}e^{-ip\vartheta} = -\frac{1}{2\pi}\sum_p \hat{\alpha}_{k-p}\hat{\beta}_p \int d\vartheta\, \cos(p\vartheta)R(|\vartheta|).\end{aligned}$$

At the second equality we make a change of variables for the second integral and introduce $\vartheta = \theta_2 - \theta_1$, after which we can integrate over $\theta$ and finally evaluate the sum over $q$ with help of $\delta_{q,k-p}$. We can split up $\exp(-ip\vartheta)$ into $\cos(p\vartheta) + i\sin(p\vartheta)$, where the latter term vanishes because $R$ is only dependent on the absolute value of $\vartheta$ and therefore symmetric, so the complete integrand is antisymmetric and therefore vanishes over symmetric integral boundaries.

The same substitutions and methods can be applied to the second part of the collision integral as well and we can write

$$\begin{aligned}
(II) =& \frac{1}{(2\pi)^2}\int d\theta \int d\theta_1 \int_{\theta_1-\pi}^{\theta_1+\pi} d\theta_2 \int_{-\infty}^{\infty} d\eta \sum_{q,p} e^{ik\theta} e^{-iq\theta_1} e^{-ip\theta_2} R(\theta_1,\theta_2) \\
&\qquad \times P(\eta)\delta_{2\pi}\left(\theta - \tfrac{\theta_1+\theta_2}{2} - \eta\right)\hat{\alpha}_q\hat{\beta}_p \\
=& \frac{1}{(2\pi)^2}\int d\theta_1 \int_{\theta_1-\pi}^{\theta_1+\pi} d\theta_2 \int_{-\infty}^{\infty} d\eta \sum_{q,p} e^{i\theta_1(k/2-q)} e^{i\theta_2(k/2-p)} e^{ik\eta} P(\eta) R(\theta_1,\theta_2)\hat{\alpha}_q\hat{\beta}_p \\
=& \frac{1}{(2\pi)^2}\int d\theta_1 \int d\vartheta \sum_{q,p} e^{i\theta_1(k-q-p)} e^{i\vartheta(k/2-p)} \hat{P}_k\hat{\alpha}_q\hat{\beta}_p R(|\vartheta|) \\
=& \frac{1}{2\pi}\int d\vartheta \sum_{q,p} \delta_{q,k-p} e^{i\vartheta(k/2-p)} \hat{P}_k\hat{\alpha}_q\hat{\beta}_p R(|\vartheta|) \\
=& \frac{1}{2\pi}\sum_p \hat{\alpha}_{k-p}\hat{\beta}_p\hat{P}_k \int d\vartheta \cos\left((\tfrac{k}{2}-p)\vartheta\right) R(|\vartheta|),
\end{aligned}$$

where we integrated over $\theta$ first to get rid of the $\delta$-distribution and used the definition of the k-th Fourier mode of $P(\eta)$, $\hat{P}_k = \exp(-k^2\sigma^2/2)$.

So in total we get for the collision term:

$$\int d\theta\, e^{ik\theta} I_{col}\,[\alpha,\beta] = (I) + (II) = \sum_p \hat{\alpha}_{k-p}\hat{\beta}_p A_{p,k}$$

$$\text{with}\;\; A_{p,k} \equiv \int \frac{d\vartheta}{2\pi} R(|\vartheta|)\left(\hat{P}_k \cos\left((\tfrac{k}{2}-p)\vartheta\right) - \cos(p\vartheta)\right) \tag{A.3}$$

The last remaining part to complete the Fourier representation of (A.1) is $I_{gt}$:

- $\int d\theta\, e^{ik\theta} I^A_{gt} = \int d\theta\, e^{ik\theta}(\tau_A b - \tau_B a) b\alpha(\theta) = (\tau_A\hat{\beta}_0 - \tau_B\hat{\alpha}_0)\hat{\beta}_0\hat{\alpha}_k$

We only demonstrated the transformation $I^A_{gt}$ here, but $I^B_{gt}$ works exactly the same way.

If we put everything together we are able to write down the complete Fourier representation. For convenience and to get rid of all constants we rescale the parameters s.t.

$$\begin{aligned}
t \to \tfrac{t}{\lambda} \qquad & \mathbf{r} \to \mathbf{r}\tfrac{v_0}{\lambda} \\
a \to a\rho_N \qquad & b \to b\rho_N
\end{aligned} \tag{A.4}$$

with $\rho_N = \frac{\lambda}{d_0 v_0}$. The remaining factors in $I_{gt}$ are then absorbed into $\tau_A$ and $\tau_B$, which are therefore rescaled as

$$\begin{aligned}
\tau_A &\to \tau_A \frac{d_0^2 v_0^2}{\lambda} \\
\tau_B &\to \tau_B \frac{d_0^2 v_0^2}{\lambda}.
\end{aligned} \tag{A.5}$$

This is equivalent to setting $\lambda = v_0 = d_0 = 1$. So in the end we arrive at

$$\begin{aligned}\partial_t\hat{\alpha}_k + \frac{1}{2}\left(\nabla\hat{\alpha}_{k-1} + \nabla^*\hat{\alpha}_{k+1}\right) &= (\hat{P}_{0,k} - 1)\hat{\alpha}_k + \sum_p \hat{\alpha}_{k-p}\hat{\alpha}_p A_{p,k} + (\tau_A\hat{\beta}_0 - \tau_B\hat{\alpha}_0)\hat{\beta}_0\hat{\alpha}_k \\ \partial_t\hat{\beta}_k + \frac{1}{2}\left(\nabla\hat{\beta}_{k-1} + \nabla^*\hat{\beta}_{k+1}\right) &= (\hat{P}_{0,k} - 1)\hat{\beta}_k + \sum_p \hat{\beta}_{k-p}\hat{\beta}_p A_{p,k} - (\tau_A\hat{\beta}_0 - \tau_B\hat{\alpha}_0)\hat{\alpha}_0\hat{\beta}_k.\end{aligned} \tag{A.6}$$

## A.2 Linear Stability of Isotropic Solution

Starting from the Fourier transformed Boltzmann equations, in chapter 5.4.2 we found the isotropic solutions for these equations. In the following we will analyze their linear stability a bit more detailed.

The fixed points are

$$\alpha_0^{fp} = \begin{cases} 0 \\ \rho \\ \rho\frac{1}{1+\lambda} \end{cases} \quad \beta_0^{fp} = \begin{cases} \rho & (I) \\ 0 & (II) \\ \rho\frac{\lambda}{1+\lambda} & (III) \end{cases} \tag{A.7}$$

To observe the behavior near these fixed points we add small perturbations $\delta\alpha_k(t)$, $\delta\beta_k(t)$ s.t. $\alpha_k(t) = \alpha_k^{fp} + \delta\alpha_k$ and $\beta_k(t) = \beta_k^{fp} + \delta\beta_k(t)$, substitute these into (5.15) and write down the first order equations

$$\begin{aligned}\partial_t\delta\alpha_k = \Big[&(P_{0,k} - 1) + (A_{k,k} + A_{0,k})\alpha_0^{fp} + \tau\left(\beta_0^{fp} - \lambda\alpha_0^{fp}\right)\beta_0^{fp} \\ &-2\tau\lambda\alpha_0^{fp}\beta_0^{fp}\delta_{0,k} - \tau\left(\beta_0^{fp} - \lambda\alpha_0^{fp}\right)\alpha_0^{fp}\delta_{0,k}\Big]\delta\alpha_k\end{aligned} \tag{A.8}$$

$$\begin{aligned}\partial_t\delta\beta_k = \Big[&(P_{0,k} - 1) + (A_{k,k} + A_{0,k})\beta_0^{fp} - \tau\left(\beta_0^{fp} - \lambda\alpha_0^{fp}\right)\alpha_0^{fp} \\ &-2\tau\alpha_0^{fp}\beta_0^{fp}\delta_{0,k} + \tau\left(\beta_0^{fp} - \lambda\alpha_0^{fp}\right)\beta_0^{fp}\delta_{0,k}\Big]\delta\beta_k.\end{aligned} \tag{A.9}$$

We can now check the stability of each fixed points by plugging in the three solutions $(I)$, $(II)$ and $(III)$:

- $(I)$: $\quad \alpha_0^{fp} = 0 \quad \beta_0^{fp} = \rho$

$$\partial_t\delta\alpha_k = \left[P_{0,k} - 1 + \tau\rho^2\right]\delta\alpha_k \tag{A.10}$$

to which the solution is an exponential function $\delta\alpha_k = \delta\alpha_k^0\exp[\mu t]$ with $\mu = P_{0,k} - 1 + \tau\rho^2$. This function and therefore the perturbation is growing when $\mu > 0$, which is equivalent to the fixed point becoming unstable. Because $P_{0,k}$ is the Fourier transformed noise, where the original distribution is $\geq 0$ everywhere and normalized, we have $P_{0,k} \leq 1$, therefore $P_{0,k} - 1 \leq 0$. Since $\tau\rho^2 \geq 0$, we can solve for a critical overall

density $\rho_{crit}$ from where on the fixed point becomes unstable.

$$\rho_{crit} = \sqrt{\frac{1 - P_{0,k}}{\tau}} \tag{A.11}$$

If we now set $k = 0$, we can see that the critical density is zero for this mode and therefore the fixed point is unstable for all $\rho$. For the second fixed point we get:

- $(II)$ : $\quad \alpha_0^{fp} = \rho \quad \beta_0^{fp} = 0$

for k=0:

$$\partial_t \delta\alpha_0 = \left[\tau\lambda\rho^2\right] \delta\alpha_0 \tag{A.12}$$

This mode is unstable again for $\rho > 0$. We could also have concluded this instability from the fact that the system is symmetric under the exchange of species $A$ and $B$ and the fixed points are symmetric as well. So therefore fixed point $(II)$ is nothing else than the mirror image of $(I)$ and has to be unstable as well. More interesting is the case of the third fixed point:

- $(III)$ : $\quad \alpha_0^{fp} = \rho\frac{1}{1+\lambda} \quad \beta_0^{fp} = \rho\frac{\lambda}{1+\lambda}$

for k=0:

$$\begin{aligned} \partial\delta\alpha_0 &= \left[-\tau\lambda\rho^2\frac{2\lambda}{(1+\lambda)^2}\right] \delta\alpha_0 \\ \partial\delta\beta_0 &= \left[-\tau\rho^2\frac{2\lambda}{(1+\lambda)^2}\right] \delta\beta_0 \end{aligned} \tag{A.13}$$

both of which are negative for all $\rho$ and therefore lead to a stable mode. For $k \neq 0$ in turn we get

$$\begin{aligned} \partial\delta\alpha_k &= \left[P_{0,k} - 1 + (A_{k,k} + A_{0,k})\rho\frac{1}{1+\lambda}\right] \delta\alpha_k \\ \partial\delta\beta_k &= \left[P_{0,k} - 1 + (A_{k,k} + A_{0,k})\rho\frac{\lambda}{1+\lambda}\right] \delta\beta_k \end{aligned} \tag{A.14}$$

with $P_{0,k} - 1 \leq 0$ again. Therefore it is crucial for the stability of the k-th mode if the second term is greater than zero. This comes down to the question if $A_{k,k} + A_{0,k} > 0$, because all other factors in the second term are positive. So if $A_{k,k} + A_{0,k} > 0$ for any $k$, we can find a critical density again which separates the regimes of stability and instability. This is indeed the case, but only for $k = 1$ and for certain values of noise variance $\sigma^2$, as shown in Appendix A.5

## A.3 Derivation of Hydrodynamic Equations

In chapter 6 we use a scaling ansatz to derive the hydrodynamic equations.

We introduce a parameter $\varepsilon$ and make the ansatz

$$\begin{aligned} \alpha_0 = \mathcal{O}(\varepsilon)\,, \quad \alpha_k &= \mathcal{O}(\varepsilon^{|k|}) \quad \forall k \neq 0 \\ \beta_0 = \mathcal{O}(\varepsilon)\,, \quad \beta_k &= \mathcal{O}(\varepsilon^{|k|}) \quad \forall k \neq 0 \end{aligned} \tag{A.15}$$

which is consistent with the fact $\alpha_{-k} = \alpha_k^*$ and we assume the scaling

$$\partial_t \sim \partial_x \sim \partial_y \sim \varepsilon. \tag{A.16}$$

Further justification for this ansatz can be found in [7] [33]. We can now expand the Fourier representation of the Boltzmann equations (5.15) up the lowest order which gives non-trivial solutions, which is $\varepsilon^3$ in our case and truncate higher orders:

- k=0:

$$\begin{aligned} \partial_t \alpha_0 + \frac{1}{2}(\nabla \alpha_1^* + \nabla^* \alpha_1) &= +\tau(\beta_0 - \lambda\alpha_0)\alpha_0\beta_0 \\ \partial_t \beta_0 + \frac{1}{2}(\nabla \beta_1^* + \nabla^* \beta_1) &= -\tau(\beta_0 - \lambda\alpha_0)\alpha_0\beta_0 \end{aligned} \tag{A.17}$$

- k=1:

$$\begin{aligned} \partial_t \alpha_1 + \tfrac{1}{2}(\nabla \alpha_0 + \nabla^* \alpha_2) &= (P_{0,1} - 1)\alpha_1 + (A_{0,1} + A_{1,1})\alpha_0\alpha_1 \\ &\quad + (A_{2,1} + A_{-1,1})\alpha_1^*\alpha_2 + \tau(\beta_0 - \lambda\alpha_0)\alpha_1\beta_0 \\ \partial_t \beta_1 + \tfrac{1}{2}(\nabla \beta_0 + \nabla^* \beta_2) &= (P_{0,1} - 1)\beta_1 + (A_{0,1} + A_{1,1})\beta_0\beta_1 \\ &\quad + (A_{2,1} + A_{-1,1})\beta_1^*\beta_2 - \tau(\beta_0 - \lambda\alpha_0)\alpha_0\beta_1 \end{aligned} \tag{A.18}$$

- k=2:

$$\begin{aligned} \partial_t \alpha_2 + \tfrac{1}{2}\nabla \alpha_1 &= (P_{0,2} - 1)\alpha_2 + (A_{0,2} + A_{2,2})\alpha_0\alpha_2 + A_{1,2}\alpha_1^2 \\ \partial_t \beta_2 + \tfrac{1}{2}\nabla \beta_1 &= (P_{0,2} - 1)\beta_2 + (A_{0,2} + A_{2,2})\beta_0\beta_2 + A_{1,2}\beta_1^2 \end{aligned} \tag{A.19}$$

Because we only want to have a maximum order of $\varepsilon^3$ in our final equation as well, we can drop the third order terms $\partial_t \alpha_2$ and $\partial_t \beta_2$ in (A.19) and solve for $\alpha_2$ and $\beta_2$. With the introduction of

$$\nu_A = -\frac{1}{4(P_{0,2} - 1 + (A_{0,2} + A_{2,2})\alpha_0)} \tag{A.20}$$

we can write

$$\alpha_2 = 4\nu_A A_{1,2}\alpha_1^2 - 2\nu_A \nabla \alpha_1 \tag{A.21}$$

If we plug this into (A.18), we get

$$\begin{aligned} \partial_t \alpha_1 = &-\tfrac{1}{2}\nabla \alpha_0 - 2\nabla^* \nu_A \left(A_{1,2}\alpha_1^2 - \tfrac{1}{2}\nabla \alpha_1\right) - 2\nu_A \left(2A_{1,2}\alpha_1 \nabla^* \alpha_1 - \tfrac{1}{2}\nabla^* \nabla \alpha_1\right) \\ &+ (P_{0,1} - 1)\alpha_1 + (A_{0,1} + A_{1,1})\alpha_0\alpha_1 + 4\nu_A A_{1,2}(A_{2,1} + A_{-1,1})\alpha_1^*\alpha_2^2 \\ &- 2\nu_A (A_{2,1} + A_{1,1})\alpha_1^* \nabla \alpha_1 + \tau(\beta_0 - \lambda\alpha_0)\beta_0\alpha_1 \end{aligned} \tag{A.22}$$

where, if we drop all orders of $\varepsilon^4$ or higher and rearrange the equation a bit, arrive at

$$\begin{aligned} = &\left[(P_{0,1} - 1) + (A_{0,1} + A_{1,1})\alpha_0 + 4(A_{2,1} + A_{-1,1})|\alpha_1|^2 \nu_A A_{1,2} + \tau(\beta_0 - \lambda\alpha_0)\beta_0\right]\alpha_1 \\ &- \tfrac{1}{2}\nabla \alpha_0 + \nu_A \nabla^* \nabla \alpha_1 - 4\nu_A A_{1,2}\alpha_1 \nabla^* \alpha_1 - 2\nu_A (A_{2,1} + A_{-1,1})\alpha_1^* \nabla \alpha_1. \end{aligned} \tag{A.23}$$

After a similar calculation for $\beta_1$ and with the introduction of the new parameters

$$\begin{aligned}
\nu_A =& -\tfrac{1}{4}\left[P_{0,2} - 1 + (A_{0,2} + A_{2,2})\alpha_0\right]^{-1} \\
\nu_B =& -\tfrac{1}{4}\left[P_{0,2} - 1 + (A_{0,2} + A_{2,2})\beta_0\right]^{-1} \\
\mu_A =& P_{0,1} - 1 + (A_{0,1} + A_{1,1})\alpha_0 + \tau(\beta_0 - \lambda\alpha_0)\beta_0 \\
\mu_B =& P_{0,1} - 1 + (A_{0,1} + A_{1,1})\beta_0 - \tau(\beta_0 - \lambda\alpha_0)\alpha_0 \\
\gamma_A =& 4\nu_A A_{1,2} \qquad \kappa_A = 2\nu_A(A_{2,1} + A_{-1,1}) \qquad \xi_A = -4(A_{2,1} + A_{-1,1})\nu_A A_{1,2} \\
\gamma_B =& 4\nu_B A_{1,2} \qquad \kappa_B = 2\nu_B(A_{2,1} + A_{-1,1}) \qquad \xi_B = -4(A_{2,1} + A_{-1,1})\nu_B A_{1,2}
\end{aligned}$$

we can write the hydrodynamic equations as

$$\partial_t\alpha_0 = -\tfrac{1}{2}(\nabla\alpha_1^* + \nabla^*\alpha_1) + \tau(\beta_0 - \lambda\alpha_0)\beta_0\alpha_0 \tag{A.24a}$$

$$\partial_t\beta_0 = -\tfrac{1}{2}(\nabla\beta_1^* + \nabla^*\beta_1) - \tau(\beta_0 - \lambda\alpha_0)\beta_0\alpha_0 \tag{A.24b}$$

$$\begin{aligned}
\partial_t\alpha_1 =& (\mu_A(\alpha_0,\beta_0) - \xi_A(\alpha_0)|\alpha_1|^2)\alpha_1 + \nu_A(\alpha_0)\nabla^*\nabla\alpha_1 - \tfrac{1}{2}\nabla\alpha_0 \\
& - \gamma_A(\alpha_0)\alpha_1\nabla^*\alpha_1 - \kappa_A(\alpha_0)\alpha_1^*\nabla\alpha_1
\end{aligned} \tag{A.24c}$$

$$\begin{aligned}
\partial_t\beta_1 =& (\mu_B(\alpha_0,\beta_0) - \xi_B(\beta_0)|\beta_1|^2)\beta_1 + \nu_B(\beta_0)\nabla^*\nabla\beta_1 - \tfrac{1}{2}\nabla\beta_0 \\
& - \gamma_B(\beta_0)\beta_1\nabla^*\beta_1 - \kappa_B(\beta_0)\beta_1^*\nabla\beta_1
\end{aligned} \tag{A.24d}$$

## A.4 Linear Stability of Hydrodynamic Equations

In chapter 6.3 we employ a linear stability analysis to study the stability of our homogeneous fixed points using inhomogeneous perturbations:

$$\begin{aligned}
\alpha_0(\mathbf{r},t) &= a + \delta a(\mathbf{r},t) \qquad & \beta_0(\mathbf{r},t) &= b + \delta b(\mathbf{r},t) \\
\alpha_1(\mathbf{r},t) &= w + \delta w(\mathbf{r},t) \qquad & \beta_1(\mathbf{r},t) &= u + \delta u(\mathbf{r},t)
\end{aligned} \tag{A.25}$$

$a$, $b$, $w$, $u$ are the homogeneous fixed points of $\alpha_0$, $\beta_0$, $\alpha_1$, $\beta_1$, respectively and $\delta a$, $\delta b$, $\delta w$, $\delta u$ the inhomogeneous perturbations.

If we plug this into our hydrodynamic equations (6.1a-d) and only write down terms up to first order, we get

$$\partial_t\delta a = -\frac{1}{2}(\nabla\delta w^* + \nabla^*\delta w) + \tau(2b - \lambda a)a\delta b + \tau(b - 2\lambda a)b\delta a \tag{A.26a}$$

$$\partial_t\delta b = -\frac{1}{2}(\nabla\delta u^* + \nabla^*\delta u) - \tau(2b - \lambda a)a\delta b - \tau(b - 2\lambda a)b\delta a \tag{A.26b}$$

$$\begin{aligned}
\partial\delta w =& \left[\left(\frac{\partial\mu_A}{\partial a} - \frac{\partial\xi_A}{\partial a}|w|^2\right)w - \frac{1}{2}\nabla\right]\delta a + \frac{\partial\mu_A}{\partial b}w\delta b - \xi_A w^2\delta w^* \\
& + (\mu_A - 2\xi_A|w|^2 + \nu_A\nabla^*\nabla - \gamma_A w\nabla^* - \kappa_A w^*\nabla)\delta w
\end{aligned} \tag{A.26c}$$

$$\begin{aligned}
\partial\delta u =& \left[\left(\frac{\partial\mu_B}{\partial b} - \frac{\partial\xi_B}{\partial b}|u|^2\right)u - \frac{1}{2}\nabla\right]\delta b + \frac{\partial\mu_B}{\partial a}u\delta a - \xi_B u^2\delta u^* \\
& + (\mu_B - 2\xi_B|u|^2 + \nu_B\nabla^*\nabla - \gamma_B u\nabla^* - \kappa_B u^*\nabla)\delta u
\end{aligned} \tag{A.26d}$$

To analyze the stability of our solutions, we employ a plane wave ansatz which can be framed as a Fourier transformation of the spatial variable like

$$\begin{aligned} f(\mathbf{r},t) =& \frac{1}{2\pi}\int_{-\infty}^{\infty} d\mathbf{q}\, e^{i\mathbf{q}\mathbf{r}} f_{\mathbf{q}} \qquad f_{\mathbf{q}} = \frac{1}{2\pi}\int_{-\infty}^{\infty} d\mathbf{r}\, e^{-i\mathbf{q}\mathbf{r}} f(\mathbf{r}) \\ f^*(\mathbf{r},t) =& \frac{1}{2\pi}\int_{-\infty}^{\infty} d\mathbf{q}\, e^{-i\mathbf{q}\mathbf{r}} f^*_{\mathbf{q}} \qquad f^*_{\mathbf{q}} = \frac{1}{2\pi}\int_{-\infty}^{\infty} d\mathbf{r}\, e^{i\mathbf{q}\mathbf{r}} f^*(\mathbf{r}) \end{aligned} \tag{A.27}$$

where $f$ is a surrogate for $\delta a$, $\delta w$, etc. Now, with this definition, we can transform the equations (A.26a-d) by multiplying with $\exp(i\mathbf{q}\mathbf{r})$ and integrating over $\mathbf{r}$ to arrive at a system of linear equations in $\delta a_{\mathbf{q}}$, $\delta b_{\mathbf{q}}$, $\delta w_{\mathbf{q}}$, $\delta w^*_{-\mathbf{q}}$, $\delta u_{\mathbf{q}}$ and $\delta u^*_{-\mathbf{q}}$.

$$\begin{aligned} \partial_t \delta a_{\mathbf{q}} =& \left[\tau(b-2\lambda a)b\right]\delta a_{\mathbf{q}} + \left[\tau(2b-\lambda a)a\right]\delta b_{\mathbf{q}} \\ &+ \left[-\tfrac{1}{2}(iq_x+q_y)\right]\delta w_{\mathbf{q}} + \left[-\tfrac{1}{2}(iq_x-q_y)\right]\delta w^*_{-\mathbf{q}} \end{aligned} \tag{A.28a}$$

$$\begin{aligned} \partial_t \delta b_{\mathbf{q}} =& \left[-\tau(b-2\lambda a)b\right]\delta a_{\mathbf{q}} + \left[-\tau(2b-\lambda a)a\right]\delta b_{\mathbf{q}} \\ &+ \left[-\tfrac{1}{2}(iq_x+q_y)\right]\delta u_{\mathbf{q}} + \left[-\tfrac{1}{2}(iq_x-q_y)\right]\delta u^*_{-\mathbf{q}} \end{aligned} \tag{A.28b}$$

$$\begin{aligned} \partial_t w_{\mathbf{q}} =& \left[\left(\frac{\partial \mu_A}{\partial a} - \frac{\partial \xi_A}{\partial a}|w|^2\right)w - \frac{1}{2}(iq_x-q_y)\right]\delta a_{\mathbf{q}} + \left[\frac{\partial \mu_A}{\partial b}w\right]\delta b_{\mathbf{q}} \\ &+ \left[\mu_A - 2\xi_A|w|^2 - \nu_A(q_x^2+q_y^2) - \gamma_A w(iq_x+q_y) - \kappa_A w^*(iq_x-q_y)\right]\delta w_{\mathbf{q}} \\ &+ \left[-\xi_A w^2\right]\delta w^*_{-\mathbf{q}} \end{aligned} \tag{A.28c}$$

$$\begin{aligned} \partial_t w^*_{-\mathbf{q}} =& \left[\left(\frac{\partial \mu_A}{\partial a} - \frac{\partial \xi_A}{\partial a}|w|^2\right)w^* - \frac{1}{2}(iq_x+q_y)\right]\delta a_{\mathbf{q}} + \left[\frac{\partial \mu_A}{\partial b}w^*\right]\delta b_{\mathbf{q}} \\ &+ \left[-\xi_A (w^*)^2\right]\delta w_{\mathbf{q}} \\ &+ \left[\mu_A - 2\xi_A|w|^2 - \nu_A(q_x^2+q_y^2) - \gamma_A w^*(iq_x-q_y) - \kappa_A w(iq_x+q_y)\right]\delta w^*_{-\mathbf{q}} \end{aligned} \tag{A.28d}$$

$$\begin{aligned} \partial_t u_{\mathbf{q}} =& \left[\frac{\partial \mu_B}{\partial a}u\right]\delta a_{\mathbf{q}} + \left[\left(\frac{\partial \mu_B}{\partial b} - \frac{\partial \xi_B}{\partial b}|u|^2\right)u - \frac{1}{2}(iq_x-q_y)\right]\delta b_{\mathbf{q}} \\ &+ \left[\mu_B - 2\xi_B|u|^2 - \nu_B(q_x^2+q_y^2) - \gamma_B w(iq_x+q_y) - \kappa_B u^*(iq_x-q_y)\right]\delta u_{\mathbf{q}} \\ &+ \left[-\xi_B u^2\right]\delta u^*_{-\mathbf{q}} \end{aligned} \tag{A.28e}$$

$$\begin{aligned} \partial_t u^*_{-\mathbf{q}} =& \left[\frac{\partial \mu_B}{\partial a}u^*\right]\delta a_{\mathbf{q}} + \left[\left(\frac{\partial \mu_B}{\partial b} - \frac{\partial \xi_B}{\partial b}|u|^2\right)u^* - \frac{1}{2}(iq_x+q_y)\right]\delta b_{\mathbf{q}} \\ &+ \left[-\xi_B (u^*)^2\right]\delta u_{\mathbf{q}} \\ &+ \left[\mu_B - 2\xi_B|u|^2 - \nu_B(q_x^2+q_y^2) - \gamma_B u^*(iq_x-q_y) - \kappa_B u(iq_x+q_y)\right]\delta u^*_{-\mathbf{q}} \end{aligned} \tag{A.28f}$$

This rather involved system of linear equations can be framed as

$$\partial_t \begin{pmatrix} \delta a \\ \delta b \\ \delta w \\ \delta w^* \\ \delta u \\ \delta u^* \end{pmatrix} = \mathcal{J} \begin{pmatrix} \delta a \\ \delta b \\ \delta w \\ \delta w^* \\ \delta u \\ \delta u^* \end{pmatrix} \tag{A.29}$$

where we dropped the subscripts to simplify the notation and introduced the Jacobian matrix $\mathcal{J}$ which can be read off (A.28a-f). As an example, we can plug in the homogeneous, isotropic fixed point with $w = w^* = u = u^* = 0$, $a = \rho\frac{1}{1+\lambda}$ and $b = \rho\frac{\lambda}{1+\lambda}$, which simplifies the expression for $\mathcal{J}$:

$$\mathcal{J} = \begin{pmatrix} -\rho^2\tau\frac{\lambda^2}{(1+\lambda)^2} & \rho^2\tau\frac{\lambda}{(1+\lambda)^2} & -\frac{(iq_x+q_y)}{2} & \frac{(q_y-iq_x)}{2} & 0 & 0 \\ \rho^2\tau\frac{\lambda^2}{(1+\lambda)^2} & -\rho^2\tau\frac{\lambda}{(1+\lambda)^2} & 0 & 0 & -\frac{(iq_x+q_y)}{2} & \frac{(q_y-iq_x)}{2} \\ -\frac{(iq_x-q_y)}{2} & 0 & \mu_A - \nu_A q^2 & 0 & 0 & 0 \\ -\frac{(iq_x+q_y)}{2} & 0 & 0 & \mu_A - \nu_A q^2 & 0 & 0 \\ 0 & -\frac{(iq_x-q_y)}{2} & 0 & 0 & \mu_B - \nu_B q^2 & 0 \\ 0 & -\frac{(iq_x+q_y)}{2} & 0 & 0 & 0 & \mu_B - \nu_B q^2 \end{pmatrix}$$

with $q^2 = q_x^2 + q_y^2$. The eigenvalues of this matrix encode the stability of the fixed point.

## A.5 Collision Factors

The collision factors $A_{p,k}$ appear in the collision term of the Boltzmann equation $I_{col}$ and later on in the hydrodynamic equations as well. They play an important part in the stability of the fixed points and are defined as

$$A_{p,k} = \int \frac{d\vartheta}{2\pi} R(|\vartheta|) \left( P_k \cos\left( (\tfrac{k}{2} - p)\vartheta \right) - \cos(p\vartheta) \right) \tag{A.30}$$

with

$$R(|\vartheta|) = 4 \left| \sin\left(\frac{\vartheta}{2}\right) \right| \tag{A.31a}$$

$$P_k = \exp\left(-\frac{\sigma^2}{2}k^2\right). \tag{A.31b}$$

The most important of these factors for our treatment are given in the following:

- $A_{0,1} = \frac{4}{\pi}\left( \exp\left[-\frac{\sigma^2}{2}\right] - 2 \right)$
- $A_{1,1} = \frac{4}{\pi}\left( \exp\left[-\frac{\sigma^2}{2}\right] + \frac{2}{3} \right)$

- $A_{0,2} = -\frac{8}{\pi}\left(\frac{1}{3}\exp\left[-2\sigma^2\right]+1\right)$
- $A_{1,2} = \frac{8}{\pi}\left(\exp\left[-2\sigma^2\right]+\frac{1}{3}\right)$
- $A_{2,2} = \frac{8}{\pi}\left(-\frac{1}{3}\exp\left[-2\sigma^2\right]+\frac{1}{15}\right)$
- $A_{2,1} = \frac{4}{\pi}\left(-\exp\left[-\frac{\sigma^2}{2}\right]+\frac{2}{15}\right)$
- $A_{-1,1} = \frac{4}{\pi}\left(-\exp\left[-\frac{\sigma^2}{2}\right]+\frac{2}{3}\right)$

# *Acknowledgements*

Ich möchte mich zuallererst bei Prof. Dr. Frey bedanken, der unsere Idee der gemeinsamen Bearbeitung eines größeren Themas im Rahmen zweier sich ergänzender Masterarbeiten von Anfang an voll unterstützt hat. In unseren Gesprächen hat er mit seinem breiten Wissen über statistische Physik und den Stand der Forschung immer das richtige Gespür für die wichtigen und essentiellen Fragestellungen und Ansätze gehabt und uns so sehr oft weitergeholfen.

Besonderen Dank möchte ich auch unseren Betreuern Jonas und Lenz aussprechen, welche uns den nötigen Freiraum gaben um sehr eigenständig arbeiten zu können, aber gleichzeitig bei jeglichen Problemen immer erreichbar waren und uns wertvolle Ratschläge und Verbesserungsvorschläge für Ansätze und Analysen gaben.

Vielen Dank an Johanna, meine Partnerin in der Bearbeitung dieses Masterarbeitsthemas. Bereits seit Beginn des Bachelors habe ich immer sehr gern mit dir gearbeitet, gelernt und diskutiert. Ich hätte mir keine bessere Partnerin für diese Masterarbeit wünschen können und bedanke mich für die schöne Zeit, die vielen Gespräche und die Motivation, wenn es mal nicht so gut lief.

Danke an meine Mitbewohner Florian und Julia, die mich besonders in der Endphase der Masterarbeit mit allem versorgten und meinen Ausführungen zu physikalischen Themen lauschten.

Ich bedanke mich bei meiner Familie, meinen Eltern und Geschwistern, meinen Freunden, die mich während des gesamten Studiums und außerhalb tatkräftig unterstützten.

Danke euch Allen!

# Bibliography


[1] Igor S. Aranson and Lev S. Tsimring. "Pattern formation of microtubules and motors: Inelastic interaction of polar rods". In: *Phys. Rev. E* 71 (5 May 2005), p. 050901. DOI: 10.1103/PhysRevE.71.050901. URL: https://link.aps.org/doi/10.1103/PhysRevE.71.050901.

[2] R Axelrod and WD Hamilton. "The evolution of cooperation". In: *Science* 211.4489 (1981), pp. 1390–1396. ISSN: 0036-8075. DOI: 10.1126/science.7466396.

[3] M Ballerini et al. "Interaction Ruling Animal Collective Behaviour Depends on Topological rather than Metric Distance: Evidence from a Field Study". In: *Proceedings of the National Academy of Sciences of the United States of America* 105 (Feb. 2008), pp. 1232–7. DOI: 10.1073/pnas.0711437105.

[4] Aparna Baskaran and M. Cristina Marchetti. "Enhanced Diffusion and Ordering of Self-Propelled Rods". In: *Phys. Rev. Lett.* 101 (26 Dec. 2008), p. 268101. DOI: 10.1103/PhysRevLett.101.268101. URL: https://link.aps.org/doi/10.1103/PhysRevLett.101.268101.

[5] Madeleine Beekman, David Sumpter, and Francis L. W. Ratnieks. "Phase transition between disordered and ordered foraging in Pharaoh's ants". In: *Proceedings of the National Academy of Sciences of the United States of America* 98 (Sept. 2001), pp. 9703–6. DOI: 10.1073/pnas.161285298.

[6] Eric Bertin, Michel Droz, and Guillaume Grégoire. "Boltzmann and hydrodynamic description for self-propelled particles". In: 74.2 (Aug. 2006), p. 022101. DOI: 10.1103/PhysRevE.74.022101. URL: https://ui.adsabs.harvard.edu/abs/2006PhRvE..74b2101B.

[7] Eric Bertin, Michel Droz, and Guillaume Grégoire. "Hydrodynamic equations for self-propelled particles: microscopic derivation and stability analysis". In: *Journal of Physics A Mathematical General* 42.44 (Nov. 2009), p. 445001. DOI: 10.1088/1751-8113/42/44/445001. URL: https://ui.adsabs.harvard.edu/abs/2009JPhA...42R5001B.

[8] H. Chaté et al. "Modeling collective motion: variations on the Vicsek model". In: *The European Physical Journal B* 64.3 (Aug. 2008), pp. 451–456. ISSN: 1434-6036. DOI: 10.1140/epjb/e2008-00275-9. URL: https://doi.org/10.1140/epjb/e2008-00275-9.

[9] Hugues Chaté et al. "Collective motion of self-propelled particles interacting without cohesion". In: *Phys. Rev. E* 77 (4 Apr. 2008), p. 046113. DOI: 10.1103/PhysRevE.77.046113. URL: https://link.aps.org/doi/10.1103/PhysRevE.77.046113.

[10] Czirók et al. "Formation of complex bacterial colonies via self-generated vortices." In: *Physical review. E, Statistical physics, plasmas, fluids, and related interdisciplinary topics* 54 2 (1996), pp. 1791–1801.

[11] András Czirók, H Eugene Stanley, and Tamás Vicsek. "Spontaneously ordered motion of self-propelled particles". In: *Journal of Physics A: Mathematical and General* 30.5 (Mar. 1997), pp. 1375–1385. DOI: 10.1088/0305-4470/30/5/009. URL: https://doi.org/10.1088/0305-4470/30/5/009.

[12] András Czirók, M Matsushita, and Tamás Vicsek. "Theory of periodic swarming of bacteria: Application to Proteus mirabilis". In: *Physical review. E, Statistical, nonlinear, and soft matter physics* 63 (Apr. 2001), p. 031915. DOI: 10.1103/PhysRevE.63.031915.

[13] Alma Dal Co, Simon van Vliet, and Martin Ackermann. *Emergent microscale gradients give rise to metabolic cross-feeding and antibiotic tolerance in clonal bacterial populations*. Jan. 2019. DOI: 10.1101/534149.

[14] R M Dawes. "Social Dilemmas". In: *Annual Review of Psychology* 31.1 (1980), pp. 169–193. DOI: 10.1146/annurev.ps.31.020180.001125. eprint: https://doi.org/10.1146/annurev.ps.31.020180.001125. URL: https://doi.org/10.1146/annurev.ps.31.020180.001125.

[15] Jonas Denk et al. "Active Curved Polymers Form Vortex Patterns on Membranes". In: *Phys. Rev. Lett.* 116 (17 Apr. 2016), p. 178301. DOI: 10.1103/PhysRevLett.116.178301. URL: https://link.aps.org/doi/10.1103/PhysRevLett.116.178301.

[16] Christopher Dombrowski et al. "Self-Concentration and Large-Scale Coherence in Bacterial Dynamics". In: *Phys. Rev. Lett.* 93 (9 Aug. 2004), p. 098103. DOI: 10.1103/PhysRevLett.93.098103. URL: https://link.aps.org/doi/10.1103/PhysRevLett.93.098103.

[17] Erwin Frey and Tobias Reichenbach. "Bacterial Games". In: Feb. 2011, pp. 297–329. DOI: 10.1007/978-3-642-18137-5_13.

[18] I. Gallagher et al. *From Newton to Boltzmann: Hard Spheres and Short-range Potentials*. Zurich lectures in advanced mathematics. European Mathematical Society, 2013. ISBN: 9783037191293. URL: https://books.google.de/books?id=SIS6FuqUvF0C.

[19] Jeff Gore, Hyun Youk, and Alexander Oudenaarden. "Gore J, Youk H, van Oudenaarden A.. Snowdrift game dynamics and facultative cheating in yeast. Nature 459: 253-256". In: *Nature* 459 (May 2009), pp. 253–6. DOI: 10.1038/nature07921.

[20] H Grubmueller et al. "Generalized Verlet Algorithm for Efficient Molecular Dynamics Simulations with Long-range Interactions". In: *Mol. Sim.* 6 (Mar. 1991), pp. 121–. DOI: 10.1080/08927029108022142.

[21] W.D. Hamilton. "The genetical evolution of social behaviour. I". In: *Journal of Theoretical Biology* 7.1 (1964), pp. 1 –16. ISSN: 0022-5193. DOI: https://doi.org/10.1016/0022-5193(64)90038-4. URL: http://www.sciencedirect.com/science/article/pii/0022519364900384.

[22] Christoph Hauert and Michael Doebeli. "Spatial structure often inhibits the evolution of cooperation in the snowdrift game". In: *Nature* 428 (Apr. 2004), pp. 643–646. DOI: 10.1038/nature02360.

[23] Josef Hofbauer and Karl Sigmund. *Evolutionary Games and Population Dynamics*. Cambridge University Press, 1998. DOI: 10.1017/CBO9781139173179.

[24] L. Huber et al. "Emergence of coexisting ordered states in active matter systems". In: *Science* 361.6399 (2018), pp. 255–258. ISSN: 0036-8075. DOI: 10.1126/science.aao5434. eprint: https://science.sciencemag.org/content/361/6399/255.full.pdf. URL: https://science.sciencemag.org/content/361/6399/255.

[25] Jolyon J. Faria et al. "Leadership and social information use in human crowds". In: *Animal Behaviour - ANIM BEHAV* 79 (Apr. 2010), pp. 895–901. DOI: 10.1016/j.anbehav.2009.12.039.

[26] Tariq Samad (eds.) John Baillieul. *Encyclopedia of Systems and Control*. Springer London, 2015. ISBN: 978-1-4471-5102-9.

[27] Oskar Morgenstern John Von Neumann. *Theory of Games and Economic Behaviour*. 3rd. Princeton University Press, 1972. ISBN: 0691041830.

[28] T. Killingback, M. Doebeli, and N. Knowlton. "Variable investment, the Continuous Prisoner's Dilemma, and the origin of cooperation". In: *Proceedings Biological sciences* 266 (1430 1999), 1723–1728. DOI: 10.1098/rspb.1999.0838.

[29] Kevin Leyton-Brown. *Essentials of game theory*. 1st ed. Synthesis Lectures on Artificial Intelligence and Machine Learning. Morgan and Claypool Publishers, 2008. ISBN: 1598295934,9781598295931.

[30] Ugo Lopez et al. "From behavioural analyses to models of collective motion in fish schools". In: *Interface focus* 2 (Dec. 2012), pp. 693–707. DOI: 10.1098/rsfs.2012.0033.

[31] Nagy M. Couzin I.D. Fiedler W. Wikelski M. and Flack A. "Synchronization, coordination and collective sensing during thermalling flight of freely migrating white storks". In: *Phil. Trans. R. Soc. B* 373 (20170011 2018). DOI: /10.1098/rstb.2017.0011. URL: http://dx.doi.org/10.1098/rstb.2017.0011.

[32] M. C. Marchetti et al. "Soft Active Matter". In: *arXiv e-prints*, arXiv:1207.2929 (July 2012), arXiv:1207.2929. arXiv: 1207.2929 [cond-mat.soft].

[33] Johanna Mayer. "Two Species of Self-Propelled Particles Interacting in a Snowdrift Game Scenario - Kinetic Approach". In: *Master Thesis, Department of Statistical Physics at LMU Munich* (2019).

[34] Shradha Mishra, Aparna Baskaran, and M Cristina Marchetti. "Fluctuations and pattern formation in self-propelled particles". In: *Physical review. E, Statistical, nonlinear, and soft matter physics* 81 (June 2010), p. 061916. DOI: 10.1103/PhysRevE.81.061916.

[35] Roger B. Myerson. "Nash Equilibrium and the History of Economic Theory". In: *Journal of Economic Literature* 37.3 (1999), pp. 1067–1082. DOI: 10.1257/jel.37.3.1067.

[36] John F. Nash. "Equilibrium points in n-person games". In: *Proceedings of the National Academy of Sciences* 36.1 (1950), pp. 48–49. ISSN: 0027-8424. DOI: 10.1073/pnas.36.1.48. eprint: https://www.pnas.org/content/36/1/48.full.pdf. URL: https://www.pnas.org/content/36/1/48.

[37] John von Neumann. "Zur Theorie der Gesellschaftsspiele." In: *Mathematische Annalen* 100 (1928), pp. 295–300. URL: https://doi.org/10.1007/BF01448847.

[38] Martin Nowak and Robert May. "Evolutionary games and spatial chaos". In: *Nature* 359 (Oct. 1992). DOI: 10.1038/359826a0. URL: https://doi.org/10.1038/359826a0.

[39] Peter Pacheco. *An Introduction to Parallel Programming*. 1st. San Francisco, CA, USA: Morgan Kaufmann Publishers Inc., 2011. ISBN: 9780123742605.

[40] A. Peshkov et al. "Boltzmann-Ginzburg-Landau approach for continuous descriptions of generic Vicsek-like models". In: *The European Physical Journal Special Topics* 223.7 (June 2014), pp. 1315–1344. ISSN: 1951-6401. DOI: 10.1140/epjst/e2014-02193-y. URL: https://doi.org/10.1140/epjst/e2014-02193-y.

[41] Anton Peshkov et al. "Nonlinear Field Equations for Aligning Self-Propelled Rods". In: *Phys. Rev. Lett.* 109 (26 Dec. 2012), p. 268701. DOI: 10.1103/PhysRevLett.109.268701. URL: https://link.aps.org/doi/10.1103/PhysRevLett.109.268701.

[42] Sriram Ramaswamy. "The Mechanics and Statistics of Active Matter". In: *Annual Review of Condensed Matter Physics* 1.1 (2010), pp. 323–345. DOI: 10.1146/annurev-conmatphys-070909-104101.

[43] Sriram Ramaswamy, R Simha, and John Toner. "Active nematics on a substrate: Giant number fluctuations and long-time tails". In: *EPL (Europhysics Letters)* 62 (Jan. 2007), p. 196. DOI: 10.1209/epl/i2003-00346-7.

[44] I. William Zartman Rudolf Avenhaus. *Diplomacy Games: Formal Models and International Negotiations*. 1st ed. Springer, 2007. ISBN: 3540683038.

[45] Bridgett K. Ryan-Payseur and Nancy E. Freitag. "Bacillus subtilis Biofilms: a Matter of Individual Choice". In: *mBio* 9.6 (2018). DOI: 10.1128/mBio.02339-18. eprint: https://mbio.asm.org/content/9/6/e02339-18.full.pdf. URL: https://mbio.asm.org/content/9/6/e02339-18.

[46] Torney CJ Grant C. Hopcraft J Morrison TA Couzin ID Levin SA. "From single steps to mass migration: the problem of scale in the movement ecology of the Serengeti wildebeest". In: *Phil. Trans. R. Soc. B* 373 (20170012 2018). DOI: /10.1098/rstb.2017.0012. URL: http://dx.doi.org/10.1098/rstb.2017.0012.

[47] John Maynard Smith. *Evolution and the Theory of Games*. Cambridge University Press, 1982. DOI: 10.1017/CBO9780511806292.

[48] Heinrich von Stackelberg (auth.) *Market Structure and Equilibrium*. 1st ed. Springer-Verlag Berlin Heidelberg, 2011. ISBN: 3642125867.

[49] Ryo Suzuki et al. "Polar Pattern Formation in Driven Filament Systems Require Non-Binary Particle Collisions". In: *Nat Phys* advance online publication (Aug. 2015). DOI: 10.1038/nphys3423.

[50] Marko Sysi-Aho et al. "Spatial snowdrift game with myopic agents". In: *Physics of Condensed Matter* 44 (Mar. 2005), pp. 129–135. DOI: 10.1140/epjb/e2005-00108-5.

[51] B. Szabó et al. "Phase transition in the collective migration of tissue cells: Experiment and model". In: *Phys. Rev. E* 74 (6 Dec. 2006), p. 061908. DOI: 10.1103/PhysRevE.74.061908. URL: https://link.aps.org/doi/10.1103/PhysRevE.74.061908.

[52] Florian Thüroff, Christoph A. Weber, and Erwin Frey. "Numerical Treatment of the Boltzmann Equation for Self-Propelled Particle Systems". In: *Phys. Rev. X* 4 (4 Nov. 2014), p. 041030. DOI: 10.1103/PhysRevX.4.041030. URL: https://link.aps.org/doi/10.1103/PhysRevX.4.041030.

[53] John Toner and Yuhai Tu. "Flocks, herds, and schools: A quantitative theory of flocking". In: *Phys. Rev. E* 58 (4 Oct. 1998), pp. 4828–4858. DOI: 10.1103/PhysRevE.58.4828. URL: https://link.aps.org/doi/10.1103/PhysRevE.58.4828.

[54] John Toner and Yuhai Tu. "Long-Range Order in a Two-Dimensional Dynamical XY Model: How Birds Fly Together". In: *Phys. Rev. Lett.* 75 (23 Dec. 1995), pp. 4326–4329. DOI: 10.1103/PhysRevLett.75.4326. URL: https://link.aps.org/doi/10.1103/PhysRevLett.75.4326.

[55] John Toner, Yuhai Tu, and Sriram Ramaswamy. "Hydrodynamics and phases of flocks". In: *Annals of Physics - ANN PHYS N Y* 318 (July 2005), pp. 170–244. DOI: 10.1016/j.aop.2005.04.011.

[56] Ali Turgut et al. "Self-organized flocking in mobile robot swarms". In: *Swarm Intelligence* 2 (Dec. 2008), pp. 97–120. DOI: 10.1007/s11721-008-0016-2.

[57] Tamás Vicsek et al. "Novel Type of Phase Transition in a System of Self-Driven Particles". In: *Phys. Rev. Lett.* 75 (6 Aug. 1995), pp. 1226–1229. DOI: 10.1103/PhysRevLett.75.1226. URL: https://link.aps.org/doi/10.1103/PhysRevLett.75.1226.

[58] Tamás Vicsek and Anna Zafeiris. "Collective motion". In: *Physics Reports* 517.3 (2012), pp. 71 –140. ISSN: 0370-1573. DOI: https://doi.org/10.1016/j.

physrep.2012.03.004. URL: http://www.sciencedirect.com/science/article/pii/S0370157312000968.

[59] H. P. Zhang et al. "Collective motion and density fluctuations in bacterial colonies". In: *Proceedings of the National Academy of Sciences* 107.31 (2010), pp. 13626–13630. ISSN: 0027-8424. DOI: 10.1073/pnas.1001651107. URL: https://www.pnas.org/content/107/31/13626.

# Declaration of Authorship

Erklärung:

Hiermit erkläre ich, Michael OBERMÜLLER, die vorliegende Arbeit selbstständig verfasst zu haben und keine anderen als die in der Arbeit angegebenen Quellen und Hilfsmittel benutzt zu haben.

München, den 12. August 2019

Unterschrift:

_____